ARCHIVES OF ACOUSTICS
14, 1-2, 3-10 (1989)

LIGHT AND ACOUSTIC PULSE INTERACTION IN THE BRAGG DIFFRACTION REGION

JERZY BODZENTA, ZYGMUNT KLESZCZEWSKI

Institute of Physics, Technical University of Silesia
(44–100 Gliwice, ul. Krzywoustego 2)

This paper presents results of a theoretical analysis of interactions between a monochromatic light wave and series of acoustic pulses in the Bragg diffraction region. An expression for the electric field intensity of a diffracted light wave was achieved on the basis of known theories. The intensity is a sum of harmonics formed due to the diffraction of inciding light onto harmonics of the acoustic wave. Individual components of the light wave resulting from diffraction are spatially separated. A numeric analysis performed for a series of perfect, rectangular acoustic pulses proved that the measurement of the angular distribution of light intensity in a diffracted beam leads to the analysis of the acoustic wave's amplitudes spectrum. Therefore, an acoustic wave spectrum analyzer can be built with the utilization of the described interaction. The possibility of measuring parameters of acoustic pulses directly during propagation in the medium without influencing these parameters is the main advantage of such an analyzer. The frequency band of the proposed analyzer is limited by the Bragg condition depends on acoustic and acousto-optics properties of the medium and the geometry of the interaction region.

W pracy przedstawiono wyniki teoretycznej analizy oddziaływania monochromatycznej fali świetlnej z ciągiem impulsów akustycznych w obszarze dyfrakcji Bragga. Na podstawie znanych teorii otrzymano wyrażenie opisujące natężenie pola elektrycznego ugiętej fali świetlnej. Natężenie to jest sumą składowych harmonicznych powstających w wyniku dyfrakcji padającego światła na składowych harmonicznych fali akustycznej. Poszczególne składowe fali świetlnej powstałej w rezultacie dyfrakcji są rozdzielone przestrzennie. Na podstawie analizy numerycznej przeprowadzonej dla ciągu idealnych, prostokątnych impulsów akustycznych wykazano, że pomiar rozkładu kątowego natężenia światła w wiązce ugiętej pozwala na analizę widma amplitud fali akustycznej. Tak więc opisywane oddziaływanie stwarza możliwość budowy analizatora widma fali akustycznej. Do głównych zalet takiego analizatora należy zaliczyć możliwość pomiaru parametrów impulsów akustycznych bezpośrednio w czasie ich propagacji w ośrodku bez zmiany tych parametrów w czasie pomiaru. Pasmo przenoszenia proponowanego analizatora jest ograniczone koniecznością wypełnienia warunku Bragga i zależy od własności akustycznych i akustooptycznych ośrodka i geometrii obszaru oddziaływania.

1. Introduction

The light-acoustic pulses interaction is one of the more important problems in acousto-optics arousing interest during the last several years. However hitherto published papers are mainly concerned with the Raman–Nath type of diffraction [1–3, 5–7].

This paper presents a theoretical analysis of light diffraction on acoustic pulses in the Bragg region.

On the basis of known theories of light diffraction on a continuous acoustic wave an angular distribution of diffracted light wave component intensities resulting from light-acoustic wave harmonics interaction. Also results of numeric calculations are presented.

2. Theoretical analysis

Let us assume an acoustic wave in the form of rectangular pulses with duration τ, repeating period T and carrier frequency Ω_0. A series of such pulses is shown in Fig. 1.

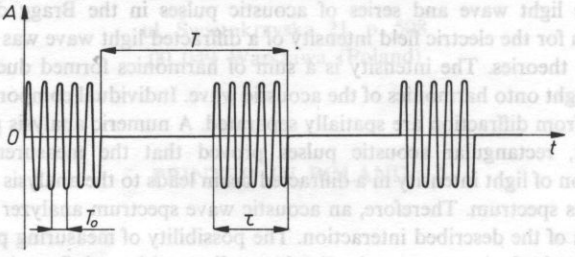

FIG. 1. Series of acoustics pulses with carrier frequencies Ω_0

Such a wave can be described with function $\Phi(\bar{r}, t)$ which is a sum of harmonics

$$\Phi(\bar{r}, t) = \sum_{l=-n}^{n} A_l \exp\{i[(\Omega_0 + l \cdot \Delta\Omega) \cdot t - \bar{K}_l \bar{r}]\} \tag{1}$$

where A_l amplitude of the l-component, $\Delta\Omega = \frac{2\pi}{T}$; $\Omega_0 = \frac{2\pi}{T_0}$, K_l wave vector of the wave l-component, equal to $\frac{\Omega_0 + l \cdot \Delta\Omega}{v}$, v propagation velocity of the acoustic wave, $\bar{r}$ vector of position.

Let us accept the geometry of interaction presented in Fig. 2. The acoustic wave propagates along the z-axis. L is the width of the acoustic beam. The light wave

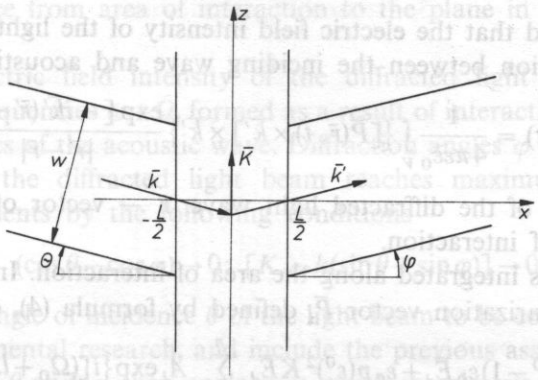

FIG. 2. Geometry of the interaction area

propagates in the xz plane under angle θ to the x-axis. The intersection of the light beam forms a square with side equal to w.

Let us assume also that these waves have constant intensity in the area of interaction. The diffracted light wave propagates in the xz plane under angle φ to the x-axis.

The electric field intensity of an inciding monochromatic light wave can be noted as

$$\bar{E}_p = \bar{E}_0 \exp[i(\omega t - \bar{k}\bar{r})], \tag{2}$$

where ω, $\bar{k}$ – frequency and wave vector respectively of the light wave.

It can be accepted that the diffracted light wave is formed as an interference result of secondary electromagnetic waves emitted by electric dipole moments, induced by the inciding light wave. By changing permittivity in the area of interaction acoustic wave causes changes of the electric polarization vector. If we accept the medium as an isotropic, non-magneti dielectric, then the vector of polarization is equal to

$$\bar{P} = (\varepsilon_0 - 1)\varepsilon_0 \bar{E}_p, \tag{3}$$

where: ε_0 – permittivity of free space, ε – relative permittivity of the medium.

When an acoustic wave propagates in the medium then the permittivity of the medium is a sum of two components: constant component ε^0 – corresponding with permittivity without disturbance, and modulating term related to the disturbance of the medium:

$$\varepsilon = \varepsilon^0 + \Delta\varepsilon = \varepsilon^0 - (\varepsilon^0)^2 ps, \tag{4}$$

where p – effective value of the medium's photo-elastic constant, s – deformation of the medium due to transition of acoustic wave.

It can be proved that the electric field intensity of the light wave generated as a result of interaction between the inciding wave and acoustic wave is equal to

$$\bar{E}_d(\bar{r};\ t) = \frac{1}{4\pi\varepsilon\varepsilon_0}\int_V \{[\bar{P}(\bar{r},\ t)\times\bar{k}']\times\bar{k}'\}\frac{\exp[-i\bar{k}'(\bar{r}'-\bar{r})]}{|\bar{r}'-\bar{r}|}dV, \tag{5}$$

where $\bar{k}$ – vector of the diffracted light wave, $\bar{r}$ – vector of position of points outside the area of interaction.

Expression (5) is integrated along the area of interaction. Including expressions (1) and (4) the polarization vector $\bar{P}$, defined by formula (4), can be expressed as

$$\bar{P}(\bar{r},\ t) = (\varepsilon^0-1)\varepsilon_0\bar{E}_d+\varepsilon_0 p(\varepsilon^0)^2 K\bar{E}_d\sum_{l=-n}^{n} A_l\exp\{i[(\Omega_0+l\Delta\Omega)t-\bar{K}_l\bar{r}]\}, \tag{6}$$

where $s = -K\Phi$, K – mean value of the wave number for acoustic wave.

The first term in expression (6) will be disregarded in further considerations, because it does not influence the generated of the diffracted light wave. Substituting (6) in formula (3) we reach

$$\bar{E}_d = \frac{1}{4\pi\varepsilon_0}\sum_{l=-n}^{n}\int_V \{[\bar{P}_{0l}\times\bar{k}']\times\bar{k}'\}\exp[-i(\bar{k}+\bar{K}_l)\bar{r}]\frac{\exp[-ik'|\bar{r}'-\bar{r}|]}{|\bar{r}'-\bar{r}|}dV, \tag{7}$$

where

$$\bar{P}_{0l} = \varepsilon_0\varepsilon pKA_l\exp[i(\omega+\Omega_l)t]\cdot\bar{E}^0, \tag{8}$$

$\bar{E}^0$ – amplitude of electric field intensity of inciding light wave

$$\Omega_l = \Omega_0 + l\cdot\Delta\Omega$$

and it was also accepted that $\varepsilon^0 \cong \varepsilon$. We accept that $\bar{E}^0 \perp \bar{k}'$ in order to simplify further considerations. Then

$$\{[\bar{P}_{0l}\times\bar{k}']\times\bar{k}'\} = -k^2 P_{0l}. \tag{9}$$

As a result the expression (7) in scalar notation will have the following form

$$E_d = \frac{k^2}{4\pi\varepsilon_0}\sum_{l=-n}^{n}\int_V P_{0l}\exp[-i(\bar{k}+\bar{K}_l)\bar{r}]\frac{\exp[-ik'|\bar{r}'-\bar{r}|]}{|\bar{r}'-\bar{r}|}dV. \tag{10}$$

The diffraction pattern is most frequently observed at a much greater distance in relation to linear dimensions of the diffraction area. Furthermore we can accept that $k \cong k'$ because $k \gg K$. This also means that angles θ and φ are small angles.

Calculating the integral in expression (10), with mentioned above assumptions, we reach the final expression for E_d

$$E_d = -\frac{k^2 K\varepsilon p}{4\pi}E_0\frac{\exp(-ikd\cdot\cos\varphi)}{d\cdot\cos\varphi}\frac{W^2 L}{\cos\theta}\frac{\sin[k(\cos\theta-\cos\varphi)L/2]}{k(\cos\theta-\cos\varphi)L/2}\times$$
$$\times\sum_{l=-n}^{n} A_l\frac{\sin\{[K_l-k(\sin\theta+\sin\varphi)]w/2\}}{[K_l-k(\sin\theta+\sin\varphi)]w/2}\exp[i(\omega+\Omega_l)t], \tag{11}$$

where d – distance from area of interaction to the plane in which diffraction is observed.

Therefore, the electric field intensity of the diffracted light wave is a sum of harmonics with frequencies $\omega+\Omega_l$ formed as a result of interaction between inciding light and harmonics of the acoustic wave. Diffraction angles φ at which the electric field intensity of the diffracted light beam reaches maximum are defined for individual components by the following conditions

$$(\cos\theta-\cos\varphi)\to 0;\ [K_l-k(\sin\theta+\sin\varphi)]\to 0 \tag{12}$$

If we assume the angle of incidence θ of the light beam to be constant, what usually happens in experimental research, and include the previous assumption concerning the value of angles θ and φ, then angle φ at which the electric field intensity of the l-component of the diffracted wave reaches maximum is expressed

$$K_l-k(\sin\varphi+\sin\theta)=0. \tag{13}$$

This means that individual harmonics of the diffracted light wave will be distributed in space and will be relatively simple to measure. The following formula expresses light intensities of individual components

$$I_{dl}=\sqrt{\frac{\varepsilon_0}{\mu_0}}\left|E_{dl}\right|^2, \tag{14}$$

where

$$E_{dl}=\frac{k^2K\varepsilon pE^0}{4\pi}\frac{\exp[-jkd\cos\varphi]}{d\cdot\cos\varphi}\frac{w^2L}{\cos\theta}\frac{\sin\left[k(\cos\theta-\cos\varphi)\frac{L}{2}\right]}{\left[k(\cos\theta-\cos\varphi)\frac{L}{2}\right]}\times$$
$$\times A_l\frac{\sin\left\{[K_l-k(\sin\theta+\sin\varphi)]\frac{w}{2}\right\}}{[K_l-k(\sin\theta+\sin\varphi)]\frac{w}{2}}\exp[j(\omega+\Omega_l)\cdot t]$$

After substitution we have

$$I_{dl}=\frac{1}{2}\sqrt{\frac{\varepsilon_0}{\mu_0}}\left\{\frac{k^2K\varepsilon pE^0}{4\pi}\frac{w^2L}{d\cdot\cos\varphi\cos\theta}\frac{\sin\left[k(\cos\theta-\cos\varphi)\frac{L}{2}\right]}{\left[k(\cos\theta-\cos\varphi)\frac{L}{2}\right]}\times\right.$$
$$\left.\times\frac{\sin\left\{[K_l-k(\sin\theta+\sin\varphi)]\frac{w}{2}\right\}}{[K_l-k(\sin\theta+\sin\varphi)]\frac{w}{2}}\right\}^2|A_l|^2 \tag{15}$$

3. Numerical calculations

The angular distribution of component intensities of a light wave diffracted on a series of ideal rectangular pulses shown in Fig. 1 was calculated on the basis of expression (15). In the case under consideration amplitudes of individual components of the acoustic wave are

$$A_l = \frac{\tau \cdot \Delta\Omega}{2\pi} \frac{\sin\left(l \cdot \Delta\Omega \frac{\tau}{2}\right)}{l \cdot \Delta\Omega\tau/2}. \tag{16}$$

If a light wave incides onto the area of interaction under the angle $\theta = \arcsin(K_0/2k)$, equal to the Bragg angle for the carrier frequency of the acoustic wave and defined by condition (13), then the ratio of the intensity of the l-component to the maximal intensity of the central component $l = 0$ is as follows

$$\frac{I_{dl}}{I_{d0}} = \left(\frac{\cos\theta}{\cos\varphi}\right)^2 \left\{ \frac{\sin(l \cdot \Delta\Omega \cdot \tau/2)}{l \cdot \Delta\Omega \cdot \tau/2} \frac{\sin\left[k(\cos\theta - \cos\varphi)\frac{L}{2}\right]}{k(\cos\theta - \cos\varphi)\frac{L}{2}} \times \right.$$

$$\left. \times \frac{\sin\left\{[K_l - k(\sin\theta + \sin\varphi)]\frac{w}{2}\right\}}{[K_l - k(\sin\theta + \sin\varphi)]\frac{w}{2}} \right\}^2. \tag{17}$$

The dependence of the l-component's intensity upon the φ angle is determined by the square of the product of $\sin x/x$ type functions; while for small θ and φ angles the last term of the product, in braces, changes most quickly with a change of the φ angle. This term conditions the width of the diffraction maximum of given component. Fig. 3 presents maximal values of (I_{dl}/I_{d0}) for components of a diffracted light wave as a function of the number of component l. Two additional axes have been drawn in the diagram. Diffraction angles φ corresponding with individual components and frequencies of acoustic wave's components Ω_l for which diffraction occurs are marked on them. Calculations were performed for following values of parameters found in (17):

$$\frac{\Omega_0}{2\pi} = 500\,\text{MHz}; \quad \frac{\Delta\Omega}{2\pi} = 1\,\text{MHz}; \quad \tau = 10^{-7}\,\text{s}; \quad L = 2 \cdot 10^{-3}\,\text{m};$$

$$w = 10^{-2}\,\text{m}; \quad \lambda = \frac{2\pi}{k} = 630\,\text{nm}; \quad v = 5000\frac{\text{m}}{\text{s}}.$$

Angle of incidence, calculated from the Bragg condition $\theta = 1°48'18''$.

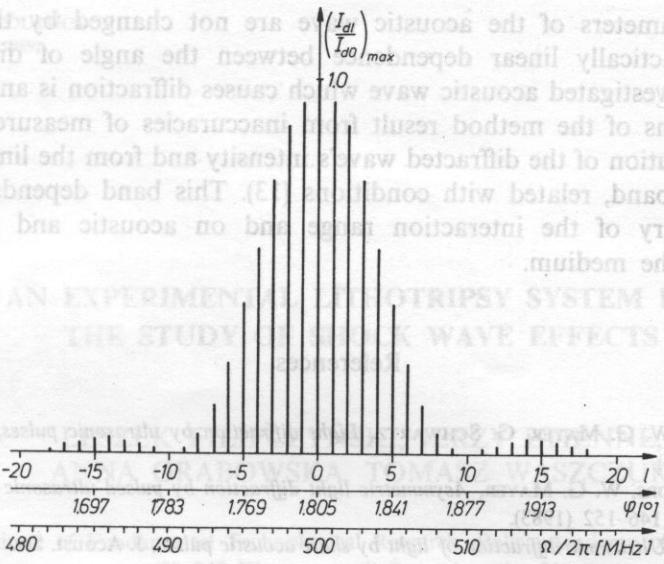

FIG. 3. Dependence of maximal values of relative intensities of diffracted light waves harmonics of the number of component l, angle of diffraction φ and frequency of component of acoustic wave Ω_l, which causes diffraction

Calculations were carried out in the range of angles expressed by inequality

$$1°36'18'' \leqslant \varphi \leqslant 2°0'18''$$

with step $\Delta\varphi = 10''$.

4. Conclusion

It results from our considerations that the interaction of a light wave with acoustic pulses provides a possibility of analysing harmonics of these pulses. Equation (15) and Fig. 3 show that the measurement of the angular distribution of light intensity in a diffracted wave can lead to the determination of the amplitude spectrum a series of acoustic pulses, calculated in the Fourier transform. Owing to the spatial resolution of individual components of the diffracted light wave measurements do not require complicated measuring methods. The direct measurement of acoustic pulses propagating in a given medium, without the necessity of converting them into electric signals (what inevitabely leads to deformations) is one of the main advantages of the spectral analysis of acoustic pulses based on the described interaction. It is also important that acousto-optic interaction do not influence the propagation of an acoustic wave when non-linear effects do not occur.

Therefore, parameters of the acoustic wave are not changed by the measuring process. A practically linear dependence between the angle of diffraction and frequency of investigated acoustic wave which causes diffraction is another facilitation. Limitations of the method result from inaccuracies of measurements of the angular distribution of the diffracted wave's intensity and from the limited width of the frequency band, related with conditions (13). This band depends also on the chosen geometry of the interaction range and on acoustic and acousto-optic properties of the medium.

References

[1] E. HÄUSLER, W. G. MAYER, G. SCHWARTZ, *Light diffraction by ultrasonic pulses*, Acoust. Lett. **4**, 180–194 (1981).

[2] T. H. NEIGHBORS, W. G. MAYER, *Asymmetric light diffraction by pulsed ultrasonic waves*, J. Acoust. Soc. Am. **74**, 146–152 (1983).

[3] R. N. ZITTER, *Ultrasonic diffraction of light by short acoustic pulses*, J. Acoust. Soc. Am., **43**, 864–870 (1968).

[4] R. W. DAMON, W. T. MALONEY, D. H. Mc MAHON in: *Физическая акустика*, [Ed.] W. P. Mason, R. N. Thurston, tom 7, Mir, Moskwa 1974, 327–336.

[5] L. JAKAB, P. RICHTER, *Spectrum analyzer with acousto-optic Bragg cell*, Proc. 3rd Spring School on Acousto-optics and Applications, Wieżyca, Gdańsk 1986, 106–112.

[6] E. MARKIEWICZ, *Some numerical results for light diffraction on ultrasonic pulses*, Proc. 3rd Spring School on Acousto-optics and Applications, Wieżyca, Gdańsk 1986, 34–45.

[7] W. G. MAYER, T. H. NEIGHBORS, *Acusto-optic interactions by pulsed ultrasound*, Proc. 3rd Spring School on Acousto-optics and Applications, Wieżyca, Gdańsk 1986, 8–21.

Received on June 16, 1987, revised version on April 6, 1988.

ARCHIVES OF ACOUSTICS
14, 1-2, 11-27 (1989)

AN EXPERIMENTAL LITHOTRIPSY SYSTEM FOR THE STUDY OF SHOCK WAVE EFFECTS

LESZEK FILIPCZYŃSKI, JERZY ETIENNE, ANNA GRABOWSKA, TOMASZ WASZCZUK

Institute of Fundamental Technological Research, Polish Academy of Sciences
(00–049 Warszawa, ul. Świętokrzyska 21)

HENRYK KOWALSKI

Department of Biophysics Medical Academy, Warsaw, Chałubińskiego 5

MICHAŁ GRYZIŃSKI, JACEK STANISŁAWSKI

Institute of Nuclear Problems, Świerk

The authors have developed a lithotripsy system and measurement set-up for the study of shock wave interaction with living tissues. The system consists of an electromagnetical shock wave generator, focusing lens and capacitance pressure pulse measuring hydrophones. The shock wave pulse pressures obtained with this system can be changed up to 40 MPa (about 400 atm). An additional ultrasonic system enables measurements of the gas bubbles generation, an important factor in the destruction process caused by cavitation. Details of the system concerning the shock wave generation, pressure field distribution, pressure time dependence and measurement technique as well as its practical application possibilities are discussed in the paper.

Autorzy opracowali system litotrypsera i układy pomiarowe dla badań oddziaływania fal uderzeniowych z żywymi tkankami. System złożony jest z elektromagnetycznego generatora fal uderzeniowych, ogniskującej soczewki i hydrofonów pojemnościowych umożliwiających bezwzględne pomiary impulsów ciśnienia.

Ciśnienia uzyskiwane za pomocą opracowanego systemu mogą osiągać wartości aż do 40 MPa (około 400 atm.). Dodatkowy układ ultradźwiękowy pozwala na pomiary generacji pęcherzyków powietrza, które są istotnym czynnikiem w procesie niszczenia tkanek powodowanym przez kawitację. Szczegóły systemu generacji fal uderzeniowych, rozkładów pól ciśnienia, zależności ciśnienia od czasu, technika pomiarowa oraz praktyczne możliwości zastosowania systemu przedyskutowano w artykule.

Introduction

Lithotripsy is becoming nowadays an important therapeutical means in the work of many urological clinical centers. However, as it is a relatively new method, mechanisms of shock wave interaction with living tissues are far from being known. Many important practical problems have to be solved, especially those connected with the dosage of this powerful technique. For the study of these problems the authors have developed a lithotripsy system and a pressure pulse measurement method.

1. The shock wave generator

The elaborated system consists of an Eisenmenger (electromagnetic) shock generator [8] with a focusing lens [18]. Figure 1 presents the idea of the system. The condenser C is charged through the rectifier D to a voltage which can be changed

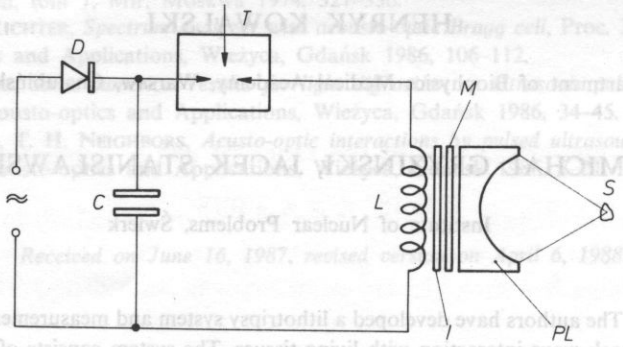

FIG. 1. The idea of the experimental lithotrypsy system

from $U_0 = 17$ to 25 kV. Then it is discharged through a plane coil L with a repetition rate about 1 Hz. The coil is coupled through an isolating plastic foil I with the metal membrane M. The high amplitude current pulse generates eddy currents in the membrane. In this way a strong magnetic field is induced which causes a force pressing the membrane in the opposite direction to the coil L. The membrane M is coupled acoustically with a plastic focusing lens PL. In this way a plane wave generated by the membrane is focused at the kidney stone S.

Figure 2 presents the shape of the high voltage pulse U and the shape of the current pulse I. The frequency of the oscillations equals 98 kHz and the current amplitude is equal to 10 kA.

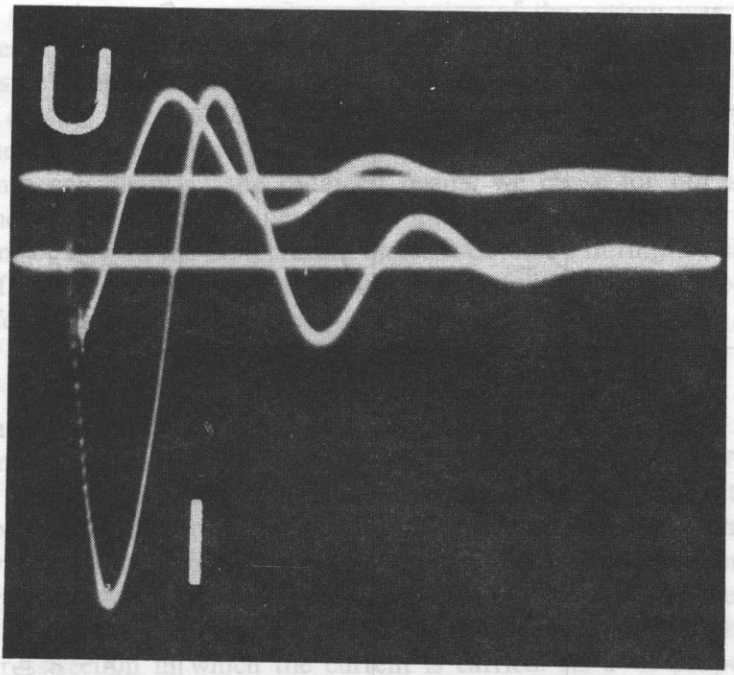

FIG. 2. Shapes of the high voltage U and current I flowing in the coil

The diameter of the plane coil equals 140 mm. To obtain a high electric coupling with the metal membrane, the coil was composed of four parallel windings of the copper wire 0.6 mm in diameter. The number of turns was equal to 4×27. The diameter of the wire was chosen taking into consideration the skin effect. The depth of the skin effect layer [20]

$$\varepsilon^E = \frac{1}{2\pi}\sqrt{\frac{\varrho^E \cdot 10^9}{\mu f}}\,[\mathrm{cm}] \underset{\mathrm{Cu},20^\circ\mathrm{C}}{=} 6.62/\sqrt{f}\ \ [\mathrm{cm}] \tag{1}$$

equals 0.2 mm for copper when $f = 100$ kHz, ϱ^E denotes here the resistivity in Ω cm, f – frequency in Hz, $\mu = 1$ is permeability for copper and aluminium.

In this way, using four instead of one winding, it was possible to decrease the distance between the current carried by the wire cross-section and the metal membrane.

The distance between the coil and the membrane, depending on the thickness of the insulating foil, was the next factor limiting the electrical coupling between the coil and the membrane. Polycarbonate foil Makrofil N (Beyer AG) was used as insulating material. Figure 3 shows the acoustic pressure in the form of our system as the function of the thickness of the insulating foil. For reasons of electric strength we chose a foil thickness ranging from 0.3 to 0.4 mm.

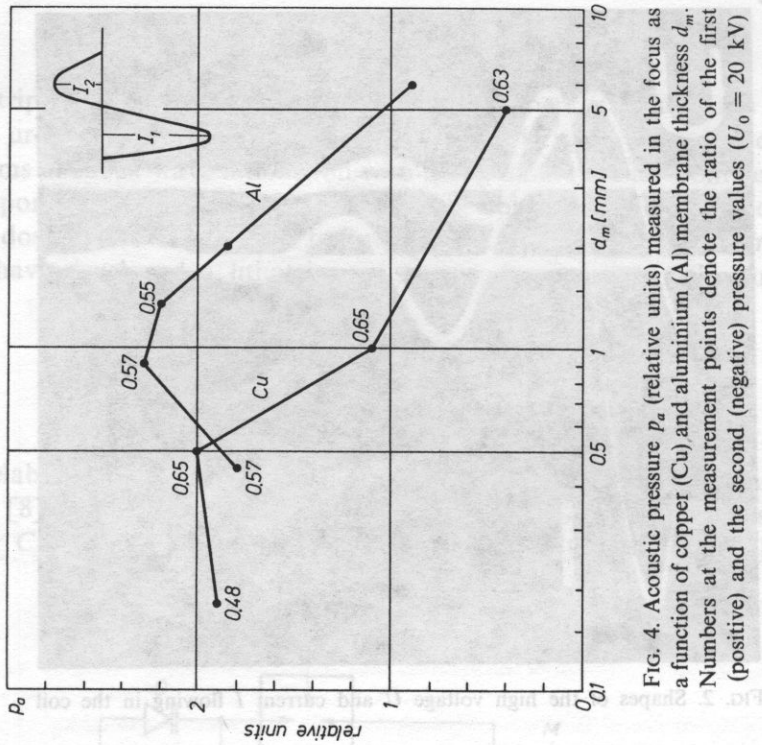

FIG. 4. Acoustic pressure p_a (relative units) measured in the focus as a function of copper (Cu) and aluminium (Al) membrane thickness d_m. Numbers at the measurement points denote the ratio of the first (positive) and the second (negative) pressure values ($U_0 = 20$ kV)

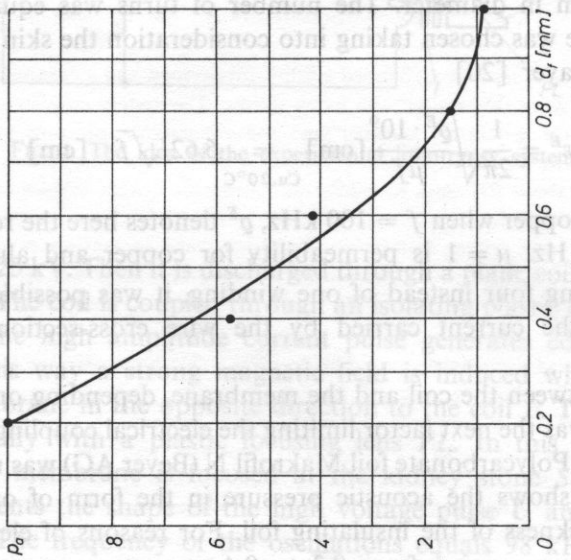

FIG. 3. Acoustic pressure p_a (relative units) measured in the focus as a function of the insulating foil thickenss d_f ($U_0 = 20$ kV)

The next experiment necessary for optimization of the system was performed with two types of membranes made of copper and aluminium. Figure 4 presents the acoustic pressure obtained in the focus as the function of the membrane thickness. It is difficult to explain this result depending on electrical and acoustical properties of the membranes as well as on electrical and acoustical conditions in which they work.

Taking into consideration the obtained results we chose for our system the aluminium membrane with a thickness of 1.35 mm. Aluminium shows an advantage from the point of view of the temperature increase observed during the shock wave generation. If the membrane diameter is constant, the following expression seems to be decisive for temperature changes:

$$CP = (c_w \varrho d)(\lambda d)/\sqrt{\varrho^E}, \tag{2}$$

where c_w denotes specific heat, d optimum thickness of the membrane, ϱ its density, λ coefficient of thermal conductivity. The product in the first brackets is proportional to the heat necessary to increase of the membrane, the product in the second brackets is proportional to the heat flowing toward a cooling brass ring, coupled mechanically with the membrane at its circumference. The last term in the denominator corresponds to electrical losses which depend on the electrical resistivity ϱ^E and on the skin depth ε^E. The value of ε^E determines the thickness of the membrane cross-section in which the current is carried. As ε^E is proportional to $\sqrt{\varrho^E}$ (see Eq. (1)), one obtains in the result the form given in Eq. (2).

The higher the value of CP, the lower the temperature increase during the shock wave generation. Inserting into Eq. (2) the corresponding coefficients [13] and optimum values of aluminium and copper membrane thickness, one obtain the ratio $CP_{AL}/CP_{Cu} \approx 3$. It shows that the increase of temperature will be smaller in the case of the aluminium membrane. Equation (2) is approximative as it does not take into account the influence of the membrane electrical resistance on the generated pressure value. However, Fig. 4 shows that the maximum measured pressure difference for copper and aluminium membranes is not higher than 15%.

2. The pressure field

The wave produced by the metal membrane becomes distorted as it travels throught the medium. In some distance called critical distance [2] the slope of the pulse front becomes infinite, i.e., a discontinuity appears in the wave. The critical distance for a plane wave equals [17]

$$x = \sigma/\beta\varepsilon k \tag{3}$$

where $\beta = 1 + B/2A$, B/A – ratio of nonlinearity parameters (for water $B/A = 5.4$ [2], for various soft tissues $B/A = 5.5$–11 [7]), c_0 – wave velocity for small amplitudes, $\varepsilon = u_0/c_0$ – acoustical Mach number, $u_0 = p/\varrho c_0$ – particle velocity at

the wave source, p – wave pressure, σ – shock parameter, $k = 2\pi f/c_0$, f – frequency of the wave.

One should take into account the fact that the wave frequency is in our case two times greater than the frequency of the electric current in the coil shown in Fig. 1. This is caused by the square dependence of the generated pressure p, on the current I carried by the coil [8]

$$p \doteq I^2. \tag{4}$$

This was confirmed by measurements of the half period time $T/2 = 2.6$ μs near the pressure source (see Fig. 7) which corresponds to the frequency of 198 kHz.

Equation (3) can be transformed to the following expression used sometimes in the literature:

$$x = c_0\sigma\left[(1+B/2A)\frac{p}{\varrho c_0}\frac{1}{c_0}2\pi f\right]^{-1} = \varrho c_0^3\sigma T[\pi(2+B/A)p]^{-1} = \varrho c_0^3\sigma[\pi(2+B/A)pf]^{-1}. \tag{5}$$

In the case of a focused wave, generated by a concave transducer, the critical is shifted by the distance [17]

$$\Delta X = Z_0\exp(-x/z_0) \tag{6}$$

toward the transducer, z_0 denotes its focal length.

The focus should be situated near the critical distance to obtain the maximum slope and, simultaneously, the maximum amplitude of the pressure pulse. According to the paper [1], for shock parameters $1.6 > \sigma \geqslant 1$ one does not observe any significant decrease of the pulse amplitude and the front slope.

Assuming the pressure in focus equal to $p' = 20$ MPa and the gain (in linear approximation) of the lens [19]

$$\frac{p'}{p} = \frac{kr^2}{2z_0} = 10, \tag{7}$$

where $k = 2\pi f/c_0$, one obtains for shock parameters $\sigma = 1.6$ and 1, for focal length $z_0 = 20$ cm, radius of the lens $r = 7$ cm, frequency $f = 198$ kHz, from Eqs. (5) and (6) the shift of the focus relatively to the critical distance. It is equal to $x = 1$ cm and 3 cm, respectively. These values seem to be acceptable since the – 6 dB drop of the pressure along the lens axis occurs in the distance of 4 cm before the focus (see Fig. 7).

To estimate the influence of the focusing lens on the pressure distribution and on its maximum value, we applied the linear theory and the continuous wave

approximation, neglecting the attenuation and internal reflections in our 1 cm thick perspex lens. However, we took into account transmission depending on acoustical parameters of the two media and on the incident angle of the acoustical rays. The transmission coefficient was determined from Eq. [14]:

$$D_{l/l} = \frac{2}{N} \frac{\varrho_W c_W \cos\alpha_L \cos 2\alpha_T}{\varrho_L c_L \cos\alpha_W}, \tag{8}$$

where

$$N = \left(\frac{c_T}{c_L}\right)^2 \sin\alpha_L \sin 2\alpha_T + \cos^2 2\alpha_T + \frac{\varrho_W c_W}{\varrho_L c_L} \frac{\cos\alpha_L}{\cos\alpha_W} \tag{9}$$

ϱ_L, ϱ_W denote, respectively, the density of lens and water, c_L, c_T – velocity of longitudinal and transverse waves in lens, c_W – wave velocity in water, α_L – incident angle of longitudinal wave, α_T – reflection angle of the transverse wave in lens, α_W refraction angle of the wave in water.

The calculated values of D as the function incident angle α_L is shown in Fig. 5.

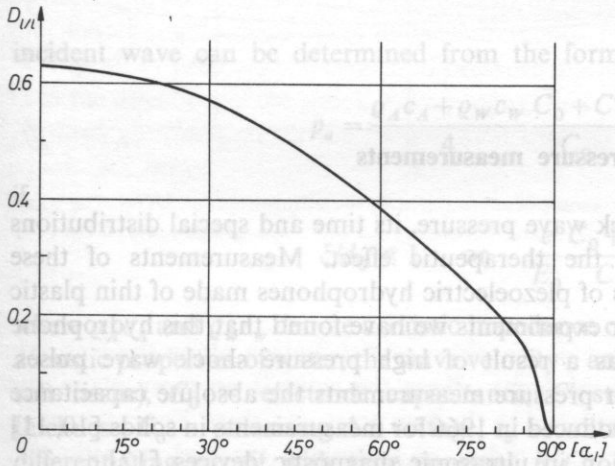

FIG. 5. Transmission coefficient $D_{L/l}$ on the concave boundary perspex water of the lens. α_L – incident angle of the longitudinal wave

Basing on the paper [19], the axial distribution of the pressure could be computed for the spherical lens taking into account the transmission loss on this concave boundary. The maximum pressure and the focal length depend strongly on the frequency as shown in Fig. 6. Hence one can conclude that the sharper the shock wave pulse, the higher the gain of the lens.

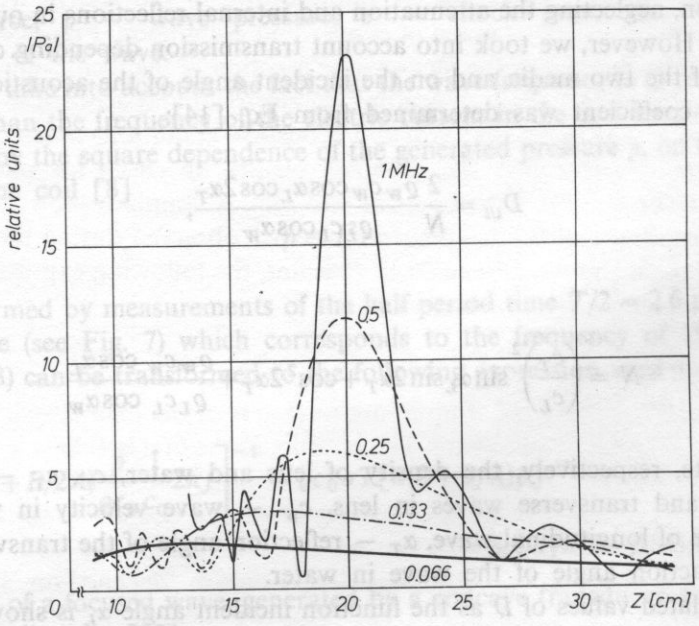

FIG. 6. Pressure distribution along the lens axis computed for various frequencies of the continuous wave. p — axial pressure in relation to the pressure on the plane lens surface (linear approximation)

3. Pressure measurements

The value of the acoustic shock wave pressure, its time and special distributions are very important factors for the therapeutic effect. Measurements of these parameters are possible by means of piezoelectric hydrophones made of thin plastic layer PVDF. However during our experiments we have found that this hydrophone was distroyed in a short time as a result of high pressure shock wave pulses. Therefore we decided to adapt for pressure measurements the absolute capacitance transducer method which was introduced in 1966 for measurements in solids [10, 11] and then for dosage determination in ultrasonic diagnostic devices [12].

The idea of this hydrophone is shown in Fig. 7. The ultrasonic pulse P penetrates the boundary water-metal plate and then it is totally reflected from the second boundary between the metal plate and air. Vibrations of this boundary change the capacitance C_0 which is formed by the second metal boundary and the electrode. The electrode is polarized with the d.c. voltage E_0 through a high value resistance R. In this way the electric charge in the capacitance C_0 remains constant while its value changes due to boundary vibrations. Hence the electric voltage on the capacitance C_0 changes, too, giving the output signal e. It is easy to show that the pressure of the

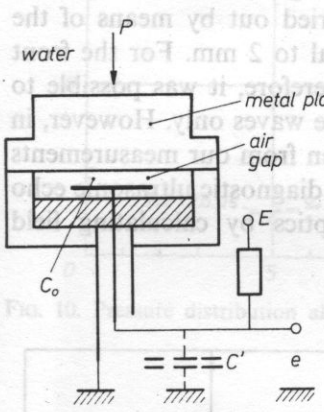

FIG. 7. Capacitance hydrophone

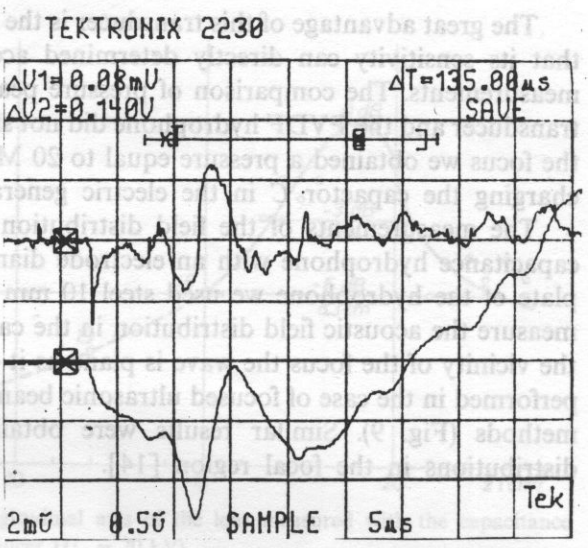

FIG. 8. Particle velocity $u \div de/dt$ (uper curve) and displacement $\xi \div e$ lower curve measured by means of the capacitance transducer (reversed polarization)

incident wave can be determined from the formula

$$p_a = \frac{\varrho_A c_A + \varrho_W c_W}{4} \frac{C_0 + C'}{C_0} \frac{d_0}{E_0} \frac{e_d}{R_d C_d} \tag{10}$$

if

$$\xi/d_0 \ll 1 \quad \text{or} \quad \frac{e}{E_0} \frac{C_0 + C'}{C_0} \ll 1, \tag{11a, b}$$

where $\varrho_A c_A$ and $\varrho_w c_w$ denote acoustic impedance of the metal plate and of water (the acoustic properties of water, the wave velocity c and density ϱ are almost the same as soft tissue), C_0 – electrode capacitance, C' stray capacitances, d_0 – air gap thickness, E_0 – polarizing d.c. voltage, e_d – voltage on the output of an additional differentiating circuit with time constant $R_d C_d$, ξ – displacement.

Figure 8 presents a typical result of measurements with the capacitance hydrophone recorded on the plotter. The lower curve is the signal e on the transducer output before differentiation. It is proportional to the displacement of ξ the medium particles. Important are the first 2 microseconds after the initial pulse. Later one obtains many internal reflections inside the transducer which form a complicated pattern due to interferences. The upper curve shows the same signal after diffraction. It represents the velocity u of the medium particles and after multiplication by the parameters shown in Eq. 7 it is equal to this pressure.

The great advantage of this transducer is the linearity of its metal [9] and the fact that its sensitivity can directly determined according to Eq. (11) from electrical measurements. The comparison of pressure peak values obtained by means of this transducer and the PVDF hydrophone did not show a difference greater than 3%. In the focus we obtained a pressure equal to 20 MPa for the d.c. voltage U_0 of 20 kV charging the capactor C in the electric generator (see Fig. 1).

The measurements of the field distribution were carried out by means of the capacitance hydrophone with an electrode diameter equal to 2 mm. For the front plate of the hydrophone we used steel 10 mm thick. Therefore, it was possible to measure the acoustic field distribution in the case of plane waves only. However, in the vicinity of the focus the wave is plane as it can be seen from our measurements performed in the case of focused ultrasonic beams used in diagnostic ultrasonic echo methods (Fig. 9). Similar results were obtained in optics by calculating field distributions in the focal region [14].

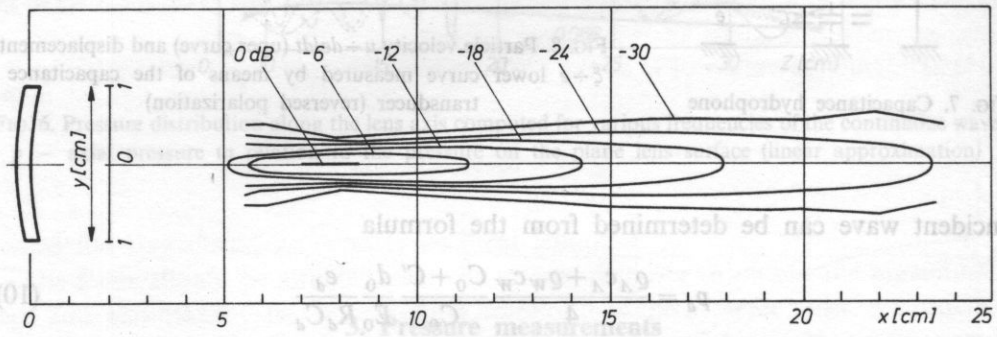

FIG. 9. Iso-echo-amplitude curves of the ultrasonic beam radiated by the ultrasonograph UG-4. The y axis is 2 times englarged when compared with the x-axis. Frequency 2.5 MHz, transducer radius 1 cm [12]

The results of our measurement of the pressure distribution along the lens axis are shown in Fig. 10. Outside of the focus, where the wave is no more plane, the measurement results may not correspond to the true pressure values. For instance, in the distance of 5 cm for the electrode radius of 1 mm the external acoustic ray, coming from the lens, will be shifted by 0.25 mm passing the aluminium plate. This may cause an error which decreases with the distance. Therefore the dotted line in Fig. 10 representing the pressure distribution measured along the longitudinal axis is an approximative one. The length of the focus measured on the $-$ 6 dB level is equal to 8.3 cm.

The numbers at the measurement points denote the duration time of the first half period of the propagation pulse. At the distance of 5 cm it was equal to 2.6 μs corresponding to the frequency of 198 kHz. With the distance the pulse became

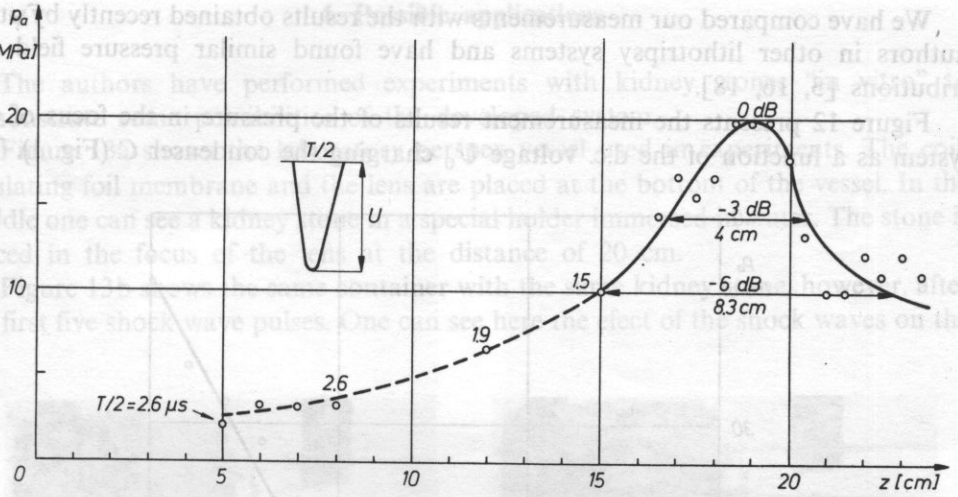

FIG. 10. Pressure distribution along the longitudinal axis of the lens measured with the capacitance transducer ($U_0 = 20$ kV)

distorted and we measured in this case the duration time between the first zero crossing points. In the focus it was equal to 0.3 μs and the rise time – 50 ns. However, in fact the rise time may be shorter since this was the sampling period of the digital oscilloscope used in measurements.

Figure 11 presents the measured pressure distribution in the focus perpendicularly to the direction of the shock wave propagation. The focus in this direction is about 10 times shorter than in the longitudinal one. Its width measured on the – 6 dB equals 8.5 mm.

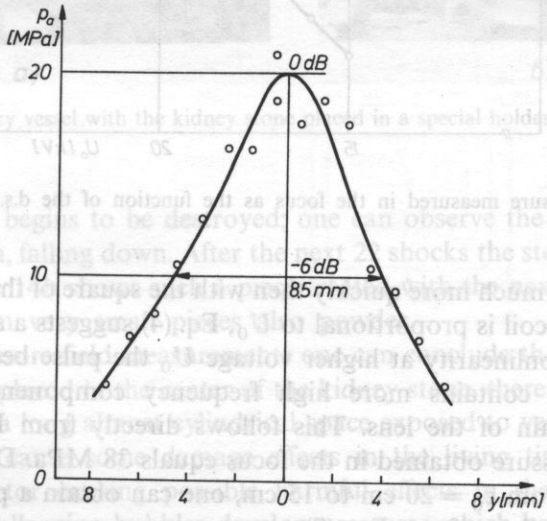

FIG. 11. Pressure distribution in the focal plane ($U_0 = 20$ kV)

We have compared our measurements with the results obtained recently by other authors in other lithotripsy systems and have found similar pressure field distributions [3, 16, 18].

Figure 12 presents the measurement results of the pressure in the focus of our system as a function of the d.c. voltage U_0 charging the condenser C (Fig. 1). The

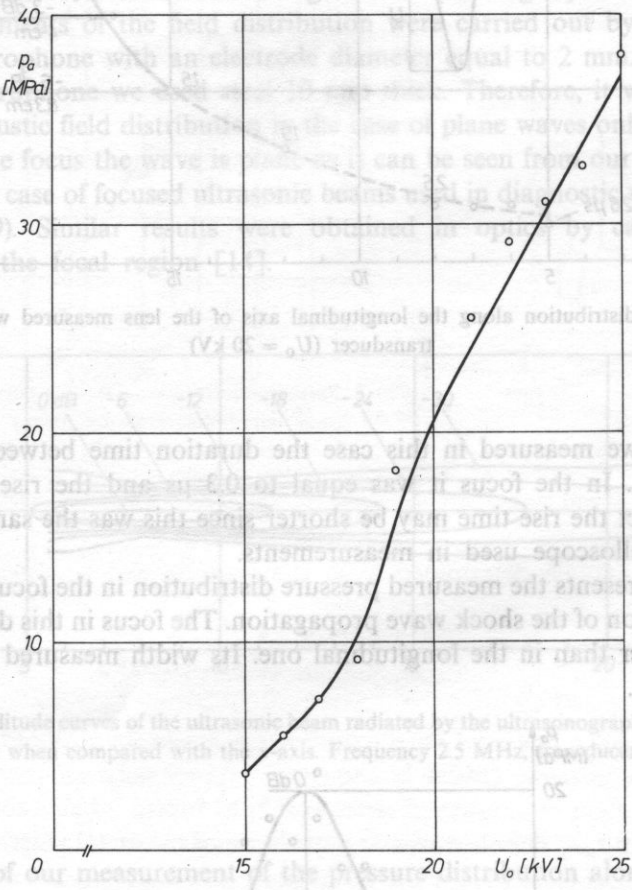

FIG. 12. Pressure measured in the focus as the function of the d.s. voltage U_0

pressure p increases much more quickly then with the square of the voltage U_0. Since the current I in the coil is proportional to U_0, Eq. (4) suggests a square dependence. However, due to nonlinearity at higher voltage U_0 the pulse becomes sharper and then the spectrum contains more high frequency components thus increasing considerably the gain of the lens. This follows directly from Fig. 6.

The highest pressure obtained in the focus equals 38 MPa. Decreasing the focal length of the lens from $z_0 = 20$ cm to 15 cm, one can obtain a pressure increase of about 10% as it follows from Eq. (7).

4. Possible applications

The authors have performed experiments with kidney stones "in vitro" to demonstrate some possibilities of the developed system.

Figure 13a shows the laboratory perspex vessel used in experiments. The coil, insulating foil membrane and the lens are placed at the bottom of the vessel. In the middle one can see a kidney stone in a special holder immersed in water. The stone is placed in the focus of the lens at the distance of 20 cm.

Figure 13b shows the same container with the same kidney stone, however, after the first five shock wave pulses. One can see here the efect of the shock waves on the

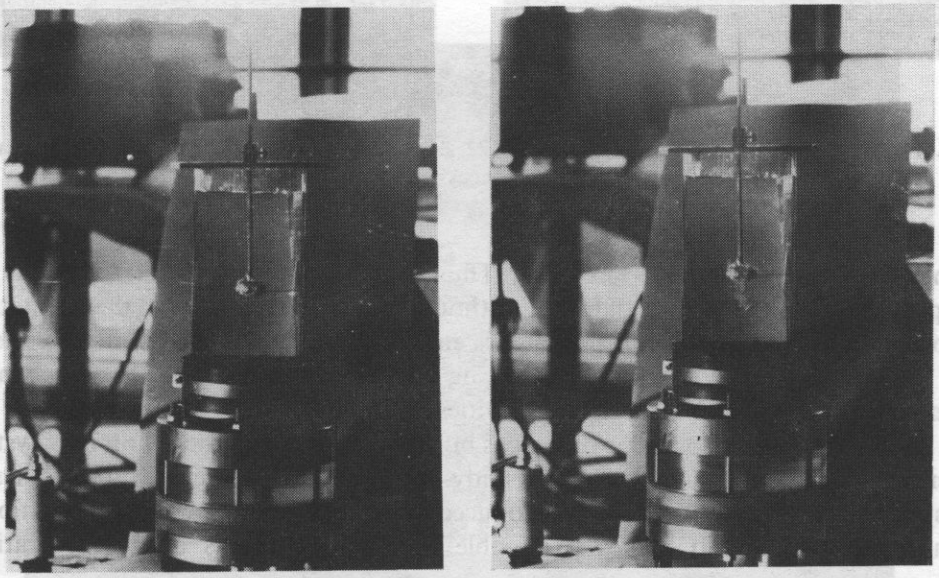

FIG. 13. The laboratory vessel with the kidney stone placed in a special holder (a) and after 5 shocks (b)

stone. The stone begins to be destroyed; one can observe the powder of the stone, caused by erosion, falling down. After the next 22 shocks the stone breaks into pieces (Fig. 14a). Figure 14b shows such a piece treated with the next 25 shocks. One can notice apart from very small pieces also powder.

From the pressure field measurements one can conclude that even if the focus of the lithotripsy is placed in the center of the kidney stone, there will be in the kidney, before the stone, a long almost cylindrical space exposed to very high pressures (see Fig. 10). It may cause some damage effects in the living tissues.

The main factor causing possible harmful effects in the tissue seems to be cavitation. The collapsing bubbles develop pressures which have been measured to

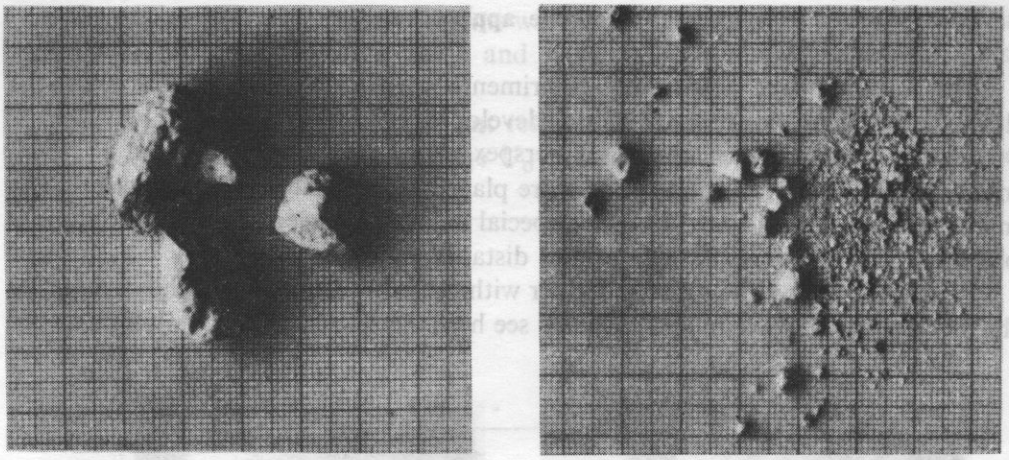

FIG. 14. The disintegrated stone after the next 22 shocks (a), one piece of the stone after the next 25 shocks (b)

achieve values as high as 300 MPa. Thus cavitation must be considered as an important factor in tissue damage. Although the total energy of the cavitation process is small, the concentration of this energy into a very small volume results in an enormous energy density, producing such very high pressures and high temperatures within the collapsing cavities [4].

In this situation knowledge of the gas bubble generation in the lithotrypsy system seems to be very important for the study of the possible damage process in soft tissues. For this purpose we have introduced into the described system an additional echoscope (Fig. 15). It makes it possible to observe the gas bubble generation,

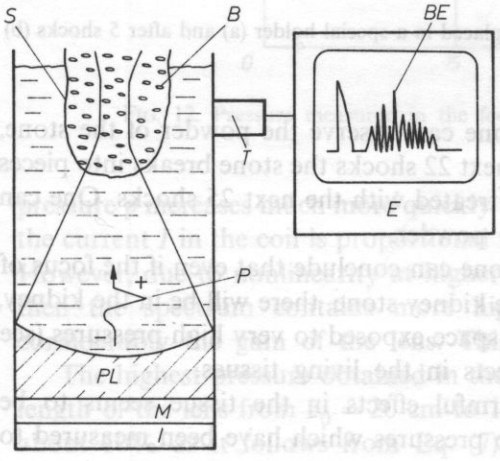

FIG. 15. The system for the gas bubble study. S – tested space, S – tested space with gas bubbles or with biological specimen, B – gas bubble, BE – bubble echoes, T – transducer, E – echoscope, P – pressure pulse, PL – plastic lens, M – membrane, I – insulating sheet

measurements of their life time to observe their growth and collapse under the action of shock wave pulses and to determine their density and size, if possible. Figure 16 presents as an example an echogram of gas bubbles were generated in water by the shock wave pulse of 20 MPa pressure.

There is of course the question whether cavitation can exist "in vivo" in the case of very short stress pulses and if it can produce damage to the living tissue. Recently, it has been demonstrated that the shock wave pulses used in lithotripsy can really produce "in vivo" acoustic cavitation in the blood vessels of pigs [5]. Also haemorrhages in all kidney structures in dogs could be shown [6]. Thus changes were dose-dependent.

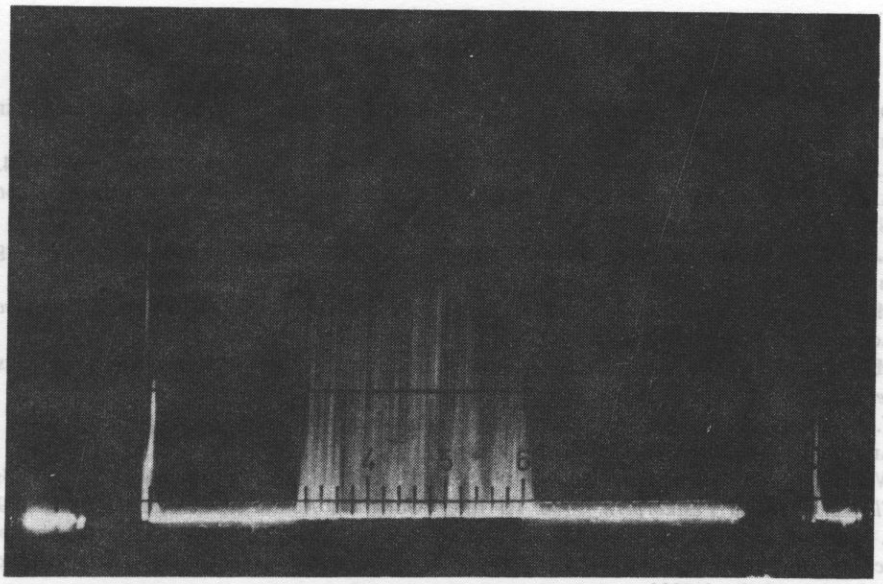

FIG. 16. Echogram of gas bubbles generated by the shock wave pulse of 20 MPa pressure. Transducer frequency — 3 MHz

In this situation one can conclude that it is important and necessary to study all the biological effects which are caused by high pressure shock wave pulses in tissues. Only by collecting many experimental data from this type of research can one elaborate dosage rules. It is necessary to answer the question what is the highest permitted pressure value, its duration time, its shape, positive and negative components, repetition period, therapy time and other factors to eliminate or to decrease the possible harmful effects in the patients treated with this powerful new therapy technique.

5. Conclusions

The developed system can be used for the study of biological effects caused by shock waves at high pressures. The values of pressures and their spatial distributions and time dependence correspond with those used in lithotripsy. This could be confirmed experimentally by destroying several kidney stones "in vitro" too. Thus the described system after some adaptations can be used as the main part of a lithotripter for clinical applications.

The applied capacitance hydrophones were verified experimentally in shock wave measurements at very high pulse pressure levels with no sign of any serious damage.

References

[1] D. BACON, *Finite amplitude distortion of the fields used in diagnostic ultrasound*, Ultrasound in Med. and Biol., **10**, 1, 189–195 (1984).

[2] R. T. BAYER, *Nonlinear acoustics*, U.S. Naval Sea Systems Command. Washington 1974.

[3] A. COLEMAN et al., *Pressure waveforms generated by a Dornier extra corporal shock-wave lithotrypter*. Ultrasound in Med and Biol, **13**, 561–657 (1987).

[4] L. A. CRUM, Cavitation microprojects as a contributory mechanisms for renal calculi desintegration in ESWL. Journal of Urology (1988) [in print].

[5] M. DELIUS, I. EIZENHOFER, R. DENK, H. LEIBICH, W. BRENDEL, *Biological effects of shock waves*, J. Acoust. Soc. Am., Suplement S XX (1988).

[6] M. DELIUS et al, *Biological effects of shock waves: Kidney damage by shock waves in dogs. Dose dependence*. Ultrasound in Med. and Biol. **14**, 117–122 (1988).

[7] F. DUNN, W. K. LAW, L. A. FRIZELL, *The ultrasonic nonlinearity parameter for biological media*, Archives of Acoustics, **9**, 1–2, 29–34 (1984).

[8] W. EISENMENGER, *Eine elektromagnetische Impulsschallquelle zur Erzeugung von Druckstössen in Flussigkeiten und Festkorpern*. Proc. III Inter. Cong. on Acoustics, Stuttgart 326–329 (1959).

[9] J. ETIENNE, L. FILIPCZYŃSKI, A. GRABOWSKA, T. WASZCZUK, *Pressure measurements in nonlinear acoustics by means of capacitance and PVDF hydrophones*, Proc. XXXV Open Seminar Acoustics, Białowieża, Poland 1988.

[10] L. FILIPCZYŃSKI, *Measuring pulse intensity of ultrasonic longitudinal and transverse waves in solids*, Proc. Vibration Problems, **7**, 1, 31–46 (1966).

[11] L. FILIPCZYŃSKI, *Absolute measurements of particle velocity displacement or intensity of ultrasonic pulses in liquids and solids*, Acoustics, **21**, 173–180 (1969).

[12] L. FILIPCZYŃSKI, G. ŁYPACEWICZ, J. SAŁKOWSKI, *Intensity determination of the inside of the abdomen by means of ultrasonics*, Proc. Vibration Problems, **7**, 3, 211–220 (1966).

[13] R. GRIMSEHL, R. TOMASCHEK, *Lehrbuch der Physik*, Bd. I p. 590, 658, Bd. II p. 197, 198.

[14] J. H. KRAUTKRÄHER, *Werkstoffprufung mit Ultrasschall*, Springer-Berlin 1961, p. 473 also Ultrasonic Testing Materials, Springer, Berlin 1983 p. 607.

[15] E. LINFOOT, E. WOLF, *Phase distribution near focus in an abberation free diffraction image*. Proc. Phys. Soc. B, **69**, 823–832 (1956).

[16] J. MESTAS, *Generation et focalization d'une onde de choc en vue de la destruction transparentale des calculs*, Int. National des Sciences Appliques. Lyon Doctor Thesis 1982.

[17] T. MUIR, L. CARSTENSEN, *Prediction of nonlinear acoustic effects at biomedical frequencies and intensities*, Ultrasound in Med. and Biol. **6**, 4, 345–357 (1980).

[18] H. REICHENBERG, G. NASER, *Electromagnetic acoustic source for the extracorporal generation of shock waves in lithotrypsy*, Siemens Forschung und Entwielungs Berichte **15**, 187–194 (1986).
[19] U. SCHLENGERMANN, *Schallfeldausbildungs bei ebenen Ultraschallquellen mit fokusierenden Linsen*, Acoustics, **30**, 6, 291–300 (1974).
[20] F. E. TERMAN, *Radio Engineers Handbook*, McGraw Hill, New York 1943, p. 34.

Received on 8 November, 1988.

ARCHIVES OF ACOUSTICS
14, 1-2, 29-43 (1989)

ACOUSTICAL SHADOW OF A SPHERE IMMERSED IN WATER. I

LESZEK FILIPCZYŃSKI, TAMARA KUJAWSKA

Department of Ultrasonics, Institute of Fundamental Technological Research,
Polish Academy of Sciences

(00-049 Warszawa, ul. Świętokrzyska 21)

In this study the acoustical field behind a rigid sphere is determined for the incidence of a plane harmonic wave on it. This field was determined as the sum of acoustic pressures of the wave incident on the sphere and reflected from it. Formulae describing the reflected wave pressure given in different form by American, Japanese and Soviet acousticians, were compared and their identity demonstrated. It was shown, that these formulae, though valid for fixed spheres, can in practical hydroacoustic cases be also used for movable spheres. On this basis directional characteristics of the shadow behind the sphere were determined for the values of $ka = 100\pi$, 40π, 20π and 8π, which are essential for hydroacoustic problems and for ultrasonic medical diagnostics. These characteristics were determined for distances falling between 10 a and 100 a, where a denotes the radius of the sphere. Moreover, the shape of directional characteristics was interpreted and the ranges of the shadow were determined for different values of ka.

W pracy wyznaczono pole akustyczne za sztywną kulą, powstające w stanie ustalonym przy padaniu na nią płaskiej fali harmonicznej. Pole to wyznaczono jako sumę ciśnienia fali padającej na kulę i ciśnienia fali od niej odbitej. Porównano wzory opisujące pole ciśnienia fali odbitej, podane w różnych postaciach przez akustyków amerykańskich, japońskich i radzieckich wykazując ich identyczność. Pokazano, że wzory te, choć słuszne dla kul nieruchomych, mogą w praktycznych przypadkach hydroakustyki być również stosowane dla kul swobodnych. Na tej podstawie wyznaczono charakterystyki kierunkowe cienia za kulą dla iloczynów liczby falowej k i promienia kuli a, $ka = 100\pi$, 40π 20π i 8π, istotnych w problematyce hydroakustycznej i ultradźwiękowej diagnostyce medycznej. Charakterystyki te, zmieniające się w zależności od odległości za kulą wyznaczono dla odległości zawartych w granicach od 10 a do 1000 a z krokiem kątowym równym 1°, 0,2° lub 0,05°. Podano przy tym interpretację kształtu tych charakterystyk oraz wyznaczono zasięgi strefy cienia dla różnych wartości ka.

1. Introduction

The problem of acoustical shadow behind solid bodies is essential for many questions of the ultrasonic technique, in particular for hydroacoustics and medical diagnostics. In the literature, many studies were devoted to wave reflection from

solid bodies, such as sphere, cylinder etc. On the other hand, the authors did not come across studies related to analysis of the shadow forming behind such solid bodies.

The object of the study is the acoustical shadow forming in the steady state behind a rigid sphere immersed in water. The obtained results can be also generalized to soft tissues since they contain more than 70% of water in their composition and their acoustical parameters are very close to those of water. The previous rather preliminary, studies by the authors [3] showed that the shadow characteristics for rigid and elastic spheres resemble each other. It was assumed, therefore, that the considered spheres are rigid. The computer time necessary for the determination of the shadow behind an elastic sphere is much longer than in the case of a rigid sphere. Moreover, this applies to homogeneous and isotropic elastic spheres, and after all, in hydrolocation practice or in medical diagnostics the inner structure of solid bodies is very complex and unknown *a priori*.

2. Wave reflection from fixed and free movable spheres

Considering the ultrasonic wave reflection from a sphere, it is necessary to distinguish between two cases: the case of a movable sphere, which can freely move in water, and that of a fixed sphere. In real sea conditions, spherical objects can be free, i.e., moving under the effect of the incident wave. This case can be considered on the basis of the result of study [9].

Between the amplitude of the harmonic plane wave of the acoustic pressure p_i incident on the sphere and the amplitude of the wave p_r reflected from the sphere, there is a relation which takes the following form for a distance which is large compares with the sphere radius and the wave-length [8]

$$p_r = \frac{a}{2r} f_\infty(ka) p_i \tag{1}$$

where a is the sphere radius, $k = \omega/c$, c is the wave velocity in water, r is the distance from its centre. The function $f_\infty(ka)$ is called the form function and depends in general on mechanical parameters of the sphere and the ambient medium. Using the complex formulae given in papers [8] and [7] it is possible to determine the function $f_\infty(ka)$ for both rigid and elastic spheres. However, the theory and the formulae derived on its grounds apply only to fixed spheres.

The above-mentioned authors [9] introduced a correction to the function $f_\infty(ka)$ which permits the use of Eq. (1) for rigid movable spheres too. Then, for movable spheres there is the modified form function in the form

$$f_\infty^M(ka) = f_\infty(ka) + \Delta f_\infty(ka), \tag{2}$$

where

$$\Delta f_\infty(ka) = \frac{6j}{ka}\left[\frac{\xi ka j_1'(ka) - j_1(ka)}{\xi ka h_1^{(2)\prime}(ka) - h_1^{(2)}(ka)} - \frac{j_1'(ka)}{h_1^{(2)\prime}(ka)}\right], \tag{3}$$

j_1 and j_1' are the spherical Bessel function of the first order and its derivative with respect to the argument. $h_1^{(2)}$ and $h_1^{(2)\prime}$ are spherical Hankel functions of the second kind, of the first order and its derivative with respect to the argument, $j = \sqrt{-1}$, ξ is the density ratio between the sphere and the ambient liquid.

Fig. 1 shows the modified shape function (modulus) calculated by the authors for a free movable sphere with density $\xi = 7.7$ g/cm^3 steel and for a fixed rigid sphere (curve R). The curve R does not depend on the density of the sphere.

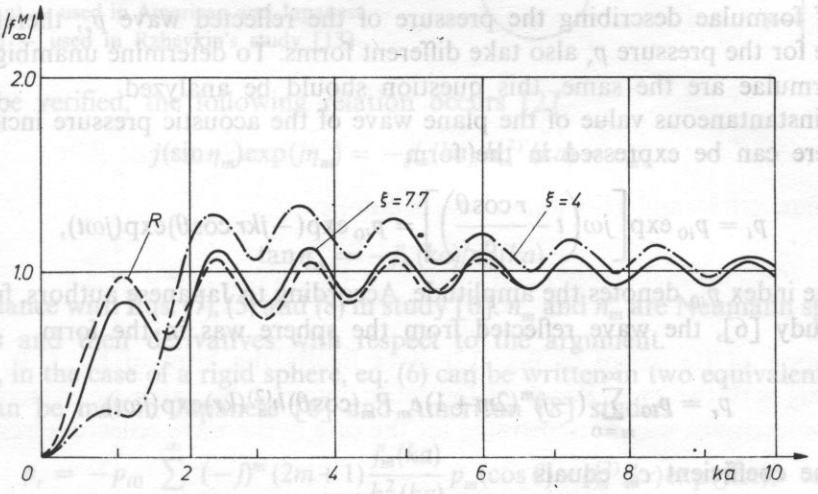

FIG. 1. The modulus of the shape function $f_\infty(ka)$ for a fixed rigid sphere (R) and the modified shape function ka for a free movable sphere with the relative density $\xi = 7.7$ (steel) and $\xi = 4$

Hence, for $ka > 6$, both curves, namely the curve R and that for steel ($\xi = 7.7$) practically coincide. On the other hand, for small values of ka, there can be large differences between the two curves (e.g. curve $\xi = 4$). Hence, it can be concluded that in the present case a sphere with large density can be treated as a fixed one. In practical cases in echo ranging this condition is usually satisfied. On the other hand the conclusion is not valid for spheres with small density and for low values of ka since, then the rigid sphere vibrates as a whole under the action of the incident wave pressure. In such a case verifying calculations should be performed according to Eqs. (2) and (3).

3. Acoustical shadow. Formulae describing wave reflection from a rigid sphere in steady state

The shadow forming arround a rigid sphere can be determined from expressions describing the acoustic pressure of the wave p_s emerging around the sphere. It is the sum of acoustic pressures of the plane wave incident on the sphere p_i and of the reflected wave p_r

$$p_s = p_i + p_r. \tag{4}$$

The acoustic pressure of the wave reflected from the sphere p_r is obtained as a result of the solution of the scalar wave equation in the medium surrounding the sphere. The boundary condition should be satisfied, namely the normal component of the acoustic velocity should vanish on the surface of the rigid sphere.

Since in the studies by American, Japanese and Soviet authors there are various forms of formulae describing the pressure of the reflected wave p_r, therefore the formulae for the pressure p_s also take different forms. To determine unambigously if these formulae are the same, this question should be analyzed.

The instantaneous value of the plane wave of the acoustic pressure incident on the sphere can be expressed in the form

$$p_i = p_{i0} \exp\left[j\omega\left(t - \frac{r\cos\theta}{c}\right)\right] = p_{i0} \exp(-jkr\cos\theta)\exp(j\omega t), \tag{5}$$

where the index p_{i0} denotes the amplitude. According to Japanese authors, from Eq. (3) in study [6], the wave reflected from the sphere was in the form

$$p_r = p_{i0} \sum_{m=0}^{\infty} (-j)^m (2m+1) c_m P_m(\cos\theta) h_m^{(2)}(kr) \exp(j\omega t), \tag{6}$$

where the coefficient c_m equals

$$c_m = -[F_m j_m(ka) - kaj'_m(ka)]/[F_m h_m^{(2)}(ka) - kah_m^{(2)'}(ka)]. \tag{7}$$

Formulae (5) and (6) are valid in a polar coordinate system in which the wave is incident on the sphere travelling from left to right (Fig. 2 a). In this system the radius was denoted by r and the azimuth by θ. $P_n(\cos\theta)$ denotes the Legendre polynomial and $h_m^{(2)}$ and $h_m^{(2)'}$ are spherical Hankel functions of the second kind and its derivative with respect to the argument.

It can be shown [2] for a rigid sphere that

$$F_m = 0. \tag{8}$$

Then, Eq. (7) becomes

$$c_m = -j'_m(ka)/h_m^{(2)'}(ka). \tag{9}$$

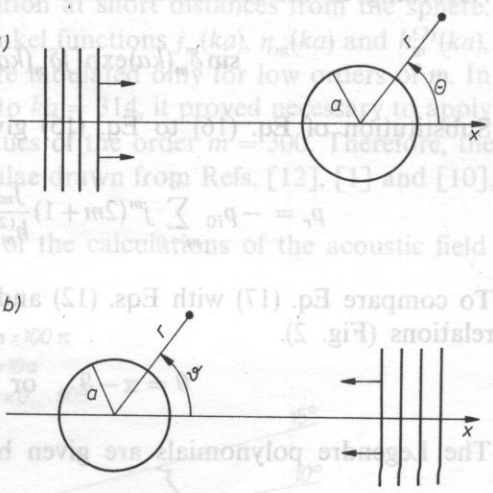

FIG. 2. The polar coordinate system and the direction of the incidence of the plane wave on the sphere. a) – used in American and Japanese studies, b) – used in Rzhevkin's study [13]

As can be verified, the following relation occurs [2]

$$j(\sin\eta_m)\exp(j\eta_m) = -j'_m(ka)/h_m^{(2)'}(ka) = c_m, \tag{10}$$

where

$$\tan\eta_m = -j'_m(ka)/n'_m(ka) \tag{11}$$

in accordance with Eqs. (7), (5) and (8) in study [6]. n_m and n'_m are Neumann spherical functions and their derivatives with respect to the argument.

Thus, in the case of a rigid sphere, eq. (6) can be written in two equivalent forms, which can be met in Japanese [6] and American [8] studies

$$p_r = -p_{i0}\sum_{m=0}^{\infty}(-j)^m(2m+1)\frac{j'_m(ka)}{h_m^2(ka)}p_m(\cos\theta)\times h_m^{(2)}(kr)\exp(j\omega t), \tag{12}$$

and

$$p_r = -p_{i0}\sum_{m=0}^{\infty}(-j)^{m+1}(2m+1)\sin\eta_m\exp(j\eta_m)P_m(\cos\theta)h_m^{(2)}(kr)\exp(j\omega t), \tag{13}$$

where $\tan\eta_m$ is expressed by Eq. (11). The above formulae are valid in the coordinate system r, θ (Fig. 2a). On the other hand in Soviet studies there are different formulae [12]. To compare them with the formulae of Japanese and American authors, let us introduce the coordinate system r, ϑ, in which the wave incident on the sphere travels from right to left (Fig. 2 b). It has the form (see [12], p. 257).

$$p_i = p_{i0}\exp\left[j\omega\left(t+\frac{r\cos\vartheta}{c}\right)\right] = p_{i0}\exp(jkr\cos\vartheta)\exp(j\omega t). \tag{14}$$

In turn, from Eq. (9.6) in the cited handbook [12], the wave reflected from the sphere is described by the formula

$$p_r = -p_{i0}\sum_{m=0}^{\infty}j^{m+1}(2m+1)\sin\delta_m(ka)\exp[j\delta_m(ka)]P_m(\cos\vartheta)h_m^{(2)}(kr)\exp(j\omega t). \tag{15}$$

According to the formulae in Ref. [12] (p. 259) for a rigid sphere

$$\sin\delta_m(ka)\exp[j\delta_m(ka)] = j[j'_m(ka)/h_m^{(2)\prime}(ka)]. \tag{16}$$

Substitution of Eq. (16) to Eq. (15) gives

$$p_r = -p_{i0}\sum_{m=0}^{\infty} j^m(2m+1)\frac{j'_m(ka)}{h_m^{(2)}(ka)}P_m(\cos\vartheta)h_m^{(2)}(kr)\exp(j\omega t). \tag{17}$$

To compare Eq. (17) with Eqs. (12) and (13) one should notice that the following relations (Fig. 2).

$$\theta = \pi - \vartheta \quad \text{or} \quad \cos\theta = -\cos\vartheta. \tag{18 a, b}$$

The Legendre polynomials are given by the expression [1]

$$P_m(x) = \frac{1}{2^m m!}\frac{d^m[(x^2-1)^m]}{dx^m}. \tag{19}$$

From Eqs. (18 b) and (19) follow the relations

$$P_m(x) = (-1)^m P_m(-x) \quad \text{or} \quad P_m(\cos\vartheta) = (-1)^m P_m(\cos\theta). \tag{20 a, b}$$

Substitution of Eq. (20 b) in Eq. (17) gives finally the form of Eq. (12).

In this way the equivalency of formulae obtained by Japanese, American and Soviet acousticians was demonstrated for the case of the wave reflection from a rigid sphere.

4. Directional characteristics of the shadow

Taking into account relations (4), (5) and (13) computer programmes elaborated from the following formula (assuming $p_{i0} = 1$) were applied for calculations of the shadow behind a rigid sphere

$$p_s = \exp(-jkr\cos\theta) - \sum_{m=0}^{\infty}(-j)^{m+1}(2m+1)\sin\eta_m(ka)\exp[j\eta_m(ka)]P_m(\cos\theta)h_m^{(2)}(kr) \tag{21}$$

where the quantity $\eta_m(ka)$ is given by Eq. (11). Eqs. (12), (13) and (21) can be simplified if the spherical Hankel function $h_m(kr)$ is replaced by approximating

formulae valid for large arguments kr. However, this simplification was abandoned in order to investigate the shadow distribution at short distances from the sphere.

The spherical Bessel, Neumann and Hankel functions $j_m(ka)$, $\eta_m(ka)$ and $h_m^{(2)}(ka)$, and also Legendre polynomials $P_m(\cos\theta)$ are tabulated only for low orders of m. In the present study, for large values of ka up to $ka = 314$, it proved necessary to apply the above mentioned functions even to values of the order $m = 300$. Therefore, the computations involved the reduction formulae drawn from Refs. [12], [1] and [10], and appropriate computer programmes.

Fig. 3, 4, 5 and 6 show chosen results of the calculations of the acoustic field

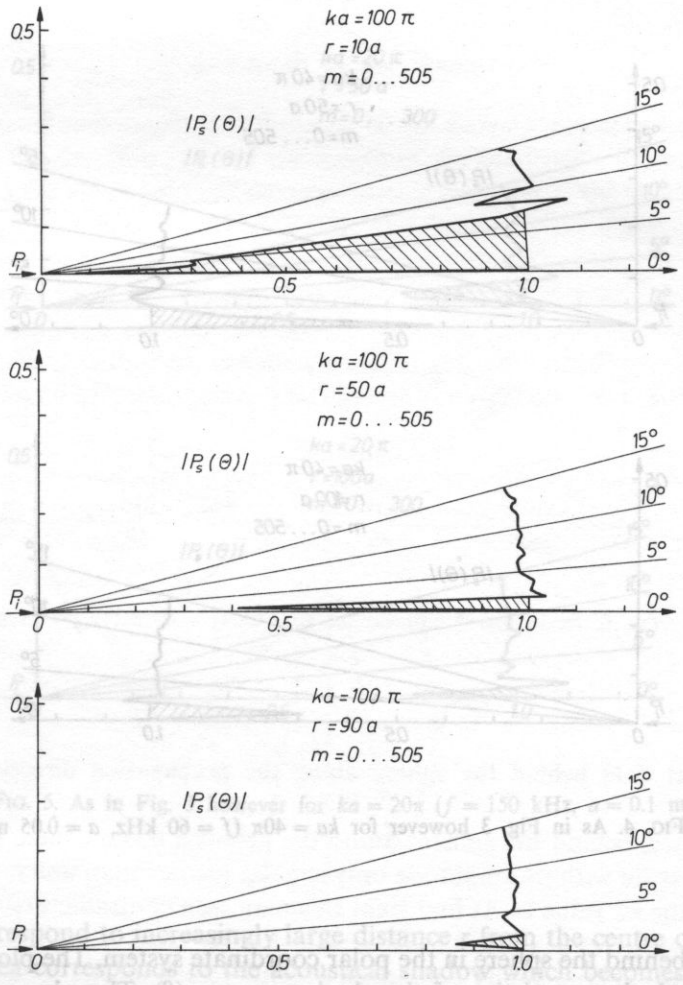

FIG. 3. Directional characteristics of the acoustic field behind the sphere for $ka = 100\pi$ ($f = 150$ kHz, $a = 0.5$ m) at different distances r. The dashed area corresponds to the shadow

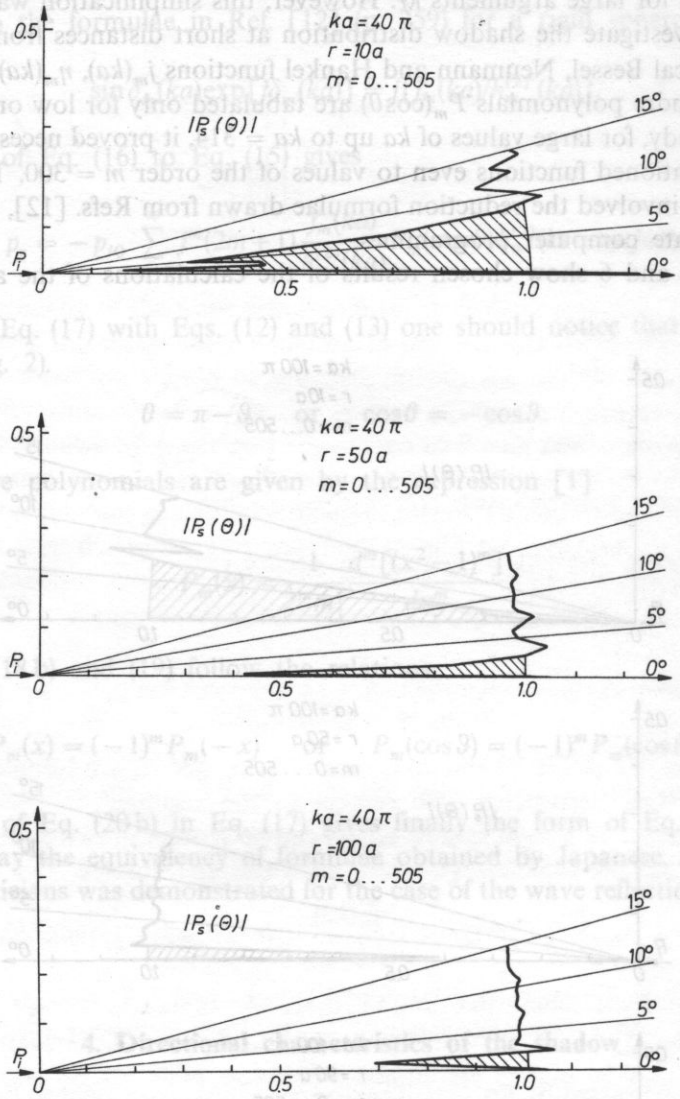

FIG. 4. As in Fig. 3 however for $ka = 40\pi$ ($f = 60$ kHz, $a = 0.05$ m)

distribution behind the sphere in the polar coordinate system. The plotted curves are the directional characteristics of the shadow $p_s = p_s(\theta)$. The plane wave with the amplitude $p_{i0} = 1$ travels from left to right along the axis $\theta = 180°$. The centre of the sphere is situated at the origin of the coordinate system. Successive curves in each of

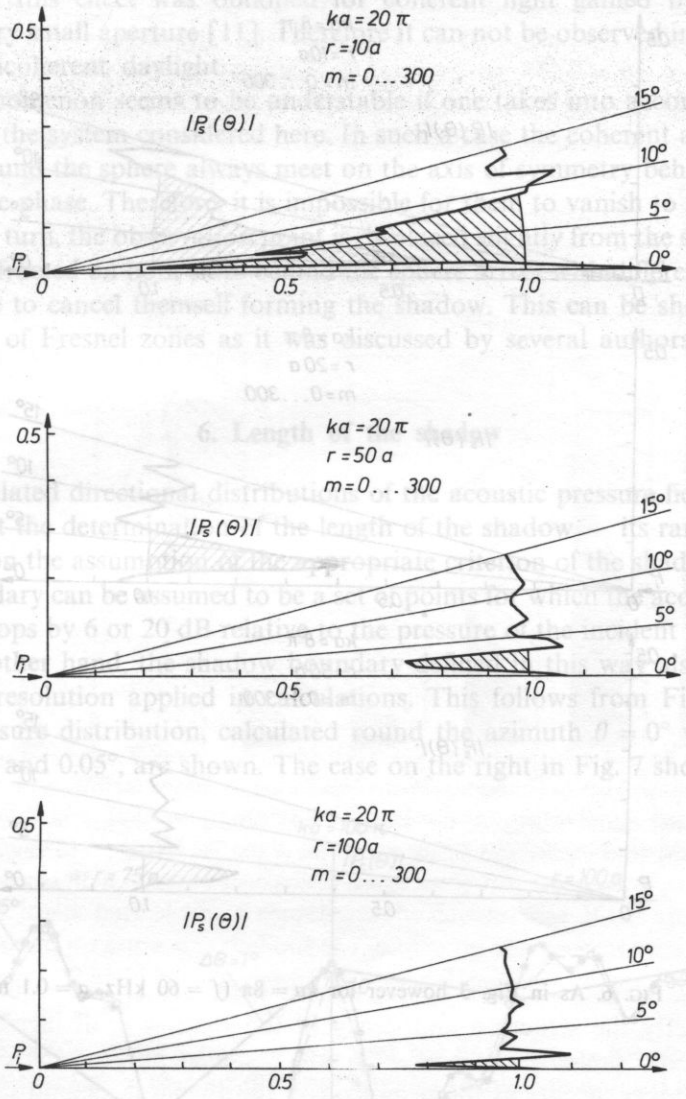

FIG. 5. As in Fig. 3 however for $ka = 20\pi$ ($f = 150$ kHz, $a = 0.1$ m)

the figures correspond to increasingly large distance r from the centre of the sphere. The dashed area corresponds to the acoustical shadow which becomes smaller and smaller as the distance from the sphere increases. The above calculations were carried out for the azimuth step $\Delta\theta = 1°$.

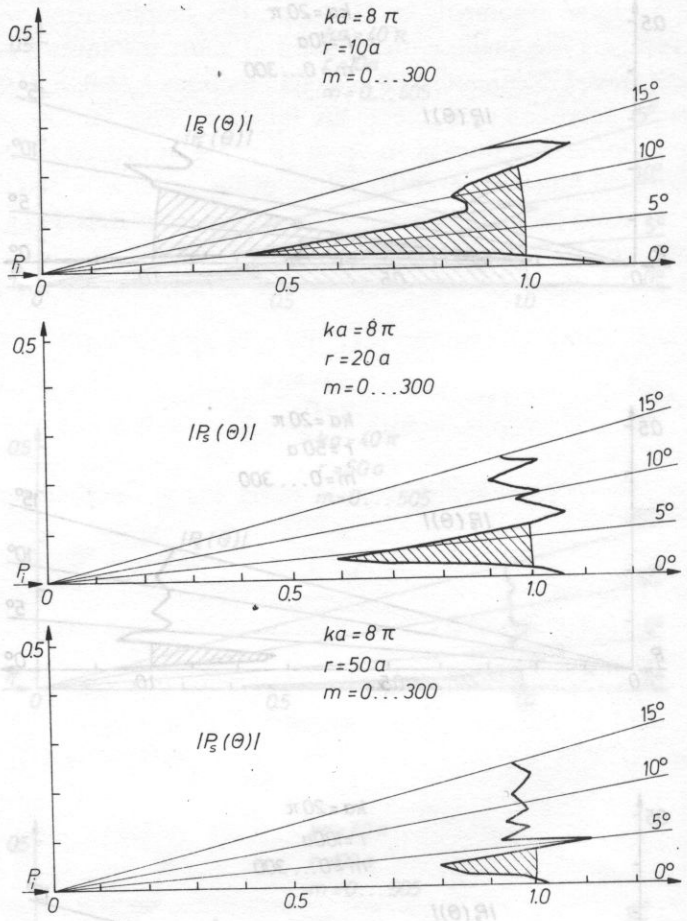

FIG. 6. As in Fig. 3 however for $ka = 8\pi$ ($f = 60$ kHz, $a = 0.1$ m)

5. Acoustical field behind the sphere along the propagation direction of the wave

In all cases, behind the sphere, round the azimuth $\theta = 0°$, there is a thin lobe of acoustic pressure with its amplitude only slightly greater than unity. It is the sharper the greater the ka value is. At first sight this may seen contradictory to our everyday experience with light shadows. However, it was exactly in optics that it was demonstrated experimentally behind an opaque screen, in the centre of its shadow, a bright spot of light [5]. This is evidence to the diffracted of light. This conclusion was drawn by Poisson on the basis of Fresnel's diffraction theory, contributing to the victory of the wave light theory. The conditions of the experiment described in [5]

indicate that this effect was obtained for coherent light gained by letting light through a very small aperture [11]. Therefore it can not be observed in everyday life, in normal incoherent daylight.

This phenomenon seems to be understable if one takes into account the perfect symmetry of the system considered here. In such a case the coherent acoustic waves difracted around the sphere always meet on the axis of symmetry behind the sphere with the same phase. Therefore, it is impossible for them to vanish to form there the shadow. If in turn, the observation point is displaced slightly from the symmetry axis, the waves diffracted on both sides behind the sphere arrive with different phases. It is then possible to cancel themself forming the shadow. This can be shown using the construction of Fresnel zones as it was discussed by several authors [4] and [5].

6. Length of the shadow

The calculated directional distributions of the acoustic pressure field behind the sphere permit the determination of the length of the shadow – its range. However, this depend on the assumption of the appropriate criterion of the shadow boundary. Such a boundary can be assumed to be a set of points for which the acoustic pressure amplitude drops by 6 or 20 dB relative to the pressure of the incident wave pressure p_{i0}. On the other hand, the shadow boundary defined in this way also depends on the angular resolution applied in calculations. This follows from Fig. 7 in which acoustic pressure distribution, calculated round the azimuth $\theta = 0°$ with the steps $\Delta\theta = 1°$, 0.2° and 0.05°, are shown. The case on the right in Fig. 7 shows that if the

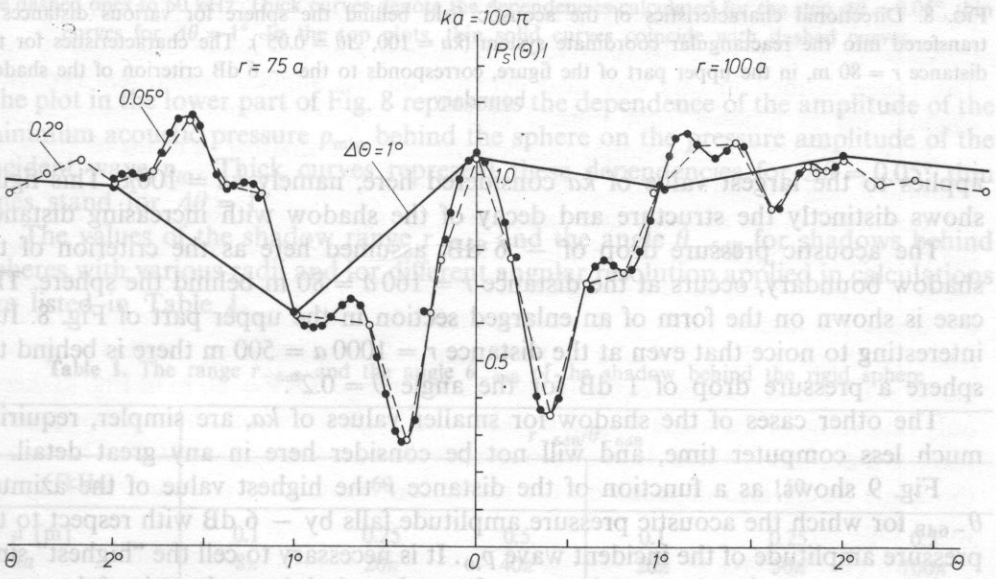

FIG. 7. The acoustic pressure distribution for low angles θ and for $ka = 100\pi$ at the distances $r = 75\,a$ and $r = 100\,a$, calculated with the steps $\Delta\theta = 1°$, 0.2° and 0.05°

criterion of the shadow boundary is set at the level of − 6 dB, the shadow is absent, assuming angular resolution of 1°. For $\Delta\theta = 0.2°$ the shadow becomes distinctly observable, for $\Delta\theta = 0.05°$ no additional changes occur.

Fig. 8 shows the directional characteristics of the acoustic field behind the sphere transfered into the rectangular coordinate system for various distances r. This case

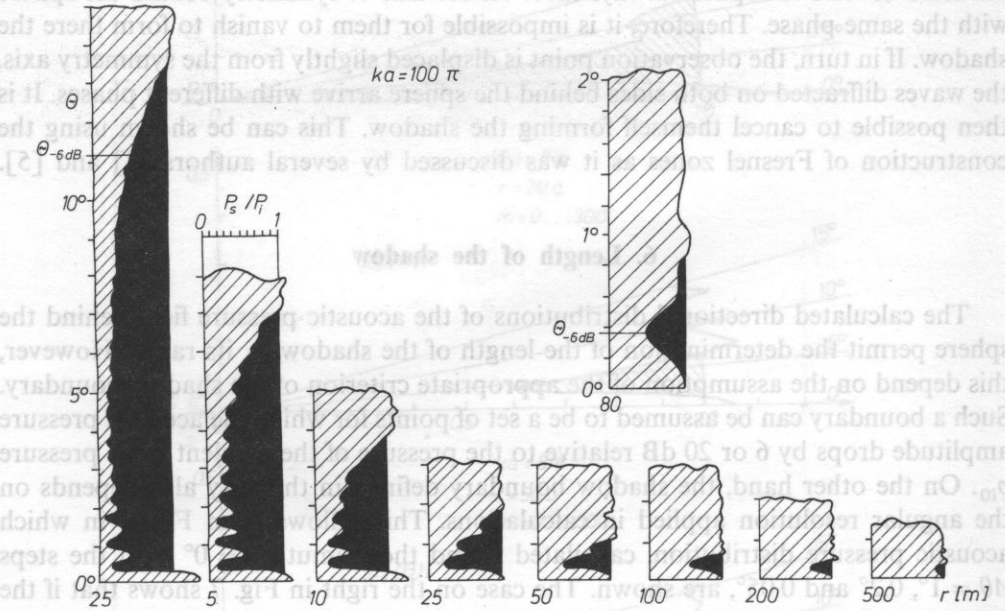

FIG. 8. Directional characteristics of the acoustic field behind the sphere for various distances r, transfered into the reactangular coordinate system ($ka = 100$, $\Delta\theta = 0.05°$). The characteristics for the distance $r = 80$ m, in the upper part of the figure, corresponds to the − 6 dB criterion of the shadow boundary

applies to the largest value of ka considered here, namely $ka = 100\pi$. This figure shows distinctly the structure and decay of the shadow with increasing distance.

The acoustic pressure drop of − 6 dB, assumed here as the criterion of the shadow boundary, occurs at the distance $r = 160\,a = 80$ m behind the sphere. This case is shown on the form of an enlarged section in the upper part of Fig. 8. It is interesting to noice that even at the distance $r = 1000\,a = 500$ m there is behind the sphere a pressure drop of 1 dB for the angle $\theta = 0.2°$.

The other cases of the shadow for smaller values of ka, are simpler, requiring much less computer time, and will not be consider here in any great detail.

Fig. 9 shows, as a function of the distance r the highest value of the azimuth $\theta_{-6\text{dB}}$ for which the acoustic pressure amplitude falls by − 6 dB with respect to the pressure amplitude of the incident wave p_{i0}. It is necessary to cell the "highest" since the second value of such an angle occurs for each main lobe at the axis of the system behind the sphere when the maximum pressure is smaller than − 6 dB (see Fig. 8).

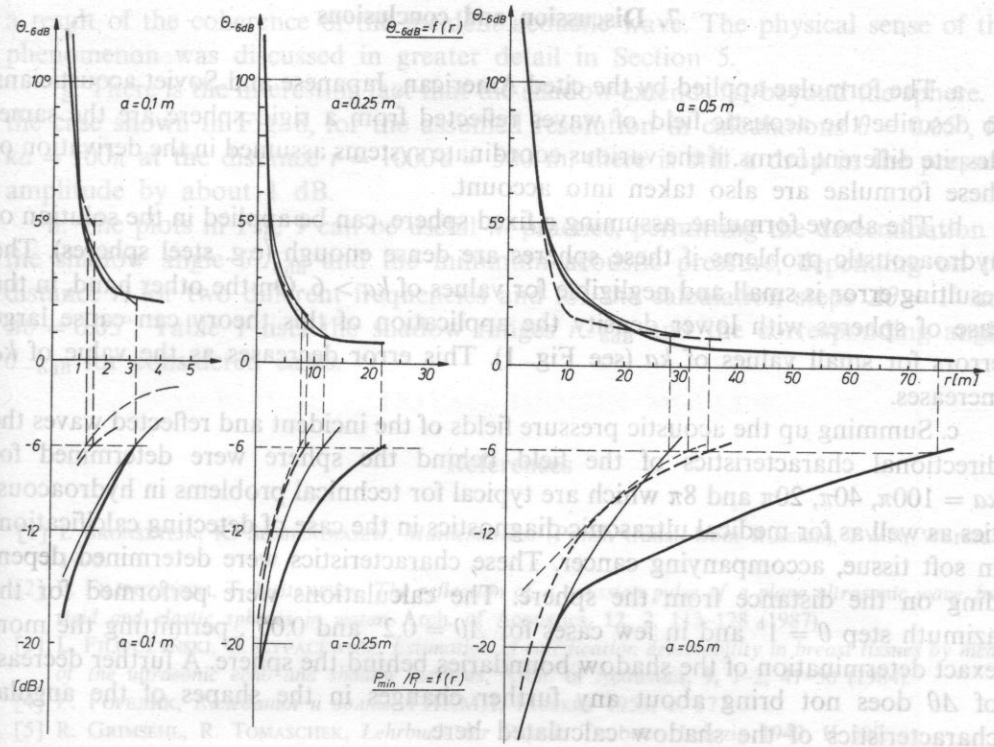

FIG. 9. The dependence of the angle $\theta_{-6\text{dB}}$ and the maximum acoustic pressure $p_{\min}$ behind the sphere on the distance r for three different sphere radius a. Solid curves correspond to the frequency $f = 150$ kHz, the dashed ones to 60 kHz. Thick curves denote the dependencies calculated for the step $\Delta\theta = 0.05°$, thin curves for $\Delta\theta = 1°$. In the top plots, thin solid curves coincide with dashed curves

The plot in the lower part of Fig. 8 represents the dependence of the amplitude of the minimum acoustic pressure $p_{\min}$ behind the sphere on the pressure amplitude of the incident wave p_{i0}. Thick curves represent these dependencies for $\Delta\theta = 0.05°$ thin ones stand for $\Delta\theta = 1°$.

The values of the shadow range $r_{-6\text{dB}}$ and the angle $\theta_{-6\text{dB}}$ for shadows behind spheres with various radii and for different angular resolution applied in calculations are listed in Table 1.

Table 1. The range $r_{-6\text{dB}}$ and the angle $\theta_{-6\text{dB}}$ of the shadow behind the rigid sphere

	$r_{-6\text{dB}}/\theta_{-6\text{dB}}$					
f [kHz]	60			150		
a [m]	0.1	0.25	0.5	0.1	0.25	0.5
ka	8π	20π	40π	20π	50π	100π
$\Delta\theta = 1°$	1.5 m/—	7.5 m/2°	30 m/1°	3 m/2°	12 m/1.2°	28 m/1°
$\Delta\theta = 0.05°$	1.3 m/5°	8.5 m/1.95°	35 m/0.95°	3.5 m/1.95°	22 m/0.76°	75 m/0.35°

7. Discussion and conclusions

a. The formulae applied by the cited American, Japanese and Soviet acousticians to describe the acoustic field of waves reflected from a rigid sphere are the same, despite different forms, if the various coordinate systems assumed in the derivation of these formulae are also taken into account.

b. The above formulae, assuming a fixed sphere, can be applied in the solution of hydroacoustic problems if these spheres are dense enough (e.g. steel spheres). The resulting error is small and negligible for values of $ka > 6$. On the other hand, in the case of spheres with lower density the application of this theory can cause large errors for small values of ka (see Fig. 1). This error decreases as the value of ka increases.

c. Summing up the acoustic pressure fields of the incident and reflected waves the directional characteristics of the field behind the sphere were determined for $ka = 100\pi$, 40π, 20π and 8π which are typical for technical problems in hydroacoustics as well as for medical ultrasonic diagnostics in the case of detecting calcifications in soft tissue, accompanying cancer. These characteristics were determined depending on the distance from the sphere. The calculations were performed for the azimuth step $\theta = 1°$ and in few cases for $\Delta\theta = 0.2°$ and $0.05°$, permitting the more exact determination of the shadow boundaries behind the sphere. A further decrease of $\Delta\theta$ does not bring about any further changes in the shapes of the angular characteristics of the shadow calculated here.

d. To evaluate quantitatively the shadow which decays in a continuous way, it was necessary to introduce a criterion permitting its unambiguous determination. For that purpose the authors proposed the criterion of a drop in the acoustic pressure amplitude by 6 dB relative to the pressure amplitude of the incident wave. The range defined in this way also depends on the angular resolution applied in calculations as follows from Figs. 7 and 9.

e. To evaluate the directional characteristics of the shadow in terms of angle, the azimuth $\theta_{-6\text{dB}}$ was introduced. It is equal to the highest value of the angle for which the amplitude of the acoustic pressure behind the sphere decreases by 6 dB relative to the pressure amplitude of the incident wave. For distances shorter than the shadow range (e.g. for $r = 2.5$ m in Fig. 8), there are two such angles, therefore it is necessary to choose the higher value of them, since there is a still smaller value of θ, resulting from the shape of the main lobe of the directional characteristics, situated near to the axis $\theta = 0°$. For a distance equal to the shadow range (for $r = 80$ m in Fig. 8) there is only one value of the angle $\theta_{-6\text{dB}}$, equal to the angle for which the acoustic pressure reaches a minimum value. In the case considered here this angle is 0, 2°. The value of the angle $\theta_{-6\text{dB}}$ also depends on the resolution assumed in calculations; it follows from Fig. 9.

f. In all the cases of the calculated directional characteristics, there is the main lobe situated round the axis $\theta = 0°$. It is the narrower the greater ka value is. This is

a result of the coherence of the incident acoustic wave. The physical sense of this phenomenon was discussed in greater detail in Section 5.

g. There is the interesting fact that the shadow extends far beyond the sphere. In the case shown in Fig. 8, for the assumed resolution in calculations $\theta = 0.05°$, for $ka = 100\pi$ at the distance $r = 1000\,a = 500$ m, there is still a drop in the pressure amplitude by about 1 dB.

h. The plots in Fig. 9 can be useful in practice, permitting the determination of the shadow angle $\theta_{-6\text{dB}}$ and the minimum acoustic pressure, depending on the distance r, for two different frequencies and for the calculation steps $\Delta\theta = 1°$ and $\Delta\theta = 0.05°$. Table 1 lists the shadow ranges $r_{-6\text{dB}}$ and the corresponding angles $\theta_{-6\text{dB}}$ for considered cases.

References

[1] I. Bronsztejn, K. Siemiendiajew, *Mathemathics* (Polish transl. from Russian), PWN, Warszawa 1970.

[2] L. Filipczyński, T. Kujawska, *The reflection of a gaussian pulse of a plane ultrasonic wave from rigid and elastic spheres in water*, Arch. of Acoustics, **12**, 2, 113–128 (1987).

[3] L. Filipczyński, G. Łypacewicz, *Estimation of calcification detectability in breast tissues by means of the ultrasonic echo and shadow methods*, Arch. of Acoustics, **9**, 1–2, 41–50 (1984).

[4] Г. Горелик, *Колебания и волны*, ГИКМЛ, Москва 1959, с. 371.

[5] R. Grimsehl, R. Tomaschek, *Lehrbuch der Physik*, Teubner, Leipzig 1943, II 590.

[6] T. Hasegawa, Y. Kitagawa, Y. Watanbe, *Sound reflection from an absorbing sphere*, J. Acoust. Soc. Am., **62**, 1298–1300 (1977).

[7] T. Hasegawa, *Comparison of two solutions for acoustic radiation pressure on a sphere*, J. Acoust. Soc. Am., **61**, 6, 1445–1448 (1977).

[8] R. Hickling, *Analysis of echoes from a solid elastic sphere in water*, J. Acoust. Soc. Am., **34**, 1582–1593 (1962).

[9] B. Hickling, N. Wang, *Scattering of sound by rigid movable sphere*, J. Acoust. Soc. Am., 39, 276–280 (1966).

[10] P. Morse, K. Ingard, *Theoretical acoustics*, Mc Graw-Hill, New York 1968.

[11] A. Piekara, Nowe oblicze optyki, PWN, Warszawa 1968, s. 155, (166).

[12] С. Ржевкин, *Курс лекций по теории звука*, ИМУ, Москва 1960.

Received on March 10, 1988.

ARCHIVES OF ACOUSTICS
14, 1-2, 45-60 (1989)

TESTING A NEW LISTENING-ROOM

BJARNE LANGVAD, HENRIK MØLLER

Institute of Electronic Systems
Aalborg University Centre

GUSTAW BUDZYŃSKI(*)

Sound Engineering Department, Gdańsk Technical University
(80-952 Gdańsk, ul. W. Majakowskiego 11/12)

New listening-rooms purposely designed and built are relatively seldom described in the literature, nevertheless problems arise especially when assessing their acoustic quality. Such problems are considered on the example of a new listening-room of the Acoustic Laboratory at the Aalborg University in Denmark. Results of the measurements and testing are discussed and some more general conclusions presented.

Nowe pomieszczenia odsłuchowe są stosunkowo rzadko opisywane w literaturze. Problemy związane z oceną ich jakości akustycznej rozpatrzono na przykładzie nowego pomieszczenia odsłuchowego Laboratorium Akustyki na Uniwersytecie w Aalborgu, w Danii. Przedyskutowano wyniki pomiarów i badań testowych oraz przedstawiono bardziej ogólne wnioski.

1. Introduction

Necessity of a high quality listening-room for all professional recording activities is still not sufficiently understood. Sound-engineers mostly listen to their recordings in their control-rooms only. However, many control-rooms in existing studios are either too small in volume or otherwise acoustically defective so that a rigorous assessment of the recordings quality can not be attained therewith. Moreover such an assessment ought very often to be performed by several people simultaneously, among them e.g. a composer, an arranger, a conductor, a producer, a sound-engineer

(*) Active as visiting professor at Aalborg University Centre since September 1987 till March 1988.

etc., while usual control-room can not afford so many seats appropriately situated acoustically.

So, purposely built and equipped listening-room became an unavoidable facility in every bigger professional recording centre, first of all at productional broadcasting-studios. Similar facilities are also needed for other purposes e.g. for psychophysiological research, for various kinds of subjective aural testing etc., as well as for didactic aims.

However, with growing number of nowly built and rebuilt control- or listening-rooms, an important question arises how to test the quality of such rooms. The question will be here partially answered on an example of testing a listening-room at the newly built Acoustic Laboratory in the Institute of Electronic Systems of the Aalborg University Centre in North Jutland, Denmark.

The listening-room has been acoustically designed by JORGEN PEDERSEN from the Scandinavisk Lydteknik, Aalborg [11], together with other special rooms of the Acoustic Laboratory, such as an anechoic-room, a reverberant-chamber, an audiometric-room, an infrasound-booth, etc. subsided by several appropriate control-rooms. The designs were based on assumptions prepared by scientific staff of the Laboratory, in accordance to recommendations mentioned beneath.

2. Objective criteria of the listening-room quality

The objective criteria, selected among more general ones concerning acoustical quality of rooms, are, first of all, contained in various recommendations edited by appropriate national or international bodies, e.g. the Scandinavian Broadcasting Corporations [20, 21], the International Electrotechnical Commission [19], Organisation Internationale de la Radio et Télévision [16, 17], Deutsche Industrie Normen [18], etc. The recommendations quote typical parameters relevant for the listening-room quality, show desirable ranges of those parameters values, and formulate some additional requirements. The particular parameters values being generally well known they will be not repeated here. Besides they were broadly discussed in many earlier [21, 25] and recent publications [3, 10, 12].

On the other hand, it might be argued that the notion of acoustical quality has not been, so far, defined and that it is frequently employed in discrepant meanings. However, such considerations are beyond the scope of this article.

The mentioned parameters and requirement neither exhaust all possible variations of the conceptual design of listening-rooms, nor preconize any important details influencing their acoustical quality. Besides, as design rules for listening-rooms are far from being stable, so variable trends may be observed actually [7, 9] and more so, when many aspects of acoustical quality of rooms are being revised and discussed again [13, 14, 15].

At any rate some of the objective criteria are unquestionable and thus the

following general requirements ought to be fulfilled for any high quality listening-room:

1) Sufficient volume of the room.
2) Appropriate shape and dimensions.
3) Optimum reverberation time characteristics.
4) Necessary outfitting.

Ad 1) The preferred volume is to be about 80 cu.m [18]. However, lower values, starting from 43 cu.m, are also recommended [5, 12, 19], while much higher ones are mostly required [16, 17, 21], going up to 150 cu.m.

Ad 2) Although irregular shapes are not excluded, the main concept remains to be a parallelepipedly shaped room.

Its length to height and width to height ratios should be different and far from integer values. Recommended ratios are [17, 21]: length/height < 1.9 or $2.1 <$ $<$ length/height and width/height $= 1.25$ to 1.45. Elsewhere, recommended dimensions are given directly [12, 19]: length $= 6.7$ m, width $= 4.2$ m, height $= 2.8$ m.

Ad 3) Recommended values of reverberation time versus frequency are fairly discrepant which is depicted in Fig. 1.

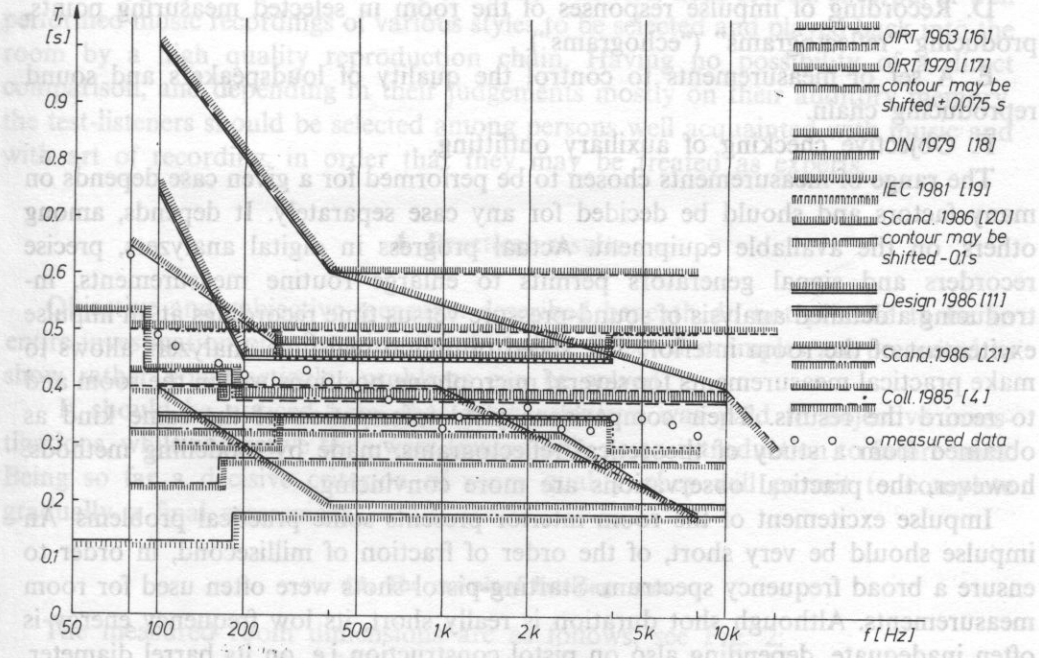

FIG. 1. Comparison of tolerances for optimum reverberation characteristics, drawn along various recommendations; the values measured in the tested room are superimposed, marked with circles. NB: The diagram seems to be unintelligible at a first glance; however, it shows how the recommendations disagree or contradict

Ad 4) Although not required decidedly several devices are mentioned in recommendations e.g.: an opaque curtain acoustically perplex, which permits to hide the assessed equipment from the listeners view; a sound-proof control window and/or a video chain linking the listening-room with an adjacent control room; appropriate seats for a limited number of listeners; mostly carpeted floor, etc.

More detailed advantageous or disadvantageous properties of listening-rooms should be taken into account yet such considerations are applicable mainly to the existing rooms, when practical measurements and tests can be undertaken. As far as possible, objective measurements should be preferred to describe room properties, although subjective tests are, of course, unavoidable.

The following objective measurements can be easily performed, provided an appropriate measuring equipment is available:

A. Measurements of dimensions and evaluation of room surfaces and volume; specification of surface-finish materials.

B. Recording of sound decays on a middle frequency and evaluation of averaged parameters: reverberation time, early-decay-time, distinctness ("Deutlichkeitsgrad"), "Schwerpunktzeit", clarity ("Klarheitsmass") etc. (see e.g. [22]).

C. Recording of sound decays in one-third octave bands and evaluation of a frequency characteristics of reverberation.

D. Recording of impulse responses of the room in selected measuring points, producing "reflectograms" ("echograms").

E. A set of measurements to control the quality of loudspeakers and sound reproducing chain.

F. Objective checking of auxiliary outfitting.

The range of measurements chosen to be performed for a given case depends on many factors and should be decided for any case separately. It depends, among others, on the available equipment. Actual progress in digital analyzers, precise recorders and signal generators permits to enlarge routine measurements, introducing a detailed analysis of sound-pressure versus time recordings at an impulse excitement of the room interior. The speed of digital real-time analyzers allows to make practical measurements for several microphone positions within the room and to record the results. Their comparisons yield information of the same kind as obtained from a study of theoretical reflectograms, made by modelling methods, however, the practical observations are more convincing.

Impulse excitement of the room interior presents some practical problems. An impulse should be very short, of the order of fraction of millisecond, in order to ensure a broad frequency spectrum. Starting-pistol shots were often used for room measurements. Although shot duration is really short, its low frequency energy is often inadequate, depending also on pistol construction i.e. on its barrel diameter. Besides, the shot sound is highly directional and difficult to be controlled in direction and position of firing. Thus the repeatibility of shot-sound impulses is poor.

Actually, impulse testing techniques use precise pulse-generators, power-amplifiers and appropriate loudspeakers to produce triggered sound impulses of

a desired shape and duration [1]. A digitally controlled excitation chain and a digital real-time analyzer permit to achieve full repeatibility of acoustic measurements within the room.

Measurement results should be analyzed and compared to some selected parameter values so as to create objective test conditions, i.e. criteria, which for a satisfying quality ought to be fulfilled.

3. Subjective assessment tests

Subjective tests performed in listening-rooms are mostly aimed at quality assessment of electroacoustic equipment and of sound quality of recordings. However, similar tests may be, and sometimes should be applied to cases when the quality of a listening-room itself is to be assessed subjectively. Such assessments are less convincing as those previously mentioned, e.g. the paired comparison method, being most efficient and very often applied in subjective testing. Unfortunately, the latter method can not be used in described case.

Nevertheless, some important properties of listening-rooms can be defined by subjective tests, if carefully designed. Useful hints on preparing such tests may be found in appropriate publications [4, 12, 19]. The tests need several excerpts of well performed music recordings of various styles to be selected and played back into the room by a high quality reproduction chain. Having no possibility of a direct comparison, and depending in their judgements mostly on their auditory memory, the test-listeners should be selected among persons well acquainted with music and with art of recording, in order that they may be treated as experts.

4. Practical results

Objective and subjective measures described beneath do not pretend to be an entire investigation of a listening-room quality. Selected examples are presented to show rather how particular problems can be solved.

It should be noticed here, that main attention was paid to objective investigations, while subjective tests were treated only as an introduction to future ones. Being so far a decisive criterion of room quality, they will permit to complete gradually a final assessment.

4.1. The examined listening-room

The measured room dimensions are as follows, see Fig. 2:

length 7.80 m; width 4.12 m; height 2.77 m.

All walls are covered with special panels; some of them suspended on rails, protruding out of the wall surface and moveable, enabling to control the diffusivity, see Fig. 3. The ceiling is covered with special plaster panels.

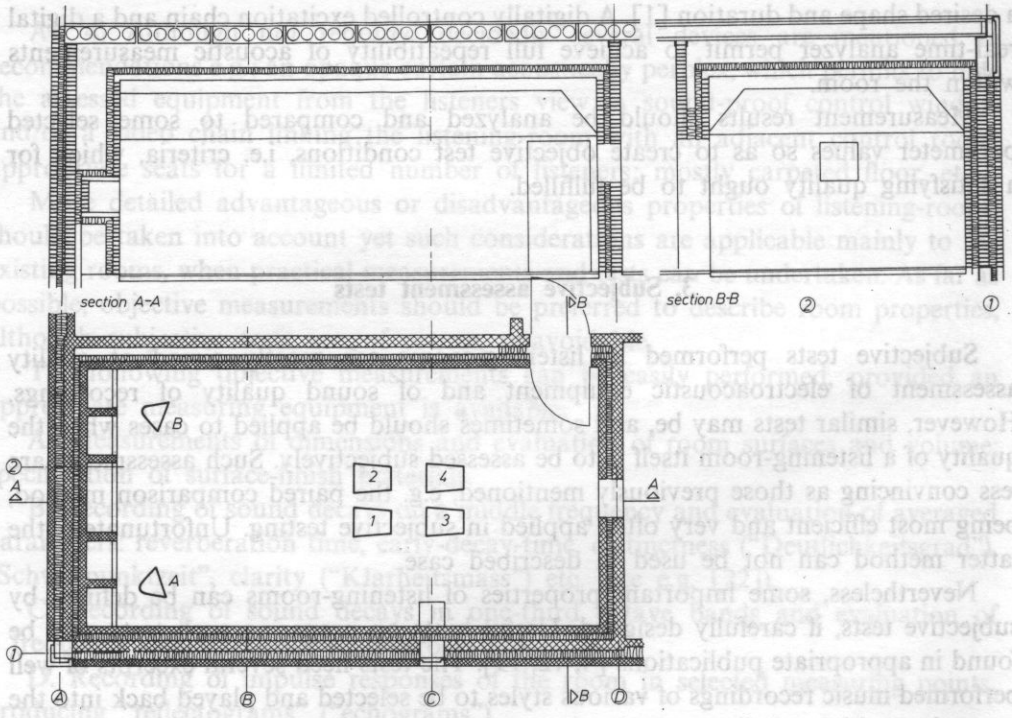

FIG. 2. Listening-room shape and dimensions. Superimposed are loudspeaker positions A and B, and seat positions No. 1, 2, 3, and 4

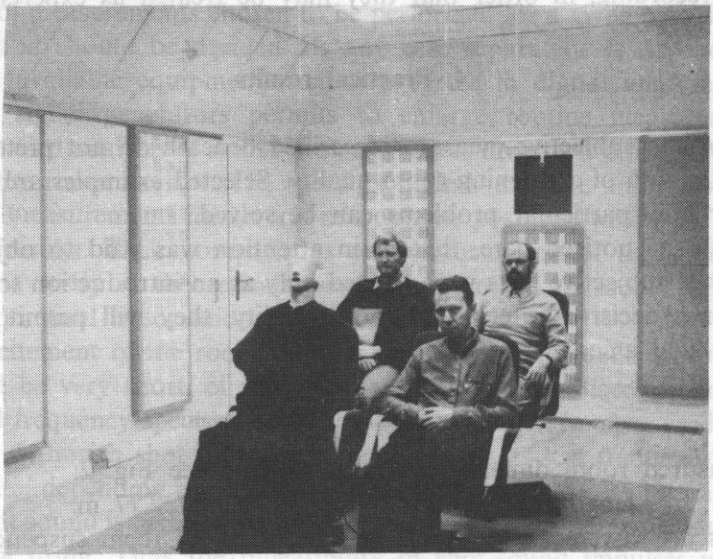

FIG. 3. Listening-room as seen from the left loudspeaker position. The seat No. 2 is occupied by a B and K artificial head- and torso-simulator in a dressing

Taking into account the angle-cut-volume between the ceiling and three walls, which has to be subtracted from the brutto volume, it makes the real volume of the room equal to 85,5 cubic metres. The relative dimension ratios are:

$$\text{lenght/height} = 7.80/2.77 = 2.8 > 2.1$$
$$\text{width/height} = 4.12/2.77 = 1.49 > 1.45(!).$$

The above ratios exceed the majority of recommended ones (see Section 2). However, augmenting the room volume by increasing its height was impossible due to architectural limitation. From the three-meter standard height of the room the 23 cm were to be devoted to a false ceiling construction necessary to improve sound insulation, mainly against impact noise coming from the rooms above.

It may be added here that other recommendations advise for medium size rooms, i.e. of about 80 cu.m volume, the higher ratios: the length/height = 2.5 and width/height = 1.6 [4] being closer to the measured above.

The angle-cut-volume, visible on Fig. 2 and 3, causes not only additional reflecting surfaces but, being separed from the room with elastic partition-panels, it acts as low-frequency absorber, which diminishes low-frequency reverberation time. This influence is mentioned beneath.

4.2. Objective results

The following parameter values were obtained from measurements:

Mean reverberation time T60 = 0.47 s;
Mean reverberation time T30 = 0.35 s;
Mean early-decay-time T10 = 0.34 s;

The frequency characteristics showing the results of reverberation measurements is depicted in Fig. 1, where it is superimposed on various contours of tolerances concerning such characteristics. The measured results can not satisfy all requirements at the same time because they are contradictory to each other. However, the measured curve fits rather well to the designed one [11], except few points in the vicinity of 1 and 3 kHz (see Sect. 5), and is in good agreement with recent recommendations [18, 20]. The presented measurements have been done with the use of B and K Precision Sound Level Meter, type 2231+1625+BZ 7104. The results, however, turned out to be strongly dependent on measurement conditions and methods, which is discussed in Sect. 5 in context of various additional measurements executed in the listening-room.

The further parameters values were processed with the use of a personal computer with appropriate software program, basing on a recorded sound impulse described above. The following parameters were evaluated:

Distinctness "Deutlichkeitsgrad" D = 85%;
"Schwerpunktzeit" t = 30 ms;
Clarity ("Klarheitmass") C80 = 14 dB;

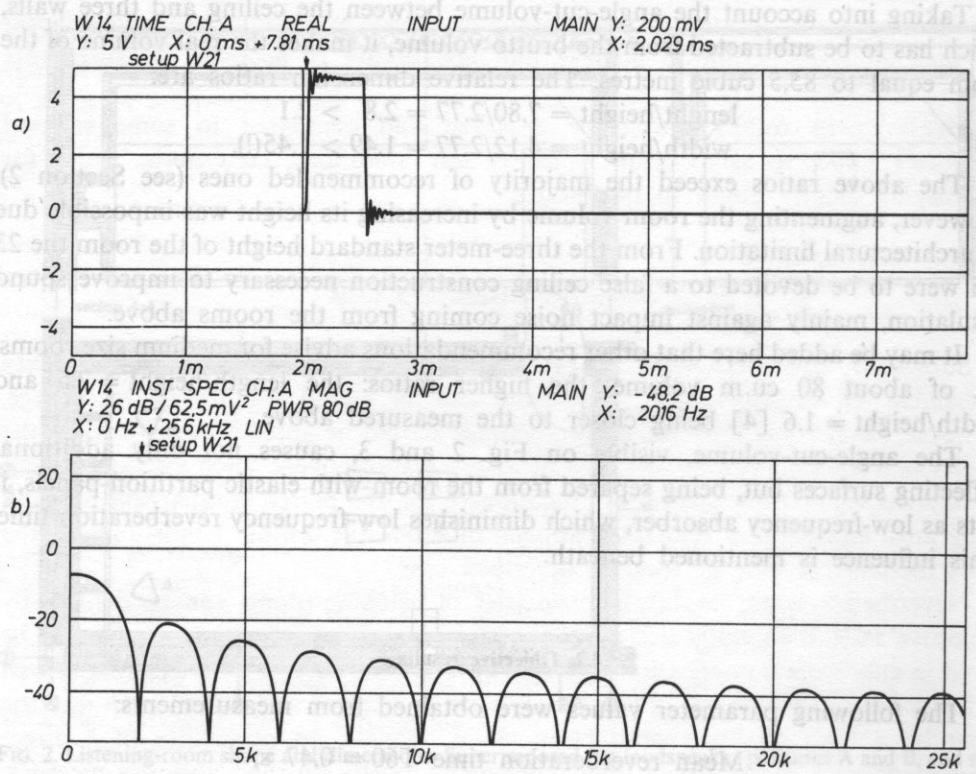

FIG. 4. An electrical excitation impulse measured at the generator output: a) time function, b) its spectrum

Furthermore, time-characteristics or reflectograms of the room were measured by means of an artificial head B and K type 4128+2812 (Head- and Torso-Simulator) and a two-channel digital analyzer B and K 2032, with a Hewlett Packard 7475A Plotter. The room was excited by triggered impulses produced by a digital generator Philips type PM 5193. Impulse duration was 0.6 ms, see Fig. 4. Those impulses were fed through a B and K power-amplifier to the pair of VIFA dynamic loudspeakers, type MD 10-39. A sound impulse radiated from such loudspeaker and recorded in an anechoic room is depicted in Fig. 5. The impulse shape and its spectrum show that the room was adequately excited. An example of reflectogram taken in the listening-room is shown in Fig. 6. Such reflectograms were made for four positions of the artificial head at each of the four seats within the room, visible in Fig. 2 and 3. A study of those reflectograms permits to appreciate the share of delay-specified groups of reflections on the envelope of perceived sound, depending on the listeners' seats. It allows also to observe the influence of minor changes in positioning of loudspeakers or listeners' seats, the result of an introduction of some reflecting surfaces within the listening-room etc.

FIG. 6. A reflectogram (echogram) of a sound impulse from the left loudspeaker (A), received by a B and K artificial head situated in the seat No. 1

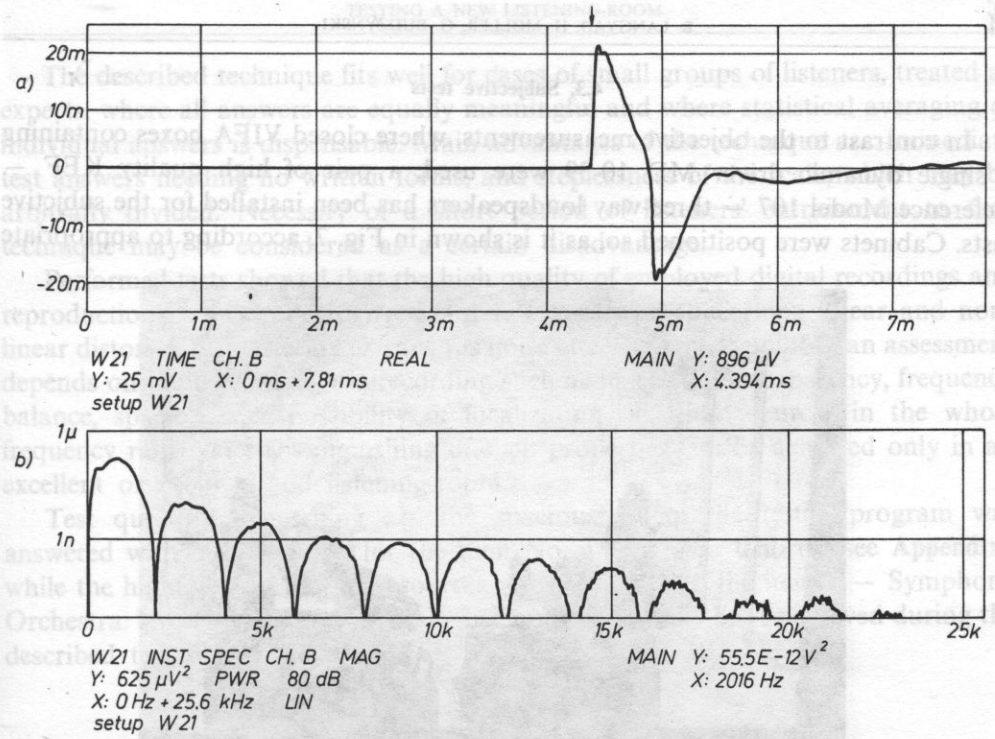

FIG. 5. A sound impulse radiated from the employed loudspeaker, measured in an anechoic-room: a) time function b) its spectrum. NB: The choice of loudspeaker type influences the degree of correspondence of the functions shown in Fig. 4 and Fig. 5, a) and b) respectively

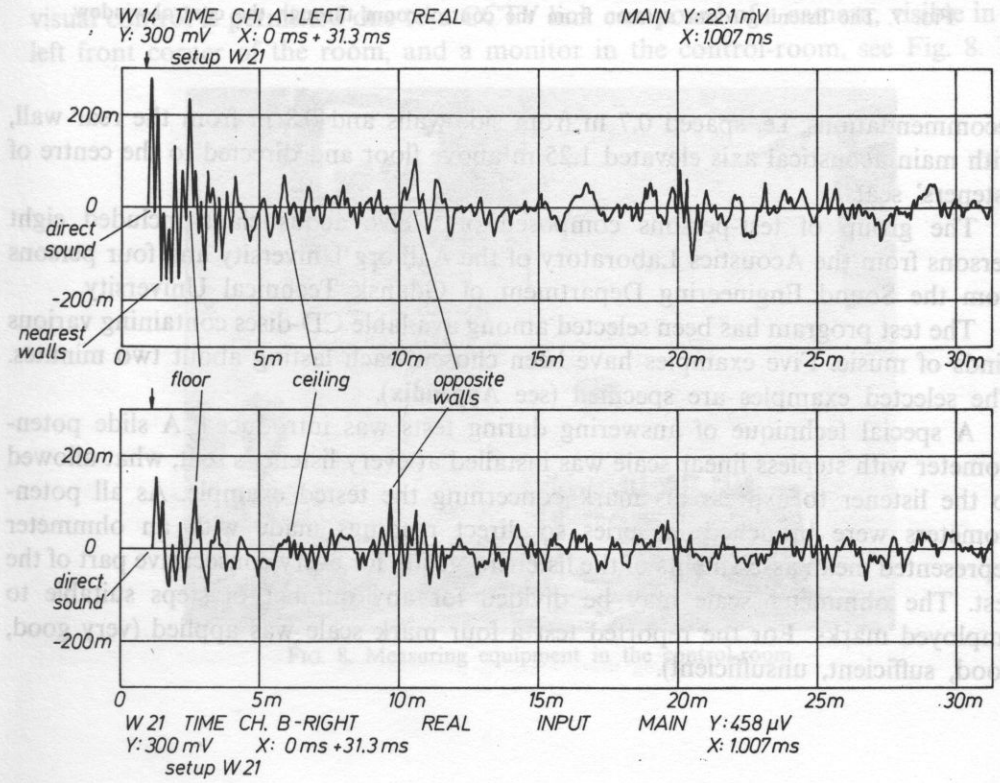

4.3. Subjective tests

In contrast to the objective measurements, where closed VIFA boxes containing a single dynamic driver MD 10-39 were used, a pair of high quality KEF – Reference Model 107 – three-way loudspeakers has been installed for the subjctive tests. Cabinets were positioned so, as it is shown in Fig. 7, according to appropriate

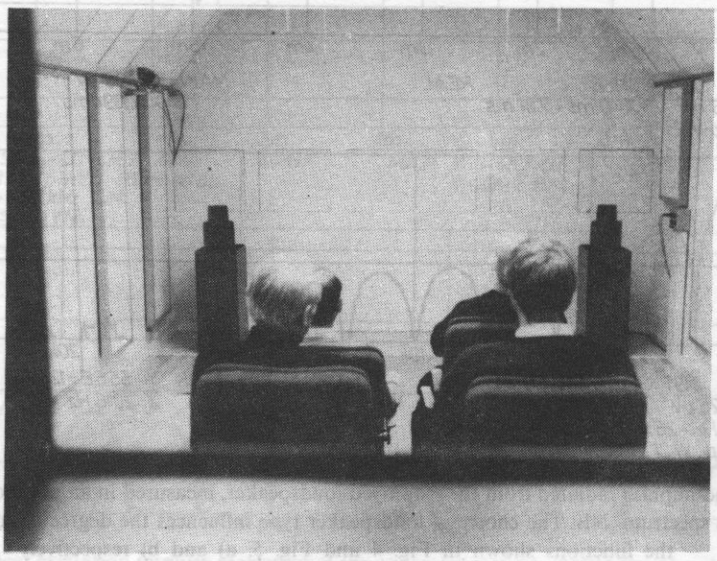

FIG. 7. The listening-room as seen from the control-room through the control-window

recommendations, i.e. spaced 0.7 m from side-walls and 0.8 m from the rear wall, with main acoustical axis elevated 1.25 m above floor and directed to the centre of listeners' seats.

The group of test-persons composed of twelve acousticians included eight persons from the Acoustics Laboratory of the Aalborg University and four persons from the Sound Engineering Department of Gdańsk Technical University.

The test program has been selected among available CD-discs containing various kinds of music. Five examples have been chosen, each lasting about two minutes. The selected examples are specified (see **Appendix**).

A special technique of answering during tests was introduced. A slide potentiometer with stepless linear scale was installed at every listener's seat, what allowed to the listener to express his mark concerning the tested example. As all potentiometers were branched in series so direct readings made with an ohmmeter represented mean assessments of the listeners' group for every consecutive part of the test. The ohmmeter scale may be divided for any number of steps suitable to employed marks. For the reported test a four mark scale was applied (very good, good, sufficient, unsufficient).

The described technique fits well for cases of small groups of listeners, treated as experts, where all answers are equally meaningful and where statistical averaging of individual answers is dispensable. Main advantages of the technique are: immediate test answers needing no written forms, and steplessness of the scale, which may be arbitrally divided. Necessity of a short period of listeners' entrainment to that technique may be considered as a certain disadvantage.

Performed tests showed that the high quality of employed digital recordings and reproduction chain rendered irrelevant test questions concerning linear and non-linear distortions, interfering extraneous noise etc. The salient point of an assessment depends on the properties of a recording such as its clarity, transparency, frequency balance, spaciousness, possibility of localization of sound sources in the whole frequency range, etc. Distinguishing of such properties can be achieved only in an excellent or a very good listening-room.

Test question concerning e.g. the spaciousness of the tested program was answered with highest mark for the item No. 3 – Opera Chorus (see **Appendix**), while the highest localization of sources was attributed to the item 1 – Symphony Orchestra. No significant faults of the listening-room have been observed during the described test sessions.

4.4 Subsidiary features

Among additional advantages of the examined room its efficient connections to neighbouring control-rooms should be emphasized. First of all, a good direct insight from the control-room is allowed due to a control-window, see Fig. 7. Other kind of visual control is permitted due to a CCTV link composed of a camera, visible in the left front corner of the room, and a monitor in the control-room, see Fig. 8. The

FIG. 8. Measuring equipment in the control-room

overview on the monitor, see Fig. 9, showing listeners' faces, facilitates and *accelerates the execution of tests.*

Additional outfittings such as a curtain and carpets on floors are visible in Fig. 10.

Subjective opinions on the listening-room general quality were very high.

FIG. 9. The listeners observed on CCTV-monitor from the control-room

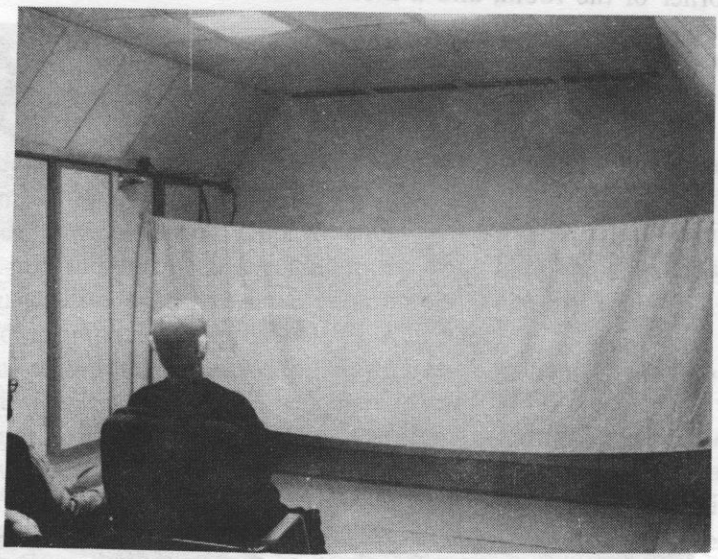

FIG. 10. Auxiliary outfitting of the listening-room: an opaque curtain, carpeted floor, markers from above showing exact listening positions, etc.

5. Discussion

As mentioned in Section 4.2, some of the objective results require further examination. First of all, the repeatibility of reverberation measurements and their dependence on employed equipment and measuring method. Besides of the results shown in Fig. 1, several other measurements have been done in the listening-room at the same or slightly altered conditions. All results are presented in Fig. 11. The

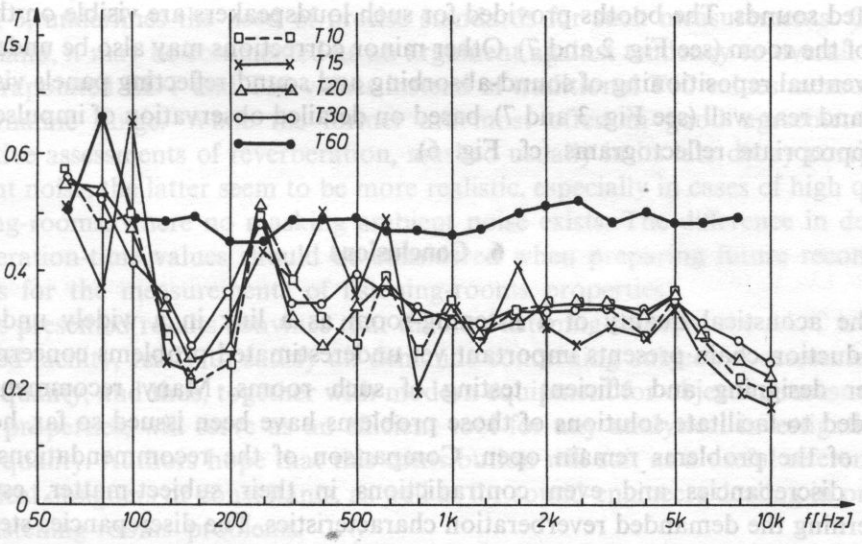

FIG. 11. Comparison of various reverberation characteristics of the listening-room

reverberation time values are processed in dependence on the analyzed portion of the sound-decays relative to 10, 15, 20 or 30 dB. An additional series of measurements has been done using a traditional evaluation of recorded decay-slopes within the 60 dB dynamic range, however, at pistol-shot room excitation.

An inspection of Fig. 11 permits to conclude that the measuring points for EDT marked T10, T15, T20 and even T30 curves are less smooth than the T60 reverberation curve. Most probably resonances within the excited room favour short lasting oscillations, which die quickly enough not to disturb the general rate of decays observed at T60 evaluation. It seems to argue for the use of T60 values rather than T30 as a characteristic parameter of the listening-room reverberation time.

For the lowest one-third octave bands of measurements i.e. 50 and 63 Hz ranges, the results are either inessential or dubious, because of stronger room resonances at lower frequencies. This observation is corroborated by subjective impressions at the listening of music tests. Some very low-pitch sound-sources, e.g. double-basses or

kettle-drums seemed unlocalizable, their resonating sound as if filling the entire room volume uniformly.

It was already noticed that some points of the measured reverberation characteristics shown in Fig. 1, especially in the vicinity of 1 and 3 kHz, did not fulfill the requirements of the design. However, in the light of above discussion such small departures of the prescribed curve seem to be unimportant. Besides, some changes in the room outfitting are foreseen, among other connected with the installation of an additional pair of flush-mounted loudspeakers, which will permit to broaden the base-width for stereophonic reproduction and reduce the amount of very early reflected sounds. The booths provided for such loudspeakers are visible on the front wall of the room (see Fig. 2 and 7). Other minor corrections may also be undertaken, e.g. eventual repositioning of sound-absorbing and sound-reflecting panels visible on side- and rear-wall (see Fig. 3 and 7), based on detailed observation of impulse delays on appropriate reflectograms (cf. Fig. 6).

6. Conclusions

The acoustical quality of a listening-room as a link in a widely understood reproduction chain presents important yet underestimated problems concerning the proper designing and efficient testing of such rooms. Many recommendations intended to facilitate solutions of those problems have been issued so far, however, most of the problems remain open. Comparison of the recommendations shows some discrepancies and even contradictions in their subject-matter, especially concerning the demanded reverberation characteristics. The discrepancies stem from different subjective preferences dependent, first of all, on style of listened music. As only in some highly specialized production-studios and in attached listening-rooms a given style of music may exclusively be recorded and listened to, so, for all other listening-rooms, a reasonable compromise between extreme demands should be accepted. The investigated listening-room of the Aalborg University Centre may serve as a good example of the fulfillment of acceptable compromise demands.

A sensitive dependence of subjective reverberation measurements on an employed measuring method and a minor changes in position of a measuring microphone, as well as of objects within the room, has been demonstrated in practice. It emphasizes the need for a precise specification of requirements to examine the acoustical properties of small rooms, in contrast to medium and large rooms, where only averaged characteristics are taken into considerations.

The properties of a listening-room referred to a specified place within the room may be precisely described due to reflectograms obtained by the use of impulse measurements aided by the technique of two-channel digital analysis. This technique experimented on the investigated example may be, and should be developed in similar future investigations. It may be especially useful for creating conditions of repeatible listening situations for assessments of stereophonic sound images.

The method of reflectograms may be generally applied to proper positioning of loudspeakers and listeners' seats, as well as reflecting or absorbing panels within a room. Such panels existing within the examined listening-room might be optimally positioned depending on concurrently measured reflectograms. Some method facilitating the time-consuming trial-and-error searching for optimal position of every panel should be invented before. Referring to the necessity of precise positioning of the listeners' seats, some method of marking their localization in the room should be applied.

The comparison of results of various reverberation measurements, discussed in section 5, underlines the need of precise standards for such measurements. On the other hand, it may be commented as an argument against tendency to overall use of the extrapolated EDT and T30 values instead of traditional T60 values measured in full dynamic range. While the former are most often in good agreement with subjective assessments of reverberation, masked usually in its late decay portion by ambient noise, the latter seem to be more realistic, especially in cases of high quality listening-rooms, where no masking ambient noise exists. The difference in defining reverberation-time values should be considered when preparing future recommendations for the measurements of listening-rooms properties.

The presented results convince that the new listening-room at the AUC is a well designed facility, ready to satisfy all demands concerning subjective assessments of sound quality, and thus, together with modern equipment for objective measuring of sound properties, will serve as an efficient tool for any analytical investigation on sound quality. Authors hope that this contribution will suit as a useful reference for acoustical designers or consultants, as well as for sound-engineers dealing in practice with listening-rooms problems.

7. Acknowledgement

This publication results from the cooperation between Aalborg Universtiy Centre and Gdańsk Technical University, enabled thanks to the Agreement of Cooperation signed by the Rectors of both Universities.

Authors gratefully appreciate participation of their colleagues of the Aalborg University Centre as well as colleagues from Gdańsk Technical University visiting Aalborg, who helped in the measurements and at preparing materials necessary for the presentation of results.

Appendix: List of recordings used as subjective test

1. G. MAHLER: *Symphony No. 7, Introduction* (*executed* by Frankfurt Symphony Orchestra, conduct. by E. Inbal) CD Denon Digital, No. 1553, 1986.
2. Fr. CHOPIN-MILSTEIN: *Nocturne C sharp minor* (played by Kyung Wha Chung, acc. by Ph. Moll) CD Decca, 1987.

3. C. M. v. WEBER: "*Viktoria, Viktoria*" (Opera Chorus) Deutsche Grammophon, Digital Recording, 1985.
4. J. BRAHMS: *Prelude from Op. 122* (played by Kurt Rapf on the Hammer Organ of the Jesus Christ Church in Berlin–Dahlem) Intercord, Digital Recording, 1985.
5. E. GARDNER: "*Misty*" Jazz – Verve Records. AAD.

(Every item, eventually faded out, lasted about 2 min.; the whole test was rerecorded on tape, using a noise reduction system Dolby C).

References

[1] M. BARRON, *Impulse testing techniques for auditoria*, Applied Acoustics, **17**, 165–181 (1984).

[2] J. BORENIUS, *On loudspeaker response in sound control rooms*, J. Audio Eng. Soc., **29**, 4, 258–261 (1981).

[3] J. BORENIUS, S. U. KORHONEN, *New aspects on listening room design*, 77th AES Conv., Hamburg, Preprint 2184 (C-2), 1985.

[4] M. COLLOMS, *High performance loudspeakers*, Pentech Press, London 1985.

[5] C. L. S. GILFORD, *The acoustic design of talks studios and listening rooms*, J. Audio Eng. Soc., **27**, 1/2, 17–31 (1979).

[6] K. HOJBERG, *Two-channel analysis in room acoustics*, 80th AES Conv., Montreux, Paper C-6, 1986.

[7] W. LAU, K. HUHN, *Der neue Bezugsabhörraum des Rundfunks der DDR*, Bericht von der dreizehnten Tonmeistertagung, S. 216–232, Munchen 1984.

[8] S. P. LIPSHITZ, *Stereo microphone techniques...* J. Audio Eng. Soc., **34**, 9, 716–744 (1986).

[9] A. MUNRO, *Developments in recording and monitoring acoustics*, Studio Sound, pp. 50–54, October, 1980.

[10] H. MØLLER, *Listening rooms for test of loudspeakers*, in Proc. of Symp. on Perception of Reproduced Sound, pp. 125–134, Ed. S. Bech and O. J. Pedersen, Aarhus, 1987.

[11] J. PEDERSEN, *Opforelse af akustiske maalerum ved Aalborg Universitetscenter*, Proc. of Nordic Acoustical Society, pp. 281–284, Aalborg, 1986.

[12] F. E. TOOLE, *Planning of the listening test – Technical and environmental variables*, in Proc. of Symp. on Perception of Reproduced Sound, pp. 41–49, Ed. S. Bech and O. J. Pedersen, Aarhus, 1987.

[13] E. J. VÖLKER, *Control rooms for music monitoring*, J. Audio Eng. Soc., **33**, 6, 452–461 (1985).

[14] J. WRIGHTSON, *Psychoacoustic considerations in the design of studio control rooms*, J. Audio Eng. Soc., **34**, 10, 789–795 (1986).

[15] J. WRIGHTSON, R. BERGER, *Influence of rear-wall reflection patterns in live-end-dead-end-type recording studio control rooms*, J. Audio Eng. Soc., **34**, 10, 796–802 (1986).

[16] *Recommendation No 22 from Technical Committee OIRT "Technical Parameters of Listening Rooms"*. Moscow 1963.

[17] *Empfehlung der technischen Komission der OIRT* Nr 86/1 "OIRT-Bezugs-Abhörraume", Varna 1979.

[18] DIN 45573, Teil 4, "*Lautsprecher-Prüfverfahren-Hörtest*", Deutsche Normen, 1979.

[19] *IEC Report on "Listening test on loudspeakers"*, International Electrotechnical Commission, Publication 268-13, Geneva 1981.

[20] *Technical recommendation from Danmarks Radio*, Norsk Rikskringkasting, Rikisutvarpid, Sveriges Radio, Yleisradio, N 12-A, Listening Conditions in Sound Control Rooms, Danmarks Radio, Soborg, Denmark, 1986.

[21] *Technical recommendation from Danmarks Radio*, Norsk Rikskringkasting, Rikisutvarpid, Sveriges Radio, Yleisradio, N 12-C, Reference listening room, Danmarks Radio, Soborg, Denmark, 1986.

[22] *Taschenbuch Akustik*, Ed. W. Fasold, W. Kraak, W. Schirmer, Verlag Technik, Berlin 1984.

Received on April 4, 1988.

ARCHIVES OF ACOUSTICS
14, 1-2, 61-65 (1989)

PROBLEM OF ACOUSTICAL RELAXATION OF LUTIDINE 3–4

B. LINDE

Institute of Experimental Physics, University of Gdańsk
(80–952 Gdańsk, ul. Wita Stwosza 57)

E. ROSENFELD

Institute of Applied Biophysics, M. Luther University, Halle, GDR

In this paper the results of acoustical absorption measurements in frequency range from 300 kHz to 9 GHz for lutidine 3–4 are presented. An acoustical relaxation process in the low frequency range between 0.3–10 MHz was observed. The relaxation process which has been noticed can be explain as a phenomenon of association and dislocation of sandwich molecules.

W pracy przedstawiono wyniki pomiarów absorpcji akustycznej w 3–4 lutydynie w zakresie częstotliwości od 300 kHz do 9 GHz. Obserwowano proces relaksacji akustycznej w zakresie niskich częstotliwości od 0,3 do 10 MHz. Proces ten można wytłumaczyć jako zjawisko asocjacji i dysocjacji cząsteczek sandwiczowych.

1. Introduction and experimental setup

The ultrasound investigations in many organic liquids indicate that it is necessary to use a set-up which gives a possibility of acoustical absorption measurements in very wide frequency range to obtain the complete information about relaxation processes in such liquids. Usually it is rather difficult.

In this paper we present the ultrasound measurements performed by four different methods. They allowed to cover five decades of frequencies. The frequency range was divided into four intervals and the following methods were applied: 0.3 MHz–3 MHz – the statistical reverberation method [4], 10–180 MHz – the pulse method [10], 0.4–1.3 GHz – the pulse method using the lithium niobate crystal

excited in the resonance cavity [1, 2], and in the highest GHz range for two 6 and 9 GHz(1) – Mandelstam Brillouin scattering method.

2. Investigations and results

The previous results of the measurements of ultrasound velocity as a function of temperature [8] in benzene derivatives liquids suggest the existence of the phase transition that could be due to breaking of the sandwich structures (Fig. 1) as it was assumed by authors conducting NMR investigations [7].

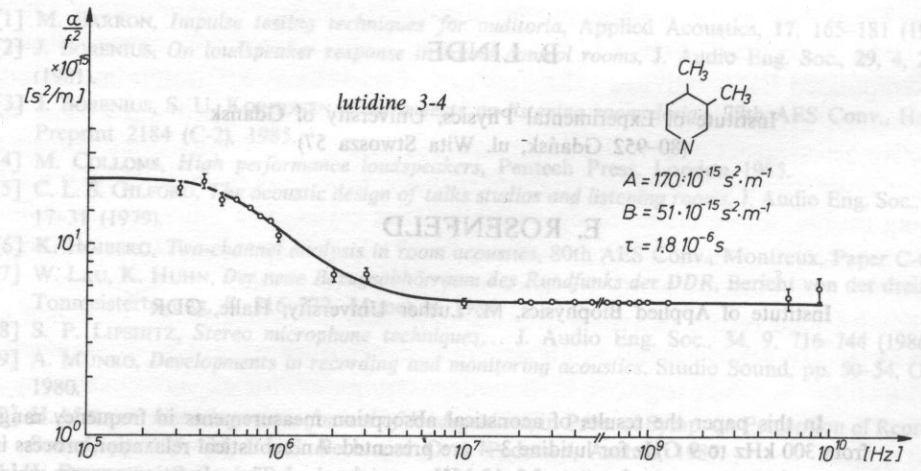

FIG. 1. Sandwich associates

The following investigations of the absorption as a function of frequency (10 MHz–1.3 GHz) [9, 12] showed us that there was no relaxation processes in this frequency range.

However the classical absorption coefficient (defined by expression [6]) is almost five times lower than experimental one (α_{exp}) (Table 1).

Table 1

$\frac{\alpha_{class}}{f^2}\left[\frac{s^2}{m}\cdot 10^{-15}\right]$	$\varrho\left[\frac{kg}{m^3}\cdot 10^3\right]$	η_s[cP]	$c\left[\frac{m}{s}\right]$	$\frac{\alpha_{exp}}{\alpha_{class}}$	$\frac{\alpha_{exp}}{f^2}\left[\frac{s^2}{m}\cdot 10^{-15}\right]$
10.4	0.9625	1.248	1487.9	4.9	51.0

$$\frac{\alpha_{class}}{f^2} = \frac{8\pi^2}{3\varrho c^3}\eta_s, \tag{1}$$

(1) The measurements for these highest frequencies were carried out by T. Pelous and M. Bassier from Laboratoire de Spectrometrie Rayleigh-Brillouin, University of Montpellier.

where c is the velocity of ultrasound waves, ϱ the density and η_s the coefficient of shear viscosity. This result is probably due to the relaxation process (Kneser relaxation [11]) for higher frequency above 10 GHz. Furthermore, the relaxation time calculated from Herzfeld equation [5] (2) is also of order of 10^{-10} s.

$$\tau = \frac{cA}{2\pi^2} \cdot \frac{C_p C_V}{C_i (C_p - C_V)} \tag{2}$$

where A is the acoustical absorption for low frequency, C_p, C_V and C_i specific heats at constant pressure, volume and vibrational specific heat (Table 2). It is possible to

Table 2

Substance	$C_i\left[\frac{\mathrm{J}}{\mathrm{mol\,K}}\right]$	$\frac{\alpha_{exp}}{f^2} - \frac{\alpha_{class}}{f^2} \approx A\left[\frac{\mathrm{s}^2}{\mathrm{m}} \cdot 10^{-15}\right]$	$\tau[\mathrm{s} \cdot 10^{-11}]$
3–4 lutidine	68.6	40.6	1.0

calculate the value of C_i from Planck-Einstein relation (3) using the frequencies of fundamental vibration ν_i determined from infrared or Raman spectra [3].

$$C_i = R \sum_i \frac{\left(\frac{h\nu_i}{kT}\right)^2}{\exp\left(\frac{h\nu_i}{kT}\right) \cdot \left[1 - \exp\left(\frac{h\nu_i}{kT}\right)\right]^2}, \tag{3}$$

where R is the gas constant, h – Planck constant, k – Boltzman constant and T – temperature.

The extension of the measurement frequency range up to 9 GHz (Table 3) did not confirm the existence of the relaxation process. There are two possible ways of

Table 3

f[MHz]	$\frac{\alpha}{f^2}$	f	$\frac{\alpha}{f^2}$	f	$\frac{\alpha}{f^2}$	f	$\frac{\alpha}{f^2}$
0.3	196.0	2.0	70.0	70.0	51.6	700.0	50.7
0.4	214.0	3.0	72.0	80.0	52.0	800.0	51.8
0.5	160.0	10.0	51.1	90.0	50.8	900.0	51.9
0.6	173.0	20.0	50.9	100.0	51.9	1000.0	50.6
0.7	155.0	30.0	51.7	180.0	51.6	1150.0	51.9
0.8	141.0	40.0	50.7	410.0	51.3	1250.0	51.1
0.9	133.0	50.0	50.2	500.0	51.1	6600.0	63 ± 6
1.0	112.0	60.0	51.2	600.0	51.9	9000.0	55 ± 10

explanation: the first one is, that the vibrational spectrum for lutidine 3 4 given in the paper by GREEN et al. [3] is not complete; and the other that the assumption (4) should not be used in calculation of the relaxation time. (Such assumption are usually adopted [5, 11] when the values of C_p and C_v are not accessible.)

$$C_p - C_i \approx 10R \quad \text{and} \quad C_p - C_V \approx 5R. \tag{4}$$

In this case the value of the relaxation time is given by the formula (5)

$$\tau = \frac{A \cdot c}{2\pi^2} \cdot \left(5 + \frac{C_i}{R}\right) \cdot \left(10 + \frac{C_i}{R}\right) \cdot \left(5 \frac{C_i}{R}\right)^{-1}. \tag{5}$$

In the lowest frequency range we have found a typical relaxation region (Fig. 2). The experimental curve α/f^2 can be well described by the relaxation equation (6) [7] with a single relaxation time τ.

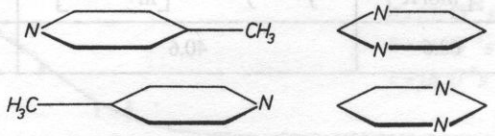

FIG. 2. Absorption coefficient α/f^2 in function of frequency (f) for lutidine 3–4 (for 293 K)

$$\frac{\alpha}{f^2} = \frac{A}{1 + (\omega\tau)^2} + B. \tag{6}$$

Similar relaxation process was found by MOKHTAR et al. [13] for toluene.

3. Conclusion

Acoustical relaxation which was observed in this low frequency range is probably in close connection with process which was mentioned above – association and dissociation of sandwich aggregates. This problem certainly needs further clasification and it is necessary to carry out the temperature investigations to obtain more precise explanation. These investigations give a possibility to calculate the activation energies of the relaxation process and allow to identify molecular process, presented in Fig. 1.

References

[1] В. А. БЕЛИНСКИ, М. КАРАБАУЕВ, А. С. ЛАГУНОВ, *Применение ультраакустики к исследовании вещества*, МОПИ, **24**, 45 (1969).

[2] Р. К. КХАБИБУЛАЕВ, М. И. ШНАКХПАРОНОВ, Акуст. Ж. **18**, 2 (1970).

[3] J. H. S. GREEN, D. T. HARRISON et al., Spectrochim. Acta, **26A**, (1970).

[4] I. ALIG, P. HAUPTMANN et al., Experimentalle Technik der Physik, **30**, 5, 417 (1982).
[5] K. F. HERZFELD, T. A. LITOWITZ, *Absorption and dispersion of ultrasonic waves*, Academic Press, New York and London 1959.
[6] A. J. MATHESON, *Molecular Acoustics*, Wiley-Interscience a Division of John Wiley Sons Ltd, London, New York, Toronto 1971.
[7] J. N. MURRELL, V. M. S. GIL, Trans. Faraday Soc., **61**, 402 (1971).
[8] B. LINDE, H. SZMACIŃSKI, A. ŚLIWIŃSKI, Acta Phys. Pol. **46A**, 5 (1974).
[9] B. LINDE, *Thesis*, Institute of Experimental Physics, University of Gdańsk 1979.
[10] J. WEHR, *Pomiary prędkości i tłumienia fal ultradźwiękowych* [in Polish] PWN, Warszawa 1972.
[11] И. Г. МИХХАУЛОВ, *Основы молекулярной акустики*, Наука, Москва 1968.
[12] B. LINDE, M. KOSMOL, A. ŚLIWIŃSKI, Archives of Acoustics, **11**, 4, 25–55 (1986).
[13] M. MOKHTAR, K. SALAMA, Acustica, **12**, 50–54 (1962).

Received on December 14, 1987.

ARCHIVES OF ACOUSTICS
14, 1-2, 67-96 (1989)

DYNAMICAL MODEL OF THE VOCAL TRACT IN CONSONANT AND NASALIZED ARTICULATION

WANDA NOWAKOWSKA, PIOTR ŻARNECKI

Laboratory of Speech Acoustics
Institute of Fundamental Technological Research, Polish Academy of Sciences
(00-049 Warszawa, ul. Świętokrzyska 21)

In the paper a simulation model of the vocal organ is presented. The model has been programmed in Turbo Pascal for an IBM PC computer. With the use of this model as a research tool the possibilities of analysing the formant structure of the speech signal has been demonstrated in the static states for the cases of oral and nasalized vowels and nasal consonants. For analysed speech sounds the approximate vocal tract cross-sections were determined. An example of simulation of continuous changes of the articulatory tract geometry which take place in natural speech has been presented and the accompanying changes of the phonetical and acoustical structure of the signal has been described. Also potential possibilities of applying the described model to the studies on the phenomenous of coarticulation and articulation in the conditions of forced nasalization has been demonstrated.

W artykule przedstawiono symulacyjny model narządu mowy, zaprogramowany w języku Turbo Pascal na komputerze IBM PC. Za pomocą opracowanego modelu jako narzędzia badawczego, pokazano możliwości analizowania struktury formantowej sygnału mowy w stanach statycznych w przypadku samogłosek ustnych, samogłosek nazalizowanych oraz spółgłosek nosowych. Dla badanych głosek wyznaczono przybliżone przekroje artykulacyjne toru głosowego. Przedstawiono przykład symulowania zmieniającej się w sposób ciągły geometrii toru artykulacyjnego, zachodzącej w mowie naturalnej oraz podano wyniki obserwacji towarzyszących temu zjawisku zmian fonetyczno-akustycznej struktury sygnału. Wykazano także potencjalne możliwości zastosowania opracowanego modelu do badania zjawiska koartykulacji oraz procesu artykulacji w warunkach nazalizacji wymuszonej.

1. Object and aim of the study

For a number of years the investigations of acoustical and phonetic features of a signal have been carried out on the basis of modelling the human articulatory organ. Modelling of the biological vocal tract, pharyngeal-oral-nasal in general case, consists in representing as a physical system its anatomical structure, and mainly its geometrical layout which changes in course of articulation of various speech sounds.

In such, it is also possible, to some extent, to take into account the individual features of the speech organ. In the case of voiced speech sounds the vocal tract model is excited by the simulated quasi-periodical laryngeal source, whereas in the case of other phones, e.g. fricatives and affricates, it is necessary to take into account the noise excitation or both kinds of excitation together. The vocal tract configuration is represented with linear equivalent systems and the nonlinear acoustic quantities which refer mainly to the source characteristics and acoustic properties of the resonance systems formed by the vocal channel are described by the linear equations system according to the generally accepted methodology (VAN DEN BERG [1], FANT [11]).

The computer simulation model of the pharyngeal-nasal-oral vocal tract which is now being worked upon turns back to the earlier works (NOWAKOWSKA [31], NOWAKOWSKA, ŻARNECKI [32, 33]). The model makes it possible to study the phonetical and acoustical features of the speech signal, in particular, the spectral structure of the oral and nasalized vowels and the nasal consonants. This is accomplished by an analysis of the transmittance of the modelled vocal tract system. The software allows for dynamical modelling of the articulatory structures which change in time, as e.g. nasal consonant – vowel syllables. It also makes it possible to model the co-articulation phenomena. These possibilities can occur useful in the automatic system for recognizing isolated words which is currently being elaborated in the Laboratory of Speech Acoustics, IFTR PAS (WIĘŹLAK [39]). The significant advantage of the present model is the possibility of investigating the articulation process in the conditions of forced nasalization that takes place in the case of cleft soft palate, which is the relatively frequent development defect of the speech organ.

2. Development of the analog modelling methods of the vocal tract

The discrete models of the vocal tract proposed in literature have taken diverse forms. The earliest model was the classical Helmholtz resonator which, being an uniresonance system, reproduced the spectral structure of a vowel only within the range of the first formant, what was not sufficient for its phonetical identification (CRANDALL [6]). The two-resonance model consisting of two coupled Helmholtz resonators (FANT [11], KACPROWSKI [20]) also appeared to be insufficient, mainly because of technical difficulties concerned with retuning systems, necessary for precise choice of such acoustical parameters as volume of the resonant cavity and dimensions of the neck, i.e. the acoustic compliance and the acoustic inertance, which describe the resonance frequencies of the system. Therefore, the acoustic models of the form of chained sectors of homogeneous tubes appeared to be far more convenient and susceptible of more precise modelling of the geometrical configuration of the vocal tract in the conditions of articulation that approached reality (DUNN [9], STEVENS and HOUSE [35], FANT [11], COKER [5]). The intense development of acoustic methods of modelling of the speech organ which emerged in

the 50-ies and 60-ies was directed at improving the modelling accuracy of the articulatory tract, what corresponded to an amelioration of acoustical structure of the speech signal and to the elevation of the limit frequency of applicability of the models. This was achieved by increasing the number of elementary cylindrical segments into which the vocal tract has been spatially partitioned by convention. Together with the increase of the number of segments the analog model of the vocal tract becomes an acoustic transmission system with unit parameters continuously distributed in space, the electrical analogue of which is a long line. The first analog voice tract worked out on this basis was a system formed by connecting 25 *T*-type four-terminal networks, each of them representing a cylindrical tract segment of length $l = 0.5$ cm (DUNN [9]). The authors of subsequent gradually improved and now already classical versions of analog configuration models, consisting usually of 17–30 segments, were STEVENS, KASSOWSKI, FANT [35] and FANT [11], STEVENS and HOUSE [36] have developed the articulatory model of vocal tract by adding a simple model of laryngeal source and VAN DEN BERG [1] has worked out an analog subglottal system which co-operated with the channel model. For the first time the numerical control of an analog configuration model was applied by DENNIS [7].

Presently, regarding the development of applications of computer systems, the analog vocal tract model have been replaced by numerical models realized by computer simulation. The essence of the computer simulation process consists in building an algorithm of the mathematical description of a physical structure of a chosen analog model and in finding the values of selected phonetical-acoustic parameters of the speech signal. According to the accessible data the first simulation model of a vocal tract was worked out by KELLY and LOCHBAUM [25]. Since then a number of simulation models have been worked out in diverse scientific centres in the world, mainly in France, Sweden, Japan and USA, the representatives of which are, among others, MRAYATI and GUERIN [29], FLANAGAN, ISCHIZAKA and SHIPLEY [13], MAEDA [27], WAKITA and FANT [37].

The present work is the first attempt in Poland to put forward a simulation model of the vocal tract and to carry out its verification with the phonetical data of Polish language, with reference to the previously developed analog articulatory model (KACPROWSKI [23, 24]).

3. Vocal tract model with variable geometry

The speech organ is anatomically complex in respect of the structure as well as the function. Nevertheless, in order to illustrate the way of modelling the speech signal the anatomical description of this biological system can be greatly simplified by limiting the considerations only to these segments of the articulatory system which are significant from the point of view of their voice generation and articulation functions.

The vocal tract consists of three cavities: pharyngeal, oral and nasal, and their

contribution in shaping the output signal depends on their current configuration; in particular it depends on:

a) the position of the soft palate (Fig. 1),

b) the position and the type of the exciting source (quasi-periodical and/or noise-type).

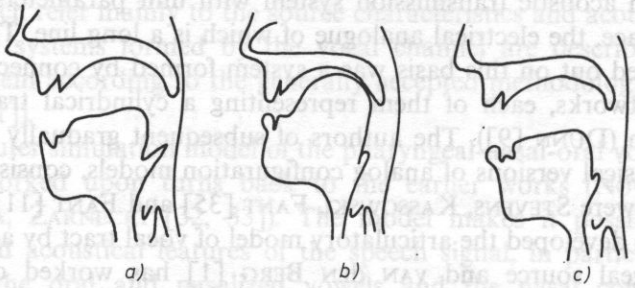

FIG. 1. Scheme of articulation with nasal cavity disengaged (a), with oral cavity disengaged (b) and scheme of oral-nasal articulation (c)

The soft palate can adhere to the back wall of the pharyngeal cavity, thus closing the air passage to the nasal cavity. In this case the air flow coming from the lungs to the larynx passes through the pharyngeal and oral cavities, subsequently (Fig. 1 a). If the soft palate forms the velar closure with the back of the tongue then the oral cavity is blocked off and the air flows through the pharyngeal-nasal cavity and comes out through the nasal appertures (Fig. 1 b). The intermediate position of the soft palate, in which it does not form the closure neither with the back wall of the pharynx nor with the back of the tongue, makes it possible for the air flow to enter both cavities, the oral and the nasal one (Fig. 1 c). In this case air can come out through the mouth and through the nostrils or, if there is an occlusion in some place in the oral cavity, only through the nostrils, as it is in the case of articulation of nasal consonants. Considerable part of the surface of pharyngeal-oral tract walls is formed by the moving articulators of the speech organ: tongue, soft palate, lips and the jaw. Hence, the geometrical configuration, i.e. the shape, length and the volume of the pharyngeal-oral tract is subject to considerable variations during the articulation process; on the contrary, the structure and the geometry of the nasal canal is constant with the exception of the inlet part formed between the uvula and the back wall of the nasal cavity. Shape of the nasal canal does not depend on the articulation conditions and exhibits only individual variations. Therefore, large simplifications can be done considering the shape function of the cross-sectional area of this tract by treating the parallel segments of the nasal canal as one tube of the cross-section equal to the sum of their cross-sections and by approximating the irregular shapes of the cross-sections by an appropriate circular shape. Similarly,

the pharyngeal-oral tract has been represented as a tube with the stepwise variable circular cross-section, constant within the range of subsequent segments. Such an approach is generally known in the literature. The usefulness and rightness of application of the circular approximation, and not, for example an ellyptical one, has been justified by WAKITA and FANT [37], who demonstrated that application of an ellyptical cross-section for the vocal tract yields the comparable results to those obtained with the circular approximation, but considerably increases the complexity of calculations what in consequence prolongs the calculations. In effect these considerations settled the question of the widespread use of models with circular cross-sections.

The basic problem in modelling the voice generating and articulating functions of the speech organ is finding the transmittance function $T(f)$ of the vocal tract, i.e. the ratio of the volume velocities or acoustic pressures in the mouth opening and/or nasal openings and in the glottal opening. The widely applied principle of analog modelling of the vocal tract consists in representing the system as a tube with stepwise variable cross-sectional area, partitioned into a finite number of elementary segments. Every elementary segment of a cylindrical tube of the length l and cross-section A is treated as a lumped-parameter system in a form of an equivalent electrical system, e.g. a four-terminal network. This four-terminal network is described by unit parameters L, C, R and G which are equivalent to the unit parameters of an acoustic tube, i.e. the acoustic inertance, acoustic compliance, friction loss resistance and heat loss conductance. Acoustic impedance of a laryngeal source Z_l (J. KACPROWSKI [22]) and acoustic radiation impedance Z_0 of this openings of mouth and nostrils are replaced by equivalent two-terminal networks (J. KACPROWSKI [20]). In the presented model the pharyngeal-oral tract has been described as a chain-type connection of seventeen ($n = 17$) elementary segments (cylindrical tubes), each of them representing a 1 cm long, tract segment. Assumption of this length of an elementary segment results from the relation of geometrical dimensions of a tract segment and length of the wave which propagates along the tract in the considered frequency range. In the Fig. 2 an elementary segment in the form of a cylindrical tube of length l (a), and it's equivalent four-terminal networks (b), (c) have been presented (KACPROWSKI [22], [24]). Similarly, the pharyngeal-nasal tract has been represented as a chain of twelve ($n = 12$) elementary segments. In both cases, the last segment of the vocal tract is loaded with the radiation impedance of a piston placed in an infinitely large flat baffle board. The radius of the nasal outlet opening is constant and equal to the radius r of the last segment, and on the basis of anatomical data it has been assumed $r = 0.27$ cm.

The equivalent system for a uniform cylindrical tube segment of the length l and cross-sectional area A for both channels is in the considered case a symmetrical T-type four-terminal network the acoustic parameters of which are described by the formulae

$$L = \frac{\varrho l}{A} \tag{1}$$

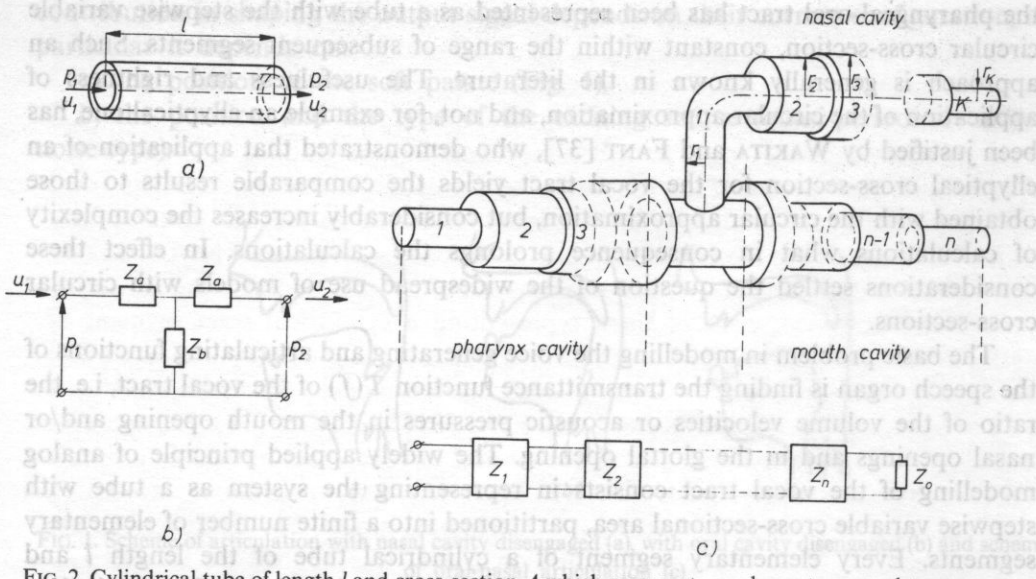

FIG. 2. Cylindrical tube of length l and cross-section A which represents an elementary vocal tract segment (a), its four-terminal network equivalent elements (P – acoustic pressure, U – volume velocity) (b, c)

acoustic inertance of the air in the tube [$kg \cdot m^{-4}$],

$$C = \frac{A \cdot l}{\varrho c^2} \tag{2}$$

acoustic compliance of the air in the tube [$kg^{-1} \cdot m^4 \cdot s^2$],

$$R = \frac{l \cdot S \sqrt{\varrho \mu \omega}}{\sqrt{2} A^2} \tag{3}$$

acoustic resistance of loss caused by viscous friction of the air near tube walls [$kg \cdot m^{-4} \cdot s^{-1}$],

$$G = \frac{(\eta - 1) lS}{\varrho c^2} \sqrt{\frac{\lambda \omega}{2 \xi \varrho}} \tag{4}$$

acoustic conductance of loss due to heat conductivity near the tube walls [$kg^{-1} \cdot m^4 \cdot s$].

The letter symbols used in Eqs. (1)–(4) and applied in the further part of this paper have the following physical meaning and numerical values:

$\varrho = 1.14$ [$kg \cdot m^{-3}$] – air density,

$\mu = 1.86 \cdot 10^{-5}$ [$N \cdot s \cdot m^{-2}$] – air viscosity coefficient in the temperature 37°C,

$\eta = 1.4$ – adiabatic constant of the air,

$\lambda = 2.3 \cdot 10^{-2}$ [$J \cdot deg^{-1} \cdot m^{-1} \cdot s^{-1}$] – thermal conductivity of the air,

$\xi = 10^3$ [$J \cdot deg^{-1} \cdot kg^{-1}$] – specific heat of the air.

Furthermore:
l – length of a single segment [m]
A – area of the tube opening [m^2]
S – parameter of the tube opening [m]
$\omega = 2\pi F$ – pulsation, angular frequency [s^{-1}]

The walls of the biological vocal tract formed of the connective tissue are not ideally rigid and smooth, as it is assumed in simplified considerations, but exhibit some loss and vibrational properties expressed by the surface impedance z_s having an initial character. In the frequency range $f > 100$ Hz this impedance can be represented as a series connection of the resistance r_s and mass m_s

$$z_s = r_s + j\omega m_s, \tag{5}$$

where $r_s[\mathrm{kg \cdot m^{-2} \cdot s^{-1}}]$ and $m_s[\mathrm{kg \cdot m^{-2}}]$ denote the mechanical loss resistance and the co-vibrating mass of wall material of the vocal tract per unit area, respectively. In the literature of the subject a lot of attention has been paid to the problem of finding the numerical values of the unit parameters r_s and m_s. The results of direct measurements carried out "in vivo" and "in vitro" on the connective tissue of human body have been taken as a starting point (cf. e.g. FLANAGAN, ISHIZAKA, SHIGLEY [13], NORD, FANT, BRANBERUD [30]) or the vibrational properties of the appropriately damped physical resonance systems have been studied (VAN DEN BERG [1], DUNN [10], FUJIMURA and LINDQVIST, [14]). The mean values obtained in the measurements and verified in model tests are $r_s \approx 16 \cdot 10^3$ $[\mathrm{kg \cdot m^{-2} \cdot s^{-1}}]$ and $m_s \approx 15$ $[\mathrm{kg \cdot m^{-2}}]$. These values have been introduced into the calculations in the present work. Because of numerical reasons and the reasons concerning the design of the scheme, it is convenient to place the impedance z_s (5) in the transversal branch of the T-type four-terminal network (Fig. 2 b), in the form of the equivalent loss admittance of the vocal tract walls related to the surface S of an elementary segment

$$Y_s = \frac{r_s Sl}{r_s^2 + \omega^2 m_s^2} - j\omega \frac{m_s Sl}{r_s^2 + \omega^2 m_s^2} = G_s + j\omega C_s, \tag{6}$$

where

$$G_s = \frac{r_s Sl}{r_s^2 + \omega^2 m_s^2} \quad [\mathrm{kg^{-1} \cdot m^4 \cdot s}] \tag{7}$$

is the acoustic loss conductance in the voice tract walls, and

$$C_s = \frac{m_s Sl}{r_s^2 + \omega^2 m_s^2} \quad [\mathrm{kg^{-1} \cdot m^4 \cdot s^2}] \tag{8}$$

is the negative acoustic compliance, equivalent to the co-vibrating acoustic mass of the vocal tract walls.

Applying the above formulae, the impedance Z_a of the longitudinal branches of the four-terminal network (according to notations in Fig. 2 b and c) and the

impedance Z_b of the transversal branch have been found as

$$Z_a = \frac{1}{2}(R + j\omega L), \tag{9}$$

$$Z_b = [(G_p + G_s) + j\omega(C_p + C_s)]^{-1}. \tag{10}$$

The analog model of the vocal tract is the system formed as a chain on n such networks (Fig. 2d), each of them representing a tract segment of length l. Every network is described by a chain matrix $\mathscr{A}_i$, $i = 1, 2, \ldots, n$ of the form

$$\mathscr{A}_i = \begin{bmatrix} 1 + \frac{Z_a}{Z_b}; & 2Z_a + \frac{Z_a^2}{Z_b} \\ \frac{1}{Z_b}; & 1 + \frac{Z_a}{Z_b} \end{bmatrix}. \tag{11}$$

The whole system is described by the matrix **A** which is the product of n such matrices A_i (Fig. 2e)

$$\mathbf{A} = \prod_{i=1}^{n} \mathscr{A}_i = \begin{bmatrix} A_{11} & A_{12} \\ A_{21} & A_{22} \end{bmatrix}. \tag{12}$$

The relations between the acoustic input values P_1, U_1 and output values P_2, U_2 of the four-terminal-network model of the vocal tract can be calculated from the matrix equation

$$\begin{bmatrix} P_1 \\ U_1 \end{bmatrix} = \begin{bmatrix} A_{11} & A_{12} \\ A_{21} & A_{22} \end{bmatrix} \begin{bmatrix} Z_0 \\ 1 \end{bmatrix} U_2, \tag{13}$$

where A_{21} and A_{22} are the elements of the chain matrix **A** (12), and opening, U_2 volume velocity in the nasal or mouth opening, Z_0 radiation impedance of the mouth or nose, P_2 acoustic pressure in the mouth or nasal opening.

The transmittance function $T(F)$ calculated for the whole tract is expressed by the relation

$$T = \frac{U_2}{U_1} = \frac{1}{A_{22} + A_{21} Z_0}, \tag{14}$$

where A_{21} and A_{22} are the elements of the chain matrix **A** (12), and

$$P_2 = U_2(f) \cdot Z_0(f) = U_1(f) \cdot T(f) \cdot Z_0(f) \tag{15}$$

where Z_0 acoustic pressure in the mouth opening.

The values of acoustic pressure have been found in relative units by referencing them to the pressure $P_2(F_0)$ where F_0 is the laryngeal tone frequency.

Hence

$$P(F) = \frac{P_2(f)}{P_2(F_0)} = \frac{U_1(f)}{U_1(F_0)} \cdot \frac{Z_0(f)}{Z_0(F_0)} \cdot \frac{T(f)}{T(F_0)}. \tag{16}$$

4. Implementation of the vocal tract simulation model on an IBM PC/XT computer

The model of the speech organ has been programmed in the Turbo Pascal language and implemented on an IBM PC/XT computer. This simulation vocal tract model serves to find the following data:

1. The frequency spectrum of acoustic pressure at the nasal or mouth openings or their sum, according to the Eq. (16), for a given geometrical configuration of the pharyngeal-oral and pharyngeal-nasal tract;

2. The instantaneous values of acoustic signal with the use of the inverse Fourier transform, which serve as input data to a D/A converter and an acoustic amplifier which generates the speech signal.

The earlier works of the authors (NOWAKOWSKA [31, 33]; NOWAKOWSKA, ŻARNECKI [32]) which concerned the development and realization of the vocal tract model allowed for finding an acoustic signal in the mouth and nasal openings for a given static articulatory configuration and for calculating the frequencies of the $F1$, $F2$, $F3$ formants as well as the formant's bands widths $B1$, $B2$, and $B3$. Utilizing the results of simulations and the results of former experiments, a vocal tract model has been constructed which makes it possible to simulate the time-variable articulatory structures. The transition from a static model to a dynamical one necessitates time description of configuration changes of the vocal tract. The structure of the simulation model of the vocal tract and the organization scheme of the program which realizes the model have been shown in the Figs. 3 and 4. The input data for the vocal tract simulation are the labels of the modelled speech sounds. The articulatory description applied here contains the information on the configuration of articulatory organs during fonation, i.e. the articulation tract geometry which corresponds to the given speech sound. Thus, the geometrical description resolves itself to the specification of the lengths l [cm] and the radii of the cross-sections r [cm] of every segment. These data are achieved and can be changed during an experiment in conversation mode by the operator. In the case of dynamical modelling, the signal segment, for one laryngeal tone period, which is stored in the computer memory, corresponds to every stationary part of the sound. Connecting these parts additionally necessitates for modelling the intermediate states resulting from the smooth change of the articulatory system. The smooth changes of the instantaneous values of the acoustic signal during transition from a stationary segment to the next one are obtained by appropriately changing the shape of the amplitude envelope modifying function in every segment, what is done after every period of the laryngeal tone. Up till now the shape of the envelope modifying function has been chosen in an informal way. The calculated frequency characteristic with the basic frequency and the envelope modifying function taken into account and with the use of the inverse Fourier transform allows for calculating a series of instantaneous values of the acoustic speech signal at the mouth opening, nasal openings or both at the same time. The series of instantaneous values are displayed on the printout as a plot. The

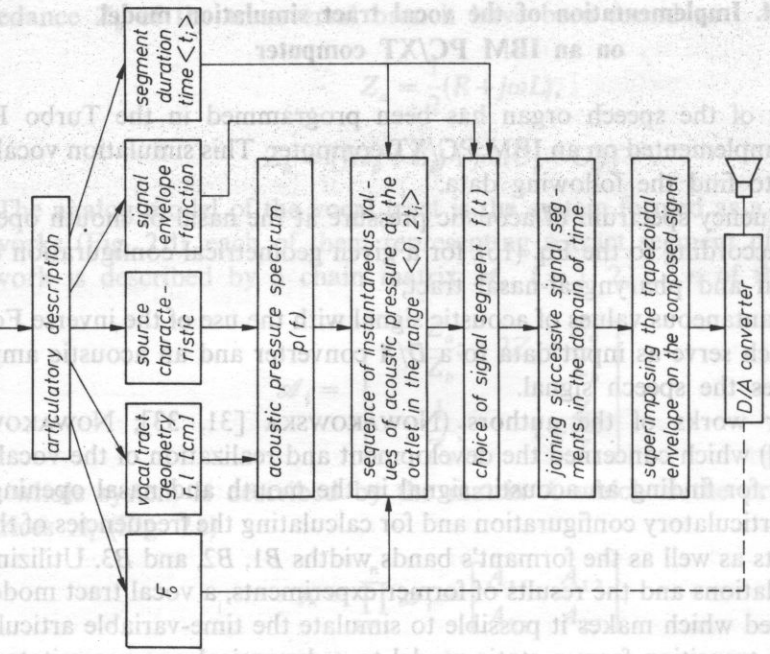

FIG. 4. Algorithm of modelling the signal at the voice tract outlet

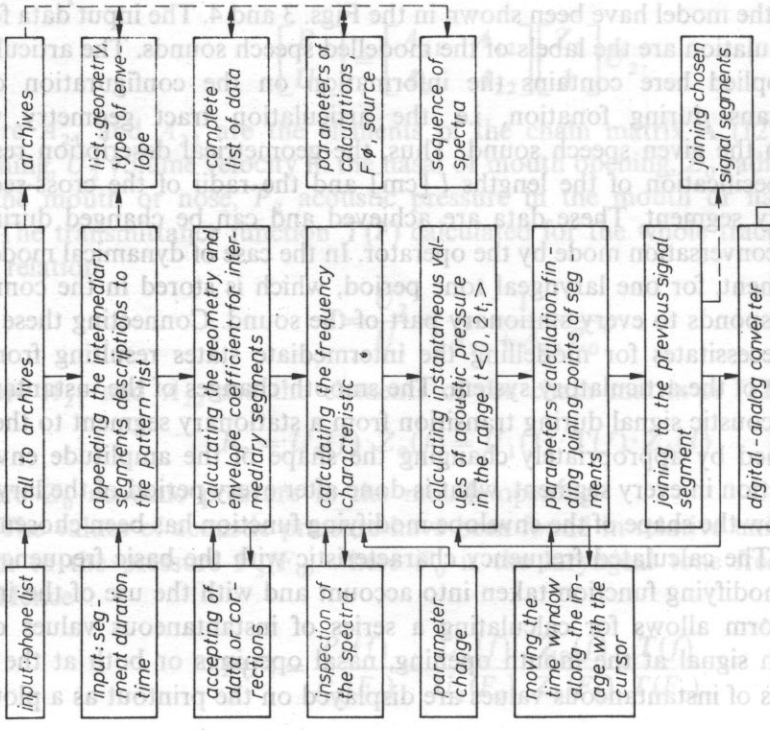

FIG. 3. Operation principle of the program realizing the vocal tract model. Broken lines represent the links which can be used in the case of utilizing the intermediate results stored in memory

calculated series of these values serves as a basis for choice of a time segment to be joined with the next segment. The part of a series is chosen which allows for a smooth signal change on the boundary between the segments when the current segment is chained with the preceding one in a specified time interval. The subsequent stage of signal processing needs the trapezoidal envelope to be imposed, to eliminate the impulse components in the monitored signal. Finally, the obtained signal is sent to an acoustic amplifier through the D/A converter. Calculations of the acoustic pressure complex form, at the mouth and nasal openings are carried out according to the algorithm showed in the Fig. 5 for subsequent vocal tract excitation

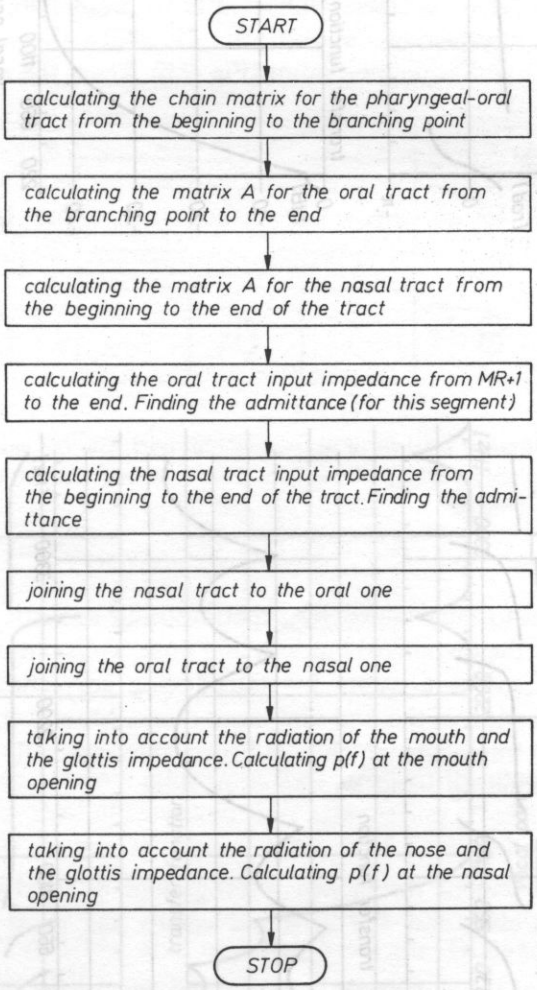

FIG. 5. Realization and way of modelling the articulatory tract for connected nasal and pharyngeal-oral tracts

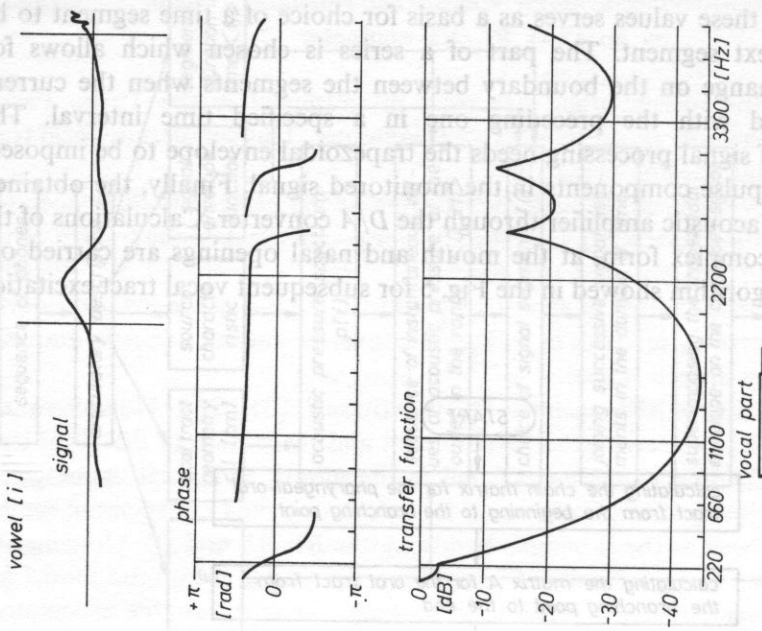
vowel [i]
signal
phase
[rad]
+π
0
-π
transfer function
[dB]
0
-10
-20
-30
-40
220
660
1100
2200
3300
[Hz]
vocal part
pharynx
mouth
nasal part
geometrical configuration
R [cm]
nose mouth
0.87 0.79 1.74 2.00 2.00 2.00 2.00 1.90 1.54 0.87 0.43 0.43 0.43 0.43 0.64 0.89 1.10 0.60 0.27

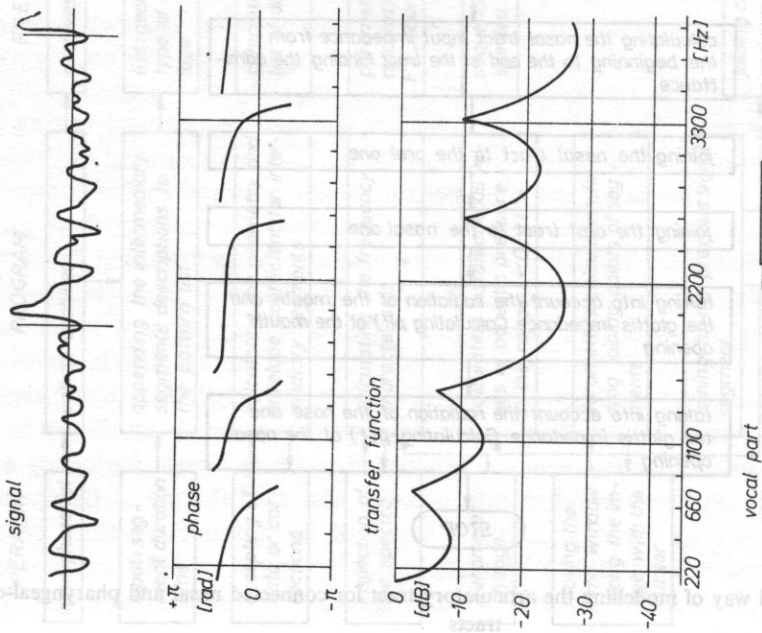
vowel [a]
signal
phase
[rad]
+π
0
-π
transfer function
[dB]
0
-10
-20
-30
-40
220
660
1100
2200
3300
[Hz]
vocal part
pharynx
mouth
nasal part
geometrical configuration
R [cm]
nose mouth
0.80 0.70 1.40 0.98 1.17 1.26 1.12 1.00 1.12 1.26 1.44 1.60 1.70 1.74 1.70 1.70 1.60 1.55 0.27

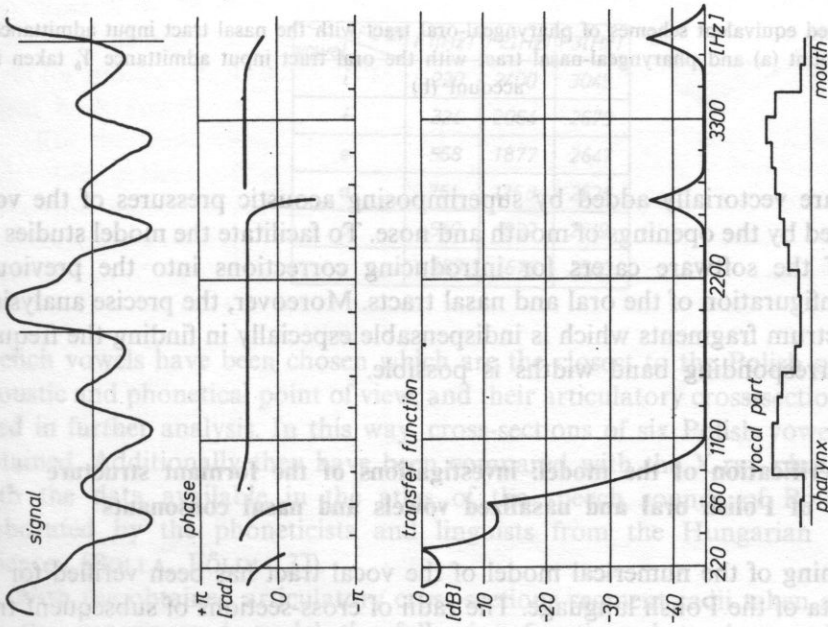

FIG. 6. Frequency characteristic corresponding to the vowels [a, i, u]

frequencies in the range between the initial frequency F_i and the final one F_f, with the specified step F_d. The results are normalized with respect to the acoustic pressure calculated for the reference frequency F_0. The spectrum is updated following the calculation of every current frequency, what gives the possibility of analysing the results before the simulation is finished and allows for corrections. In the printouts the values of the acoustic pressure modulus and phase at the mouth opening are separately plotted. The example printouts with the data concerning the [a], [i] and [u] vowels are presented in Figs. 6a, b, c.

Calculation of the spectrum of an acoustic signal in the case of two tracts being active is carried out as follows. First the acoustic pressure is calculated at the output of the tracts in two cases: a) with the input admittance of the nasal tract Y_n, which shunts the pharyngeal-oral tract, connected in the branching point (Fig. 7a), and b) with the input admittance of the oral tract Y_b, which shunts the pharyngeal-nasal tract, connected in the branching point (Fig. 7b). Then, the output signals from the

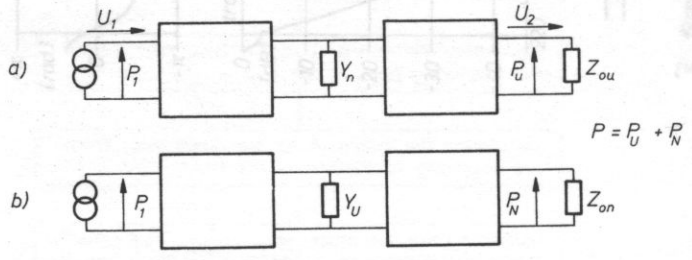

FIG. 7. Simplified equivalent schemes of pharyngeal-oral tract with the nasal tract input admittance Y_n taken into account (a) and pharyngeal-nasal tract with the oral tract input admittance Y_b taken into account (b)

two tracts are vectorially added by superimposing acoustic pressures of the voice waves emitted by the openings of mouth and nose. To facilitate the model studies the structure of the software caters for introducing corrections into the previously specified configuration of the oral and nasal tracts. Moreover, the precise analysis of narrow spectrum fragments which is indispensable especially in finding the frequencies and corresponding band widths is possible.

5. Verification of the model: investigations of the formant structure of Polish oral and nasalized vowels and nasal consonants

Functioning of the numerical model of the vocal tract has been verified for the phonetic data of the Polish language. The radii of cross-sections of subsequent tract segments were the input data for the program. For Polish vowels the detailed

descriptions of articulatory cross-sections of the pharyngeal-nasal tract during fonation do not exist. Those which can be found in various phonetic and phonological works can provide only approximate informations because the articulatory system is considered there as a static object. Because there was no possibility of taking tomographic images of vocal tract during the pronouncement of Polish phones it has been desired to use the indirect method of finding the articulatory cross-sections which has been applied (among others) by MRAYATI [28]. As a starting point the articulatory cross-sections of a pharyngeal-oral tract given in the cited paper have been taken. Comparative analysis of Polish and French vowels in respect of their place of articulation, described by their mutual position in the vowel diagram and their phonetical description based on the frequencies of first three formants $F1$, $F2$, $F3$, has been carried out (Tables 1 and 2). These among the eleven

Table 1. Formant frequencies for French vowels (MRAYATI [28]).

[Hz]	u	o	ɔ	ɑ	a	ɛ	e	i	Y	ø	œ
F1	240	350	510	650	725	510	350	240	240	350	510
F2	750	865	1000	1200	1300	1950	2200	2500	1850	1600	1400
F3	2200	2450	2250	2200	2640	2300	2500	3140	2110	2500	2300

Table 2. Formant frequencies for Polish vowels (JASSEM [19])

vowel \ F [Hz]	F1[Hz]	F2[Hz]	F3[Hz]
i	220	2400	3045
ɨ	324	2064	2679
e	568	1877	2647
a	751	1268	2526
o	540	922	2619
u	285	675	2580

French vowels have been chosen which are the closest to the Polish ones from the acoustic and phonetical point of view, and their articulatory cross-sections have been used in further analysis. In this way, cross-sections of six Polish vowels have been obtained. Additionally they have been compared with the X-ray photographs and with the data available in the atlas of the speech sounds of Polish language elaborated by the phoneticists and linguists from the Hungarian Academy of Sciences (BOLLA, FÖLDI [3]).

With the obtained articulatory cross-sections segment radii taken as input data for the programmed model the following functions have been calculated: the

transmittance functions, frequencies of the formants $F1$, $F2$, and $F3$ and the corresponding formant band widths $B1$, $B2$, and $B3$ of the considered vowels. In the Table 3 the formant frequencies obtained from the model have been compared with the results obtained by other authors.

Table 3. Formant frequencies and formant band widths obtained with the model for Polish vowels (column A), the same data according to JASSEM [19] (column B) and according to WAKITA and FANT [37] (column C).

vowel	F1 [Hz]			B1 [Hz]	
	A	B	C	A	C
ɜ	549		529	15	20
i	255	220	289	23	36
ɨ	320	324		21	
e	441	568	462	16	20
a	647	750	739	26	26
o	600	540	575	20	29
u	291	285	290	24	37

vowel	F2 [Hz]			B2 [Hz]	
	A	B	C	A	C
ɜ	1518		1475	30	41
i	2420	2400	2354	30	29
ɨ	2121	2064		41	
e	1779	1877	2011	30	65
a	1280	1268	1142	40	40
o	1070	922	894	32	30
u	621	675	636	17	24

vowel	F3 [Hz]			B3 [Hz]	
	A	B	C	A	C
ɜ	2490		2443	80	85
i	2890	3045	2888	210	266
ɨ	2530	2679		210	
e	2650	2647	2777	95	234
a	2510	2526	2491	80	64
o	2530	2619	2428	60	32
u	2720	2580	2441	20	26

With the use of the developed model the influence of the phenomenon of nasalization on the spectral structure of the investigated vowels has been studied. Flexibility of the model makes it possible to simulate the types of configuration which differ with each other in an arbitrary way and which in consequence give significantly different formant structures. The aim of the presented analysis is to verify the model as a research tool, by making an attempt of specifying formally and quantitatively the qualitative rules which concern the phenomenon of nasalization, known from the literature.

Studies on the influence of configuration changes on the transmittance functions have been carried out with the following assumptions:

– the point of connection of the nasal canal to the pharyngeal-oral tract have been constant during the analysis;

– the acoustic coupling between tracts expressed by the cross-sectional radius of the first segment of nasal canal, has been variable. In the subsequent simulations the radius was assigned the values $r_1 = 0.001$, 0.2, 0.5, 1.0, 1.4 cm;

– the pharyngeal-oral tract articulation configuration has been variable.

As it is known, the nasalization of vowels manifests itself by perceptible changes in spectral structure. Most generally speaking this phenomenon consists in changes of the spectrum envelope shape and in enriching the formant structure of the spectrum with new minima and maxima. This results from shunting the oral tract by the nasal canal. The examples of the shapes of acoustic pressure characteristics at the mouth and nasal openings for various intertract acoustic coupling values, obtained with the described model, are presented in Figs. 8 a, b, c. The influence of attaching the nasal tract to the oral one on the signal as a whole (from mouth and nose) grows together with the inter-tract coupling and it is more apparent for low frequencies than for the high ones. More detailed analysis of this phenomenon has been carried out for subsequent-formant ranges of the vowels divided into groups of front, central and back vowels.

For the front, closed vowels [i,ɨ] which are characterized by maximal tongue elevation in the front part of the oral cavity and by the low first formant, $F1 \simeq 300$ Hz, the influence of enlarging the degree of coupling between tracts (for r_1 successively assuming the values 0.001, 0.2, 0.5, 1.0, 1.4 cm) consists in the apparent movement of the first formant towards higher frequencies (Fig. 8 a). The similar effect takes place for the following vowels: back [u] (Fig. 8 c) and central [e] (Fig. 8 b). In the second formant range of the front closed vowels [i, ɨ] as the effect of nasalization a clear splitting of the second formant in the total signal spectrum takes place. This is due mainly to the lowering of the spectrum level in this frequency range for the nasal tract. The antiformant which emerges in this way appears for the frequency of about 2500 Hz. This frequency corresponds to the formant $F2$ for the [i] and [ɨ] vowels. The stronger the inter-tract acoustic coupling, the more clear the phenomenon of splitting the second formant. Within the third formant the influence of nasalization on the shape of the investigated signal is much smaller than for the above discussed formant ranges.

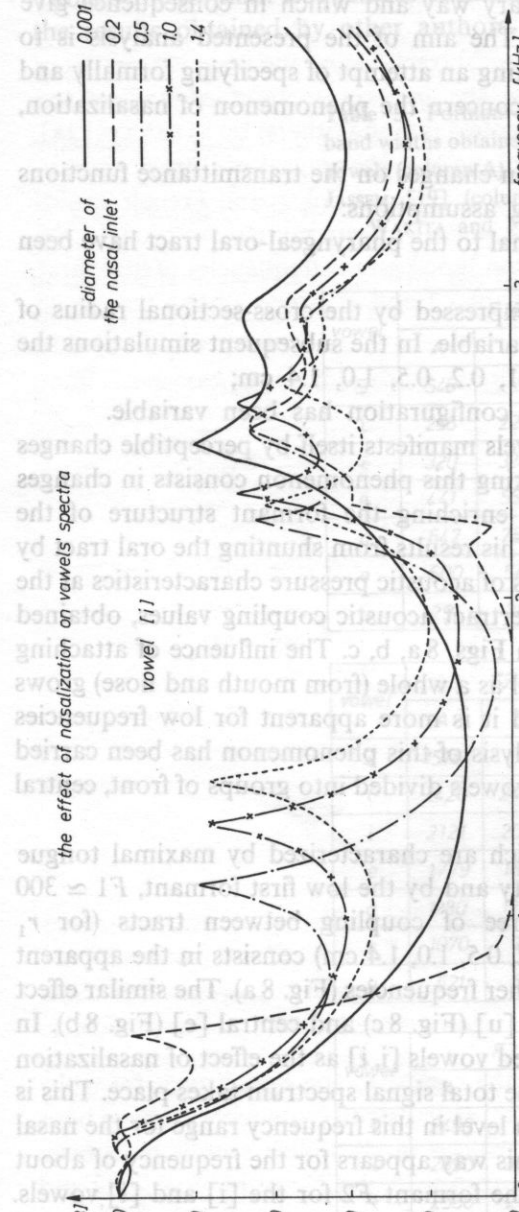
the effect of nasalization on vowels' spectra
diameter of the nasal inlet
0.001
0.2
0.5
1.0
1.4 [cm]
vowel [i]
vowel [ɨ]
frequency [kHz]
[dB]
0
-10
-20
-30
-40
-50
1
2
3
a)

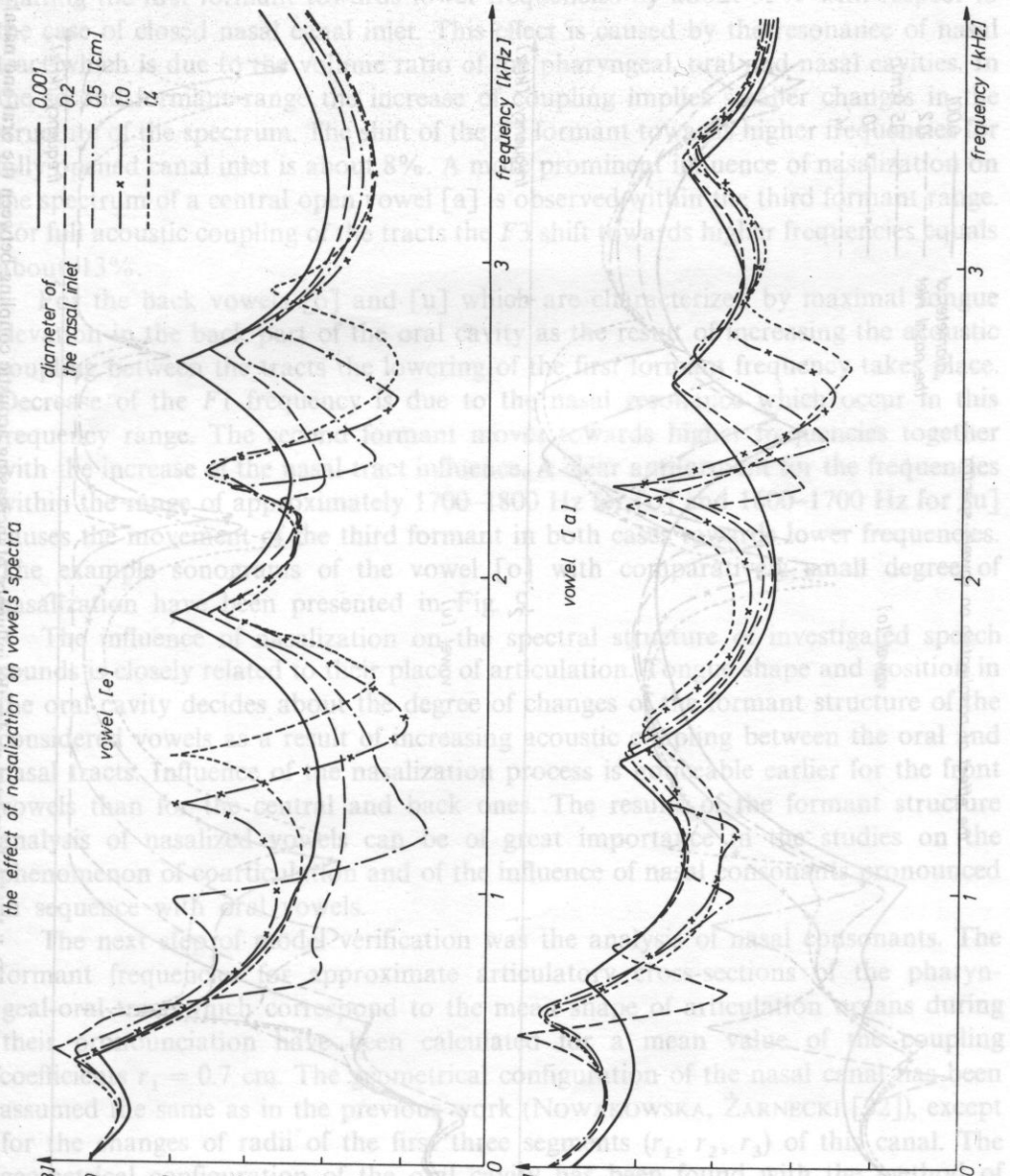
b)
the effect of nasalization on vowels' spectra
diameter of the nasal inlet
0.001
0.2
0.5 [cm]
1.0
1.4
vowel [e]
vowel [a]
[dB]
0
-10
-20
-30
-40
-50
1
2
3
frequency [kHz]

FIG. 8 a, b, c. Formant structure changes of Polish vowels spectra under the influence of increasing acoustic coupling between the oral and nasal tracts

In the case of the central open vowel [a] the nasalization phenomenon for full inter-tract acoustic coupling ($r_1 = 1.4$ cm for the first nasal canal segment) results in shafting the first formant towards lower frequencies by about 33% with respect to the case of closed nasal canal inlet. This effect is caused by the resonance of nasal tract which is due to the volume ratio of the pharyngeal, oral and nasal cavities. In the second formant range the increase of coupling implies smaller changes in the structure of the spectrum. The shift of the $F2$ formant towards higher frequencies for fully opened canal inlet is about 8%. A more prominent influence of nasalization on the spectrum of a central open vowel [a] is observed within the third formant range. For full acoustic coupling of the tracts the $F3$ shift towards higher frequencies equals about 13%.

For the back vowels [o] and [u] which are characterized by maximal tongue elevation in the back part of the oral cavity as the result of increasing the acoustic coupling between the tracts the lowering of the first formant frequency takes place. Decrease of the $F1$ frequency is due to the nasal resonance which occur in this frequency range. The second formant moves towards higher frequencies together with the increase of the nasal tract influence. A clear antiformant for the frequencies within the range of approximately 1700–1800 Hz for [o] and 1600–1700 Hz for [u] causes the movement of the third formant in both cases towards lower frequencies. The example sonograms of the vowel [o] with comparatively small degree of nasalization have been presented in Fig. 9.

The influence of nasalization on the spectral structure of investigated speech sounds is closely related to their place of articulation. Tongue shape and position in the oral cavity decides about the degree of changes of the formant structure of the considered vowels as a result of increasing acoustic coupling between the oral and nasal tracts. Influence of the nasalization process is noticeable earlier for the front vowels than for the central and back ones. The results of the formant structure analysis of nasalized vowels can be of great importance in the studies on the phenomenon of coarticulation and of the influence of nasal consonants pronounced in sequence with oral vowels.

The next step of model verification was the analysis of nasal consonants. The formant frequencies for approximate articulatory cross-sections of the pharyngeal-oral tract which correspond to the mean shape of articulation organs during their pronounciation have been calculated for a mean value of the coupling coefficients $r_1 = 0.7$ cm. The geometrical configuration of the nasal canal has been assumed the same as in the previous work (NOWAKOWSKA, ŻARNECKI [32]), except for the changes of radii of the first three segments (r_1, r_2, r_3) of this canal. The geometrical configuration of the oral cavity has been found with the method of successive approximations according to the criterion of the frequency characteristic conformity in respect of the displacement of poles and zeros with the data given by JASSEM [19] which concerned the nasal consonants articulation and their formant frequencies. In order to find an approximate oral tract configuration during the pronounciation nasal consonants an analysis of the influence of the oral tract length

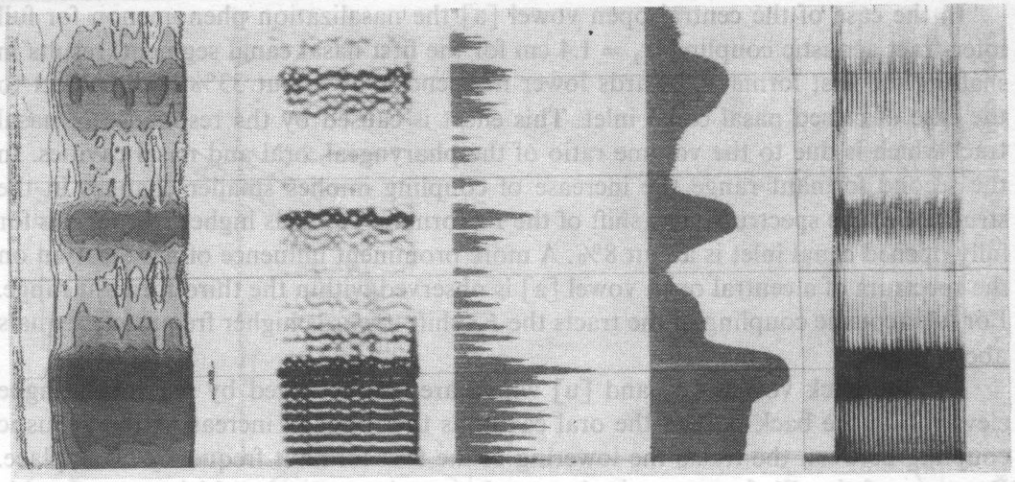

a)

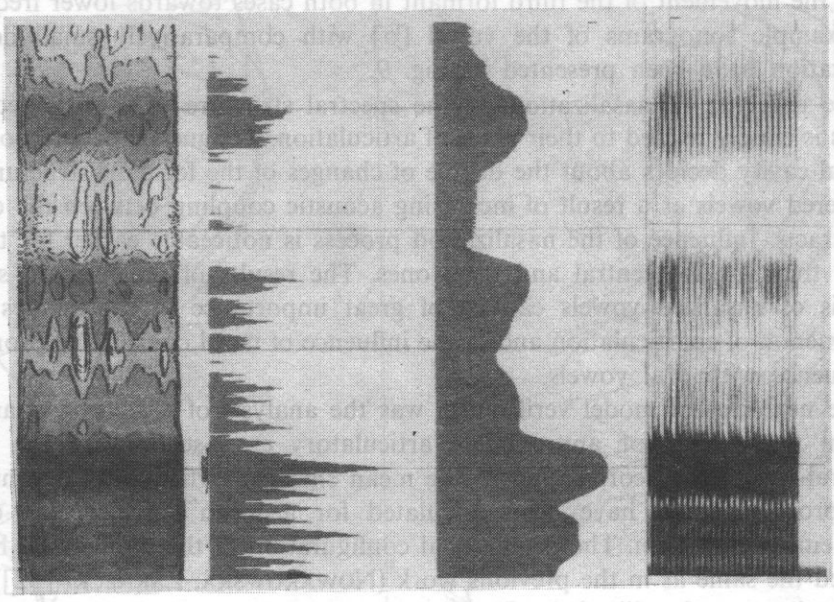

b)

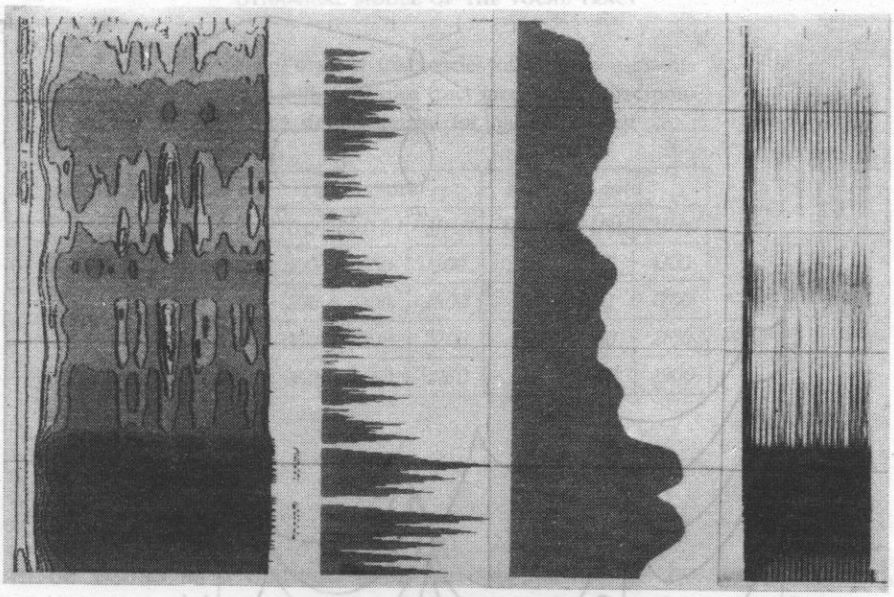

FIG. 9. Sonogram of the vowel [o] in the case of oral (a) and nasalized articulation $r_1 = 0.1$ cm (b) and $r_2 = 0.2$ cm (c). From left to right there are presented: three-dimensional spectrogram with 5 dB level contours, spectral cross-section with a band-pass filter of width 45 Hz, spectral section with a band-pass filter of width 300 Hz and three-dimensional spectrogram with the 300 Hz filter

on the displacement of poles and zeros for a constant, average acoustic inter-tract coupling has been carried out. The oral tract length was being reduced from the seventeenth segment to the eleventh one, for constant cross-section along the whole tract. The frequency characteristics corresponding to various oral tract lengths have been shown in Fig. 10. In the first approximation it can be assumed that during the articulation of a nasal consonant [m] this length equals 17 segments; for the consonant [n] – 14–15 segments, for [ɳ] about 12–13 segments and for [ŋ] – 10 11 segments. Basing on the above analysis and the data presented in the paper BOLLA, FÖLDI [23] the approximate articulatory cross-sections of the pharyngeal-oral tract for nasal consonants articulation have been found and the formant frequencies have been calculated (Table 4). The acoustic pressure courses at the mouth and nasal openings for hypothetical articulation cross-section of nasal consonants obtained with the computer model are displayed in Figs. 11 a, b, c, d.

In the nasal consonants spectra the formant caused by the pharyngeal cavity resonance with frequency about 300 Hz dominates. The formant resulting from the oral resonant cavity partly coincides with the nasal formants. The formant frequencies of the given speech sounds depend on the length of the oral resonant

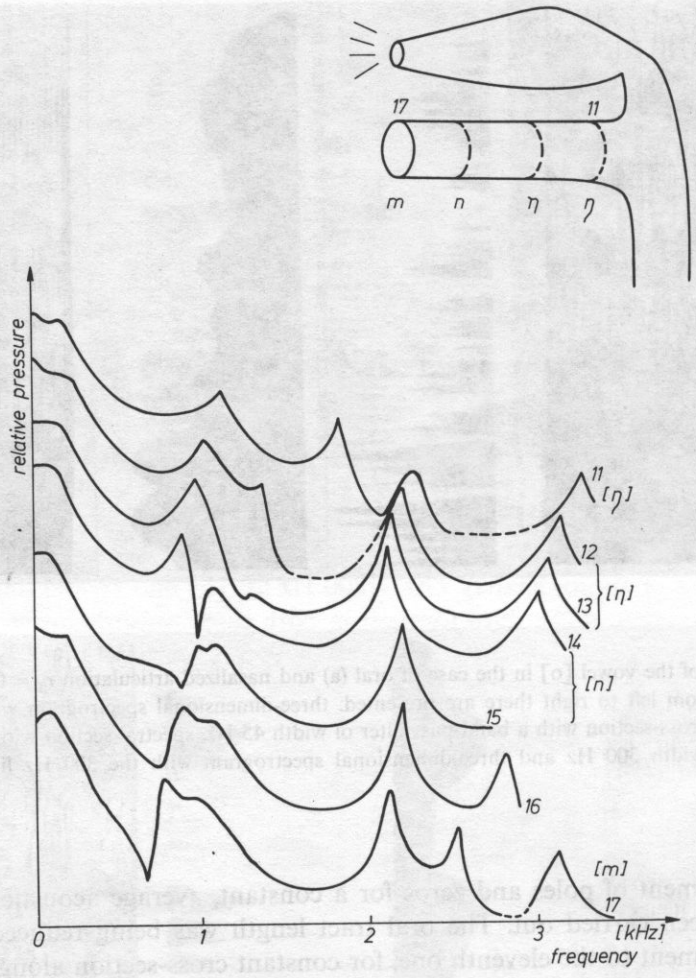

FIG. 10. Frequency characteristics of the signal generated with diverse oral tract lengths from 11 to 17 segments

cavity coupled in parallel with the pharyngeal-nasal tract with closed outlet, in the case of [m] and [n]. The dependence is such that the longer the cavity the lower the formant frequencies. In the spectrum of the nasal consonant an antiformant appears which usually manifests itself as a clear amplitude level decrease in a certain frequency range, characteristic for a given speech sound. This phenomenon takes place if an antiformant appears between the formants, whereas in the case of an antiformant which is near one of the formant frequencies the effect can be blurred to some extent. In general, the influence of a formant is stronger and an antiformant

Table 4. Formant frequencies of nasal consonants obtained with the voice tract model and corresponding data obtained for natural speech

	from model			phonetic data		
	F1[Hz]	F2[Hz]	F3[Hz]	F1[Hz]	F2[Hz]	F3[Hz]
[m]	300	900	1300	300	750	1300
[n]	300	1100	1600	320	1100	1700
[ɲ]	350	1200	2200	350	1250	2100
[ŋ]	350	1160	2160	350	1100	1900

cases to be visible as a distinct, characteristic saddle in the spectrum level, but manifests itself as a considerable level decrease of a superimposing formant. The antiformant frequency depends mainly on the oral tract length in such a way that the longer the length, the lower the frequency.

The above discussed results concerned the modelling of the speech sounds for a constant configuration of pharyngeal-oral-nasal tract. For verification of the model in the dynamical state an example of time-varying articulatory tract configuration has been chosen which corresponds to a syllable of the type: nasal consonant – vowel, i.e. a syllable [ma] which stationary segments [m] and [a] had been analyzed and discussed before.

The essence of the modelling of dynamical assemblies is the appropriate description of articulatory configurations of successive intermediary segments in the transition from one sound to another. The involved changes on a boundary between stationary sounds have been assumed to be proportional. This means that the slow process of opening the mouth when pronouncing [m] is accompanied by simultaneous process of closing the inlet to the nasal canal to obtain [a]. Such description of dynamics of the movements of articulatory organs is a considerable simplification notwithstanding this it allows to observe the changes in the spectral structure caused by articulatory movements. This simplifying assumption is not completely irrelevant to the real working conditions of the speach organ, the cases of synchronization of such type having been known e.g. in French language in the Parisian pronounciation, in some Polish dialects and in not very solicitous colloquial speech (WIERZCHOWSKA [38]). In the Fig. 12 the three-dimensional image of spectrum changes of the syllable [am] has been shown. This dynamical spectrum in the domains of time, frequency and amplitude level shows in a synthetic way the moments of formants and antiformant. Gradual vanishing of the first and second formant range of the [a] is visible and emering of the nasal antiformant of the [m].

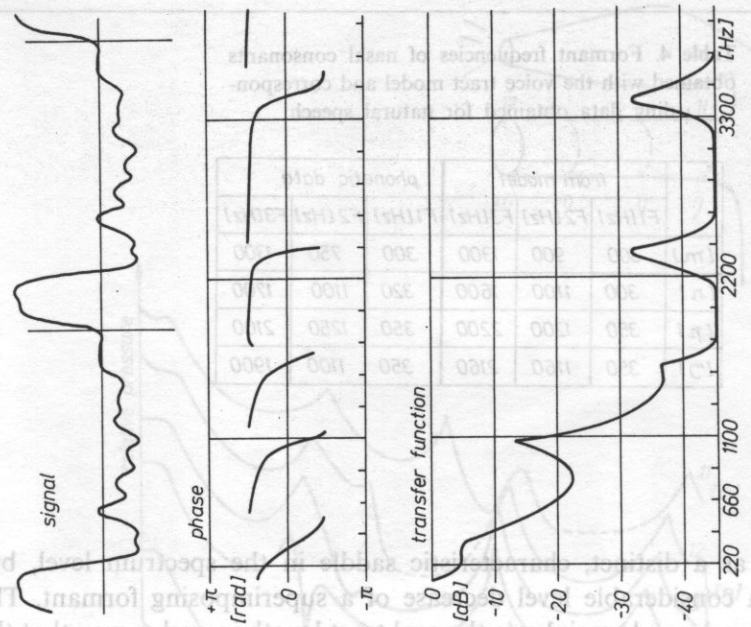
nasal [n]
signal
phase
+π
[rad]
0
-π
transfer function
0
[dB]
-10
-20
-30
-40
220
660
1100
2200
3300
[Hz]
vocal part
pharynx
mouth
nasal part
geometrical configuration
R [cm]
nose
mouth
0.70
0.95
1.26
1.12
1.10
1.00
0.98
0.70
0.75
0.80
1.20
1.10
1.48
1.00
1.48
0.60
0.91
0.35
0.91
0.01
0.91
0.91
0.60
0.60
0.27

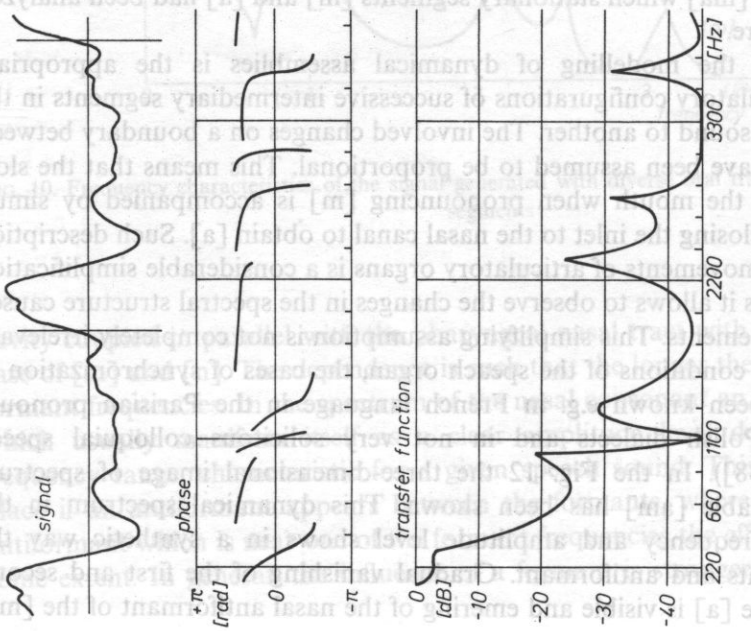
nasal [m]
signal
phase
+π
[rad]
0
-π
transfer function
0
[dB]
-10
-20
-30
-40
220
660
1100
2200
3300
[Hz]
vocal part
pharynx
mouth
nasal part
geometrical configuration
R [cm]
nose
mouth
0.70
0.95
0.75
1.00
0.80
1.10
1.48
1.20
1.48
1.20
0.91
1.10
0.91
0.90
0.91
0.90
0.91
0.50
0.60
0.01
0.60
0.60
0.27

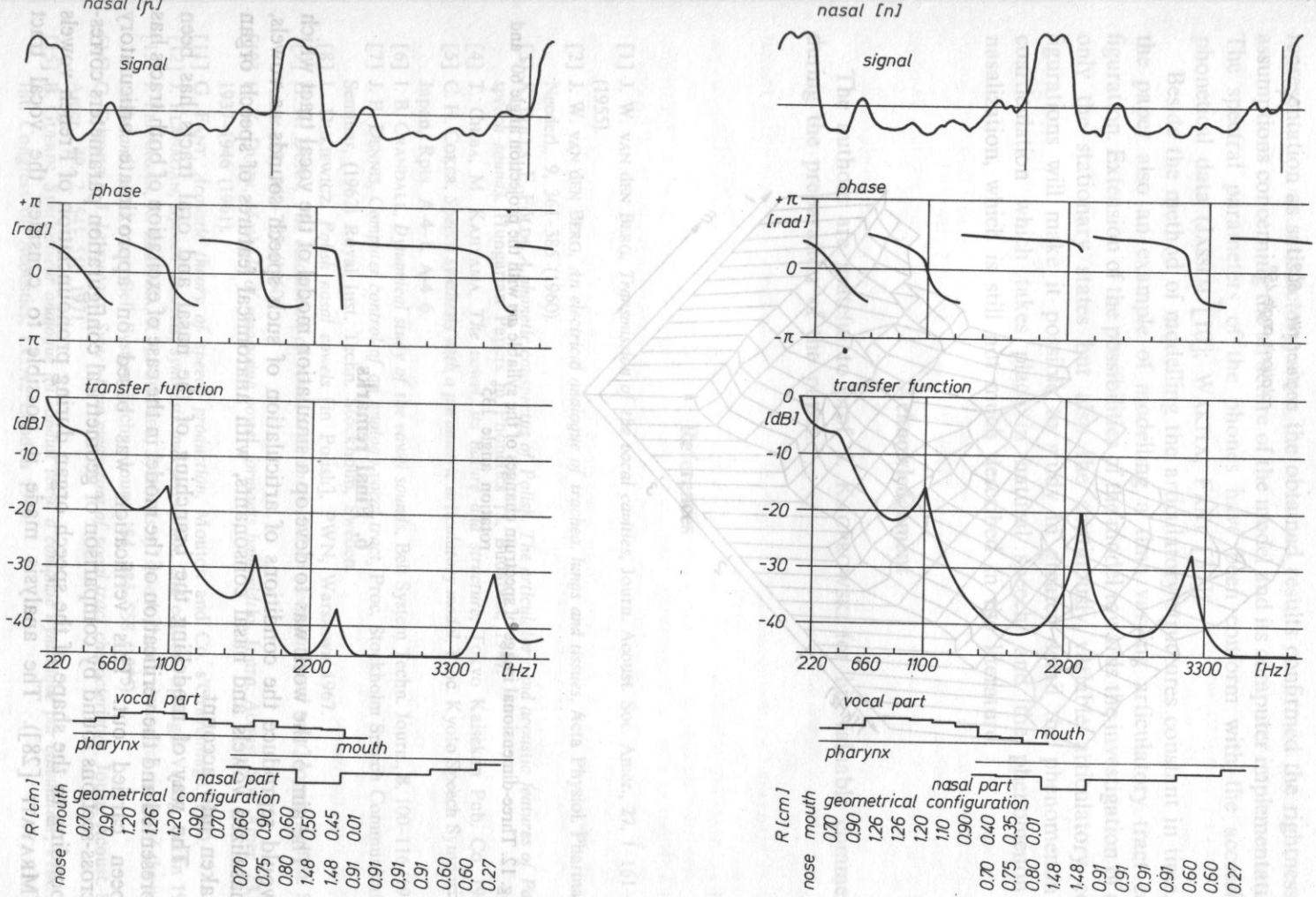

FIG. 11 a, b, c, d. Frequency characteristics of Polish nasal consonants obtained with the model

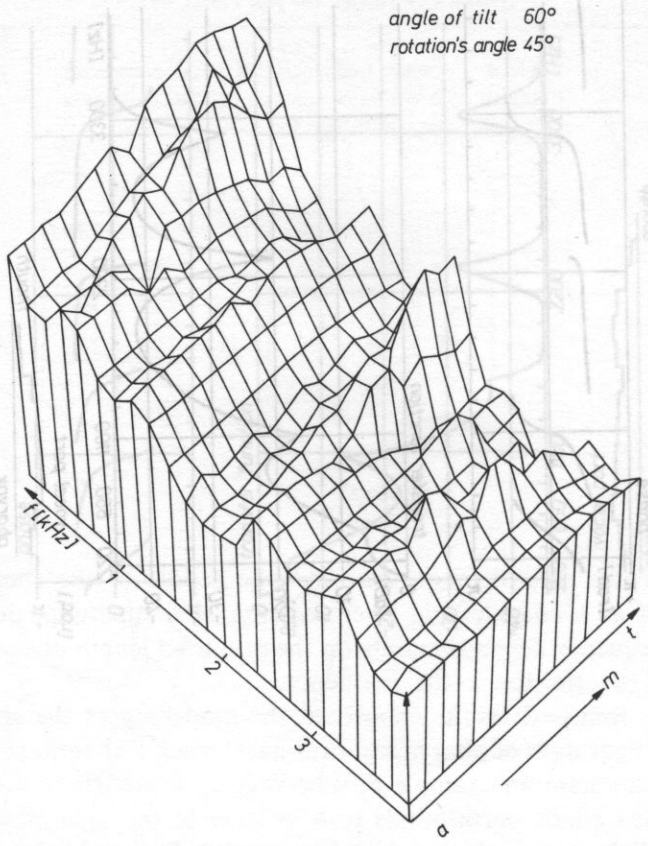

Fig. 12. Three-dimensional image of spectrum changes of the syllable *am* with the projection angle 60° and rotation angle 135°

6. Final remarks

The aim of the work was to develop a simulation model of the vocal tract which would reproduce the conditions of articulation of such speech sounds as vowels, nasalized vowels and nasal consonants, with anatomical features of speech organ taken into account.

The way of modelling the branching of the nasal and oral tracts has been presented and the verification of the model in the case of excitation of both tracts has been carried out. This verification was based on approximate articulatory cross-sections found by comparison of geometrical configuration parameters corresponding to the shape of the speech organ during pronounciation of French vowels (MRAYATI [28]). The analysis made it possible to consider the vocal tract

representation as satisfactory, since the obtained results confirmed the rightness of assumptions concerning the structure of the model and its computer implementation. The spectral parameters of the phones have been conform with the accessible phonetical data (JASSEM [10]; WAKITA, FANT [37]).

Beside the method of modelling the articulatory structures constant in time, in the paper also an example of modelling a time varying articulatory tract configuration. Extension of the possibilities of the model towards the investigation of not only the stationary states but also the continously variable articulatory configurations will make it possible to study in greater detail the phenomenon of coarticulation which takes place in natural speech, and the phenomenon of nasalization, which is still not much described in the literature.

Acknowledgement

The authors are grateful to prof. J. KACPROWSKI for his valuable comments during the preparation of the paper.

References

[1] J. W. VAN DEN BERG, *Transmission of the vocal cavities*, Journ. Acoust. Soc. Amer., **27**, 1–161–168 (1955).

[2] J. W. VAN DEN BERG, *An electrical analogue of trachea, lungs and tissues*, Acta Physiol. Pharmacol. Neederl., **9**, 361–385 (1960).

[3] K. BOLLA, E. FÖLDI, *A phonetic conspectus of Polish. The articulatory and acoustic features of Polish speech sounds.* Hungarian Papers in Phonetics 18, Budapest, 1987.

[4] T. CHIBA, M. KAJIYAMA, *The vowel, its nature and structure*, Tokyo Kaisekan Pub. Co, 1941.

[5] C. H. COKER, *Speech synthesis with a parametric articulatory model*, Proc. Kyoto Speech Symposium, Japan, Rpts. A-4–1, A-4–6.

[6] I. B. CRANDALL, *Dynamical study of the vowel sounds*, Bell System Techn. Journ., **8**, 100–116 (1927).

[7] J. B. DENNIS, *Computer control of an analogy vocal tract*, Proc. Stockholm Speech Communication Seminar, (1962) Royal Inst. Techn. Stockholm, Sweden.

[8] L. DUKIEWICZ, *Polish nasal vowels* [in Polish], PWN, Warszawa 1967.

[9] H. K. DUNN, *The calculation of vowel resonances and an electrical vocal tract*, Journ. Acoust. Soc. Amer. **22**, 740–753 (1950).

[10] H. K. DUNN, *Methods of measuring vowel formants bandwidths*, Journ. Acoust. Soc. Amer. **23**, 12, 1937–1946 (1961).

[11] G. FANT, *Acoustic theory of speech production*, Mouton and Co. s'Gravenhage, 1960.

[12] J. FLANAGAN, *Speech analysis, synthesis and perception*, 2nd edition, Springer-Verlag, Berlin 1972.

[13] J. FLANAGAN, K. ISHIZAKA, K. L. SHIPLEY, *Synthesis of speech from a dynamical model of the vocal cords and vocal tract*, Bell System Techn. Journ., **54**, 485–558 (1975).

[14] G. FUJIMURA, J. LINDQVIST, *Sweep-tone measuring of vocal tract characteristics*, Journ. Acoust. Soc. Amer., **49**, 2, 541–558 1971.

[15] B. GUERIN, *Synthetiseur analogue du conduit vocal a comande dynamique par calculateur*, Proc. 8th Int. Congress on Acoustics, I.C.A., London 1974.

[16] H. L. HECKER, *Studies of nasal consonants with an articulatory speech synthesizer*, Journ. Acoust. Soc. Amer., 34, 179–188, 1962.
[17] J. M. HEINZ, *An analysis of speech spectra in terms of a model of articulation*, Proc. Stockholm Speech Communication Seminar, Royal Inst. Techn., Stockholm, 1962.
[18] K. ISHIZAKA, *On model of the larynx*, Journ. Acoust. Soc. Amer. **22**, 293–294 (1968).
[19] W. JASSEM, *Foundations of acoustic phonetics* [in Polish] PWN, Warszawa 1979.
[20] J. KACPROWSKI, *Theoretical bases of the synthesis of Polish vowels in resonance circuits*, in: Speech Analysis and Synthesis vol. 1 [ed.] W. Jassem, PWN, Warszawa, 219–287 (1968).
[21] J. KACPROWSKI, W. MIKIEL, A. SZEWCZYK, *Acoustical modelling of cleft palate*, Archives of Acoustics, **1**, 2, 137–158 (1976).
[22] J. KACPROWSKI, *Physical models of the larynx source*, Archives of Acoustics, **2**, 1, 47–70 (1977).
[23] J. KACPROWSKI, *A simulative model of the vocal tract including the effect of nasalization*, Archives of Acoustics, **2**, 4, 236–256 (1977).
[24] J. KACPROWSKI, *An acoustical model of the vocal tract for the diagnostics of cleft palate*, in: Speech Analysis Synthesis, vol. 5 [ed.] W. Jassem, PWN, Warszawa, 165–183 (1981).
[25] J. L. KELLY, C. LOCHBAUM, *Speech synthesis*, Proc. Stockholm Speech Communication Seminar, Royal Inst. Techn., Stockholm, (1962).
[26] D. MADEJ, W. NOWAKOWSKA, *Realisation of a microcomputer model of speech signal generator* (in Polish), IFTR Reports 3 (1986).
[27] S. MAEDA, *A digital simulation method of the vocal tract system*, Speech Communication, **1**, 3–4, 199–229 (1982).
[28] M. MRAYATI, *Contribution aux études sur la production de la parole*. These de Docteur d'Etat. Institut National Polytèchnique de Grenoble.
[29] M. MRAYATI, B. GUERIN, *Étude des caracteristiques acoustiques des voyelles orales françaises par simulation du conduit vocal avec pertes*, Revue d'Acoustique, **9**, 36, 18–32 (1976).
[30] L. NORD, G. FANT, P. BRANDERUD, *A note on the vocal tract impedance*, STL-QPSR, **4**, 13–20 (1976).
[31] W. NOWAKOWSKA, *A simulation model of pharyngeal-oral voice tract* (in Polish), IFTR Reports 41 (1983).
[32] W. NOWAKOWSKA, P. ŻARNECKI, *Preliminary model investigations on the influence of nasalization phenomenon on the spectral structure of vowels* (in Polish), IFTR Reports 39 (1984).
[33] W. NOWAKOWSKA, *Investigations of the influence of nasalization on the spectral structure of Polish vowels and consonants* (in Polish), IFTR Reports 46 (1985).
[34] G. ROSEN, *Dynamic analog speech synthesizer*, Journ. Acoustic. Soc. Amer., **30**, 201–209 (1958).
[35] K. N. STEVENS, S. KOSSOWSKI, G. FANT, *An electrical analog of the vocal tract*, Journ. Acoust. Soc. Amer., **25**, 734–742 (1953).
[36] K. STEVENS, A. HOUSE, *Development of a quantitative description of vowel articulation*, Journ. Acoust. Soc. Amer. **27**, 484–493 (1955).
[37] H. WAKITA, G. FANT, *Toward a better vocal tract model*, STL-QPSR, **1**, 9–29 (1978).
[38] B. WIERZCHOWSKA, *Phonetics and phonology of the Polish language* (in Polish) Ossolineum Warsaw (1980).
[39] W. WIĘŹLAK, *Application of the simplified articulatory description of speach signal to the recognition of a limited set of isolated words* (in Polish), Ph.D. thesis, IFTR PAS Warsaw (1987).

Received on February 2, 1988.

ARCHIVES OF ACOUSTICS
14, 1-2, 97-109 (1989)

STUDY OF THE AE FREQUENCY SPECTRA OF SOME ROCKS

MARIE-CHRISTINE REYMOND

E. R. Mecanique des Surfaces, C.R.N.S., Laboratoire Central des Ponts et Chaussées
(58, Boulevard Lefèbvre, 75732 Paris CEDES 15)

ANNA JAROSZEWSKA

Institute of Fundamental Technological Research, Polish Academy of Sciences
(00-049 Warszawa, ul. Świętokrzyska 21)

Results of investigation of the acoustic emission frequency spectra in sandstone, dolomite and marble samples under uniaxial incremental compressive load are presented. The measurements of AE peak hold spectra within each incremental loading cycle in frequency range from 100 Hz–100 kHz, and averaged over 30 s interval spectra in the range from 5 kHz to 100 kHz, were made.

It was found that for nonhomogeneous rocks i.e. sandstone and dolomite the dominant frequency bands shifted towards higher frequencies with the increase of load. Prior to failure of these samples, the increase of low frequency components was observed. For the marble (carrare) which has more homogeneous structure the spectra were less differentiated and their evolution less pronounced.

The results obtained support the hypothesis of stress concentration on limits of the defects in regions of eventual failure planes. The observed increase of low frequency components could be used in practice in the prediction of failure of heterogeneous rocks.

W pracy przedstawiono wyniki badań widma częstotliwości emisji akustycznej próbek: piaskowca, dolomitu i marmuru, w funkcji jednoosiowych obciążeń ściskających, wzrastających skokowo. Wykonano pomiary maksymalnych gęstości widmowych AE, procedurą „peak hold", dla każdego cyklu obciążenia w zakresie częstotliwości 100 Hz–100 kHz oraz widm uśrednionych w czasie 30 s, w zakresie 5 kHz – 100 kHz.

Stwierdzono, że dla skał niejednorodnych: piaskowców i dolomitów LGOM, zakresy widma o maksymalnych gęstościach amplitudy przesuwały się ze wzrostem obciążenia w kierunku dużych częstotliwości. Bezpośrednio przed zniszczeniem tych skał obserwowano wzrost składowych o małych częstotliwościach. Dla marmuru (carrare), o jednorodnej strukturze, widma były mniej zróżnicowane a ich ewolucja mniej wyraźna.

Otrzymane wyniki badań potwierdzają hipotezę o koncentracji naprężeń na powierzchni wad, w strefach przyszłego zniszczenia. Obserwowany wzrost składowych o małych częstotliwościach może być wykorzystany w praktyce do przewidywań rozpadu skał niejednorodnych.

1. Introduction

The evolution of acoustic emission has been used in investigation of structure and of mechanical failure process of rock subjected to external stress. The present work has been aimed at the investigation of the AE accompanying the fracturing process of some rocks: dolomite, sandstone and marble, under uniaxial compression leading to failure. Specifically the AE frequency spectra evolution of these rocks were investigated, and found to provide significant information pertaining to the nature of fracturing process. The available experimental data on the AE frequency spectra evolution during the deformation of rocks indicate, that the observed shift towards low or high frequencies with increasing stress, remains open to question. CHUGH et al., KUSUNOSE et al., OHNAKA and MOGI and also REYMOND [1, 7, 8, 9, 10, 12, 13], examined the AE frequency spectra of the rocks under uniaxial incremental load, however, their observations were not fully consistent.

One of the first general studies on the AE frequency spectra belonging to classics but still of importance today, was published by CHUGH et al. [1]. The subject of investigation was the AE frequency spectra of a limestone, sandstone and granite samples under increasing tensile stress in the frequency range between 0.5 and 15.0 kHz only. The results of this work could be summarized as follows:

– each of the examined rocks was characterized by one or several dominant frequency bands (DFB) in which the most of AE energy was generated.

– for high stresses, the energy of acoustic emission increased in the range of higher frequencies.

KUSUNOSE et al. [7] studied the AE in granite samples under uniaxial compression in the range of frequencies from 100 kHz to 1 MHz. The comparative analysis of the most pronounced AE amplitudes in 5 μs intervals and frequency ranges: from 100 to 400 kHz and from 500 kHz to 1 MHz, indicates, that in accordance with the theory given in their work, waveforms of acoustic emission were more abundant in high frequency components as the applied stress increased.

OHNAKA and MOGI [8, 9, 10] carried out the comparative analysis of the AE event rate monitored through the windows of different frequency bands in the range from 10 kHz to 2 MHz. They observed the increased low frequency AE event rate with incrementally increased load and, immediately before and during the sample's failure, the increased high frequency AE event rate. In case of the application of constant load (creep test) the increased low frequency AE event rate as a function of time up to failure was observed.

The works by REYMOND [11, 12, 13] were concerned with examination of the AE frequency spectra of some rocks (e.g. limestone) as a function of incrementally increased compression, in the range from 100 Hz to 20 kHz. The results obtained show, that the maximal spectrum density shifts towards high frequencies as the load applied is increased. As the rock approached failure, very high spectral density was observed in the whole frequency range to decrease immediately prior to the failure, particularly in the range of very high frequencies.

Evolution of dominant spectral density was also a subject of numerous investigations with reference to earthquake prediction. The results of these investigations have significant general value on account of the scale invariable character of the fracture process of rocks under external stresses.

FEDOTOV et al., ISHIDA et al. and UTSU [2, 4, 16], obtained contradictory results in this respect. Investigations by ISHIDA and by UTSU indicate, that the foreshocks prior to earthquake, i.e. so called precursors, are characterized by frequency spectra shifted towards higher frequencies relative to the earlier events. On the contrary, FEDOTOV et al. [2] observed the shift of spectral components towards low frequencies immediately prior to a large earthquake.

SALA [14], in his works on AE, assumed that elastic wave generation in the rocks subjected to deformation, in cases of their elasto – brittle behaviour, is identical with earthquakes within the crusts of the earth which exhibit substantial tectonic stresses.

In accord with the results of granite investigation under indirect tensile stress (brasilian test), a shift of the dominant AE spectra components from low to high frequencies, up to the stress approaching strength, followed by the increase of low frequency components, was observed. In case of AE spectra measurements of granite under compressive stress, the results exhibit analogous evolution of the spectra however, the last phase of this evolution occuring earlier and being more pronounced.

In the present work cumulative results of the AE investigation in rocks carried out within the Polish-French scientific cooperation are given. This investigation were aimed, among others, at the analysis and the estimation of AE spectral width of some rocks and at its evolution as a function of uniaxial, incremental compression. Subjected to this investigation were samples of sandstone and dolomite from Legnica-Glogow Copper District in Poland and of marble (carrare) from France.

Spectral analysis of the AE in some samples and the measurements of their physical parameters were performed in France. To these authors knowledge no data were published, in the two countries, with reference to the spectral analysis of the AE in brittle rock, in the range of frequencies up to 100 kHz, under uniaxial compression.

2. Experimental Procedure

Cylindrical specimens of the examined rock, measuring 60 mm in length and 30 mm in diameter, were subjected to uniaxial compressive load until fracture occured, using large hydraulic press. The load was varied incrementally in the following way: very slow 1 tone increment of load was used and kept constant over a period of 3 to 14 min duration. Prolongation of that period over 3 min was used only in cases of observable acoustic activity and was kept until it ceased.

Test specimens were measured also with reference to their physical parameters

such as elastic longitudinal wave velocity in samples dry and in samples water saturated, mass density, bulk density and porosity. These parameters and the samples' compressive strength are give in Table 1.

Table 1

Rock type sample number	Longitudinal wave velocity c_p m/s	Longitudinal wave velocity (water saturated) c_{ps} m/s	Bulk density ϱ_v g/cm^2	Mass density ϱ g/cm^2	Porosity p %	Compressive strength σ_r MPa
Sandstone P1	3200	3150	2.13	2.71	21.3	31.1
Sandstone P2	3560	3370	2.25	2.69	16.1	83.37
Sandstone P3	4460	4040	2.42	2.74	11.8	111.16
Dolomite D1	6000	5630	2.67	2.72	1.8	152.8
Dolomite D2	5910	6030	2.71	2.73	0.6	127.3
Dolomite D3	6000	6050	2.71	2.72	0.5	194.5
Marble C1	3880	5190	2.70	2.71	0.3	86.3
Marble C2	3730	5190	2.70	2.71	0.3	111.16
Marble C3	3730	5260	2.70	2.71	0.3	111.16

In order to detect the AE during loading, a Bruel and Kjaer type 4344 piezoelectric accelerometer was cemented to one side of the examined cylindrical specimen. The accelerometer frequency response was: 2Hz to 100 kHz.

The amplified waveforms were fed to a wide band (100 Hz to 150 kHz) magnetic tape recorder. The frequency spectra of the recorded AE events were analysed using the Fast Fourier Transform. To obtain maximum spectral density, within each incremental loading cycle a peak hold procedure was used.

3. Results

The AE peak hold frequency spectra for the sandstone samples at 0.16 and 0.90 of the failure stress are shown for illustration in Fig. 1. Detailed analysis of the results obtained shows, that for loads below 0.16 of the failure stress, a pronounced domination of low frequency components (up to approx. 10 kHz) is observed. As the load is increased, a shift of the dominant frequency bands towards higher frequencies is observed.

Peak hold spectra for the dolomite samples also shows domination of low frequency components below 0.14 of the failure stress. For higher loads the dominant frequency bands shifted in the direction of higher frequencies, amounting 70 to 90 kHz for 0.90 of the failure stress. For illustration of the AE spectrum evolution, the representative spectra for 0.14, 0.57 and 0.92 of the failure stress for dolomite samples, are given in Fig. 2.

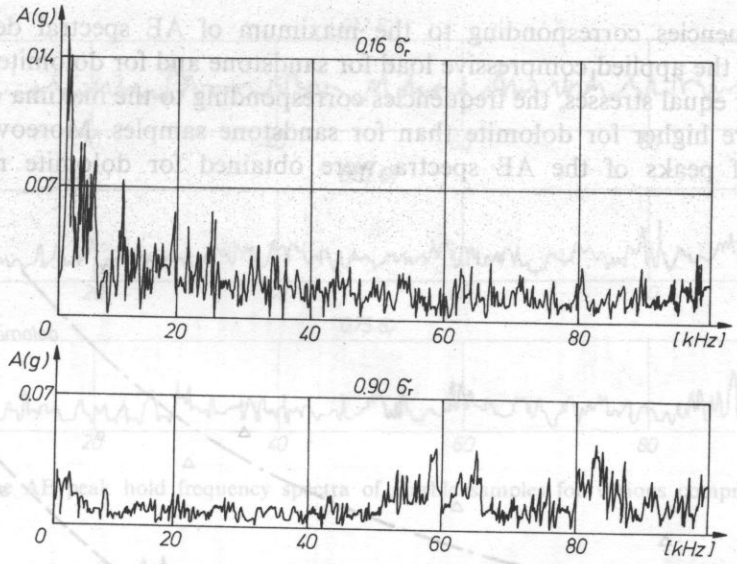

FIG. 1. The AE peak hold frequency spectra of sandstone samples for various compressive stresses

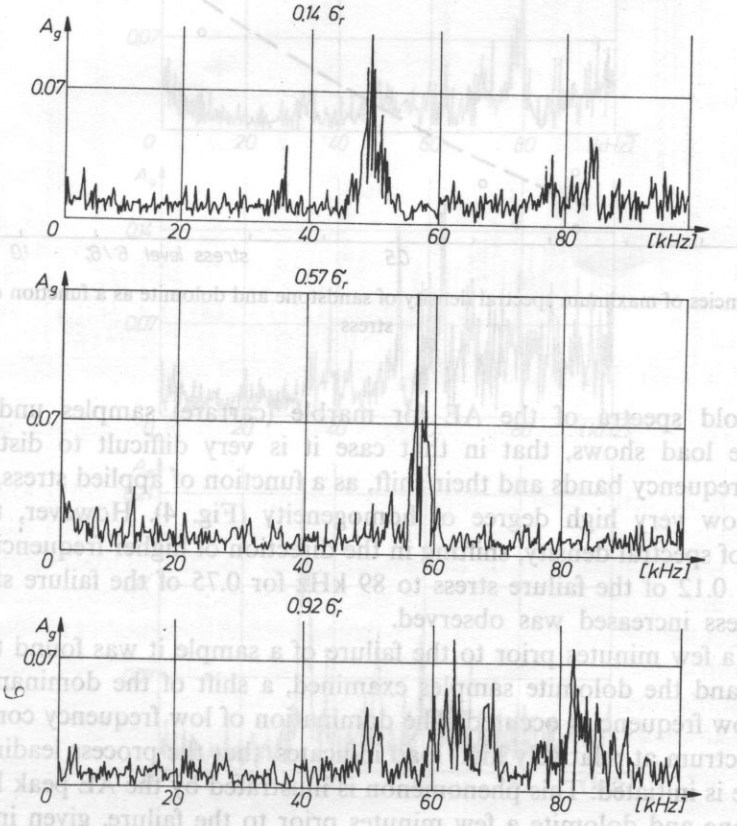

FIG. 2. The AE peak hold frequency spectra of dolomite samples for various compressive stresses

The frequencies corresponding to the maximum of AE spectral densities as a function of the applied compressive load for sandstone and for dolomite are given in Fig. 3. For equal stresses, the frequencies corresponding to the maxima of spectral densities were higher for dolomite than for sandstone samples. Moreover, higher amplitude of peaks of the AE spectra were obtained for dolomite relative to a sandstone.

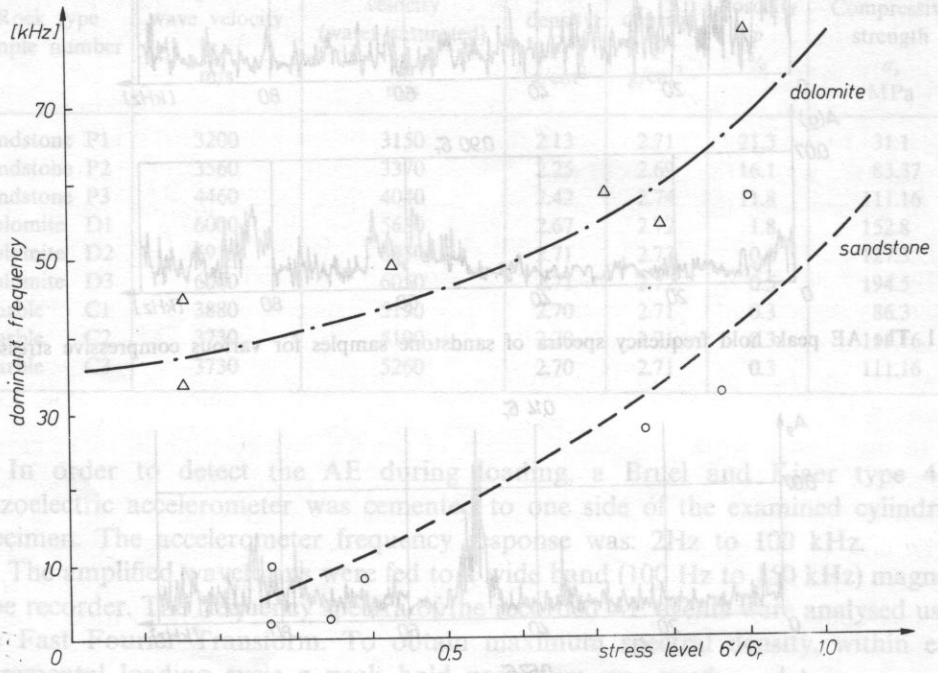

FIG. 3. Frequencies of maximum spectral density of sandstone and dolomite as a function of compressive stress

Peak hold spectra of the AE for marble (carrare) samples under uniaxial compressive load shows, that in that case it is very difficult to distinguish the dominant frequency bands and their shift, as a function of applied stress, since these samples show very high degree of homogeneity (Fig. 4). However, the discrete maximum of spectral density, shifting in the direction of higher frequencies i.e., from 28 kHz for 0.12 of the failure stress to 89 kHz for 0.75 of the failure stress, as the applied stress increased was observed.

Within a few minutes prior to the failure of a sample it was found that, for the sandstone and the dolomite samples examined, a shift of the dominant frequency bands to low frequencies occured. The domination of low frequency components in the AE spectrum at relatively high load indicates, that the process leading to failure of a sample is initiated. This phenomenon is illustrated by the AE peak hold spectra for sandstone and dolomite a few minutes prior to the failure, given in Fig. 5 and Fig. 6.

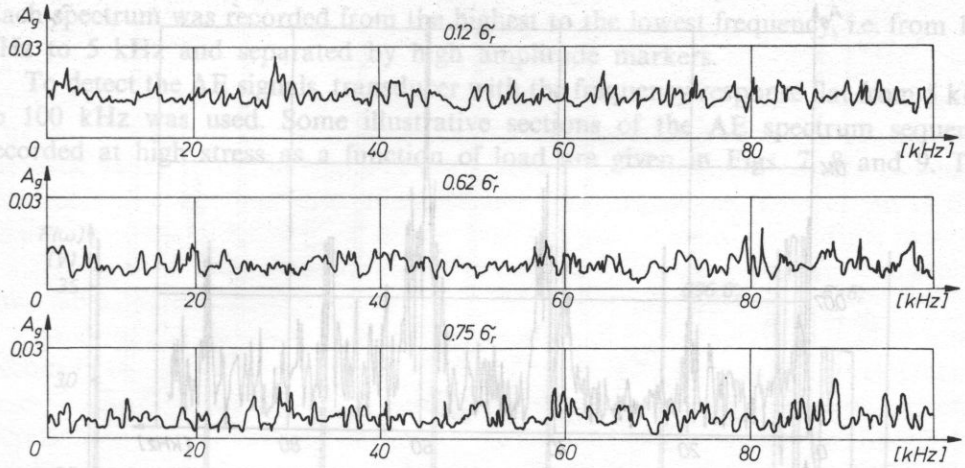

FIG. 4. The AE peak hold frequency spectra of marble samples for various compressive stresses

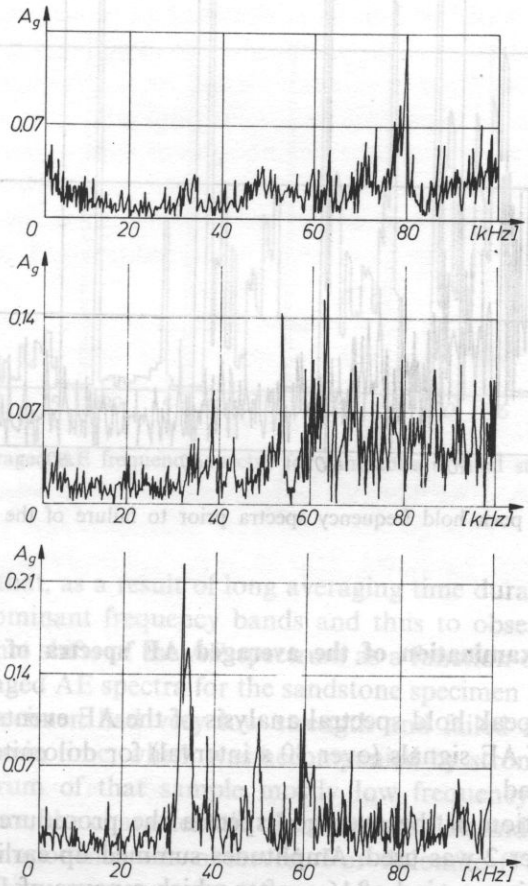

FIG. 5. The AE peak hold frequency spectra prior to failure of the sandstone sample

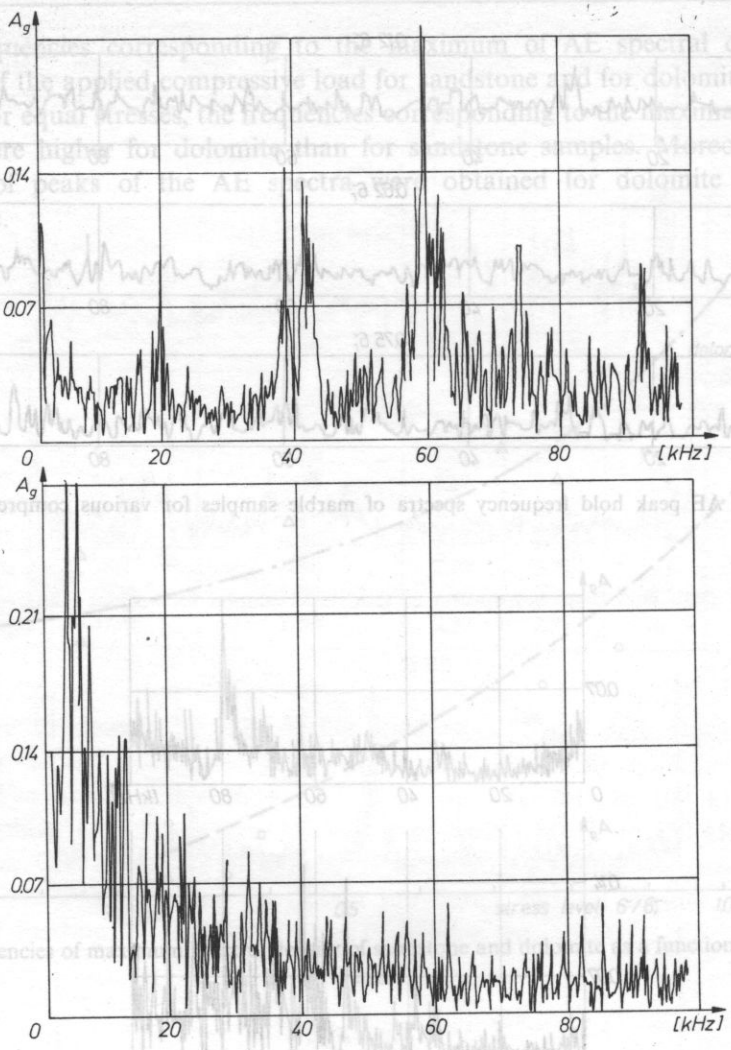

FIG. 6. The AE peak hold frequency spectra prior to failure of the dolomite sample

4. Examination of the averaged AE spectra of rocks

Along with the peak hold spectral analysis of the AE events, examination of the averaged spectra of AE signals (over 30 s interval) for dolomite and sandstone was performed in Poland.

In the examination of the averaged spectra the procedure of load application described in Chapter 2 was used. Amplitudes summed up earlier over 30 s interval are registered in a time period of 16 s, after which a pause of 14 s duration follows.

Each spectrum was recorded from the highest to the lowest frequency, i.e. from 100 kHz to 5 kHz and separated by high amplitude markers.

To detect the AE signals, transducer with the frequency response flat from 5 kHz to 100 kHz was used. Some illustrative sections of the AE spectrum sequence recorded at high stress as a function of load are given in Figs. 7, 8 and 9. The

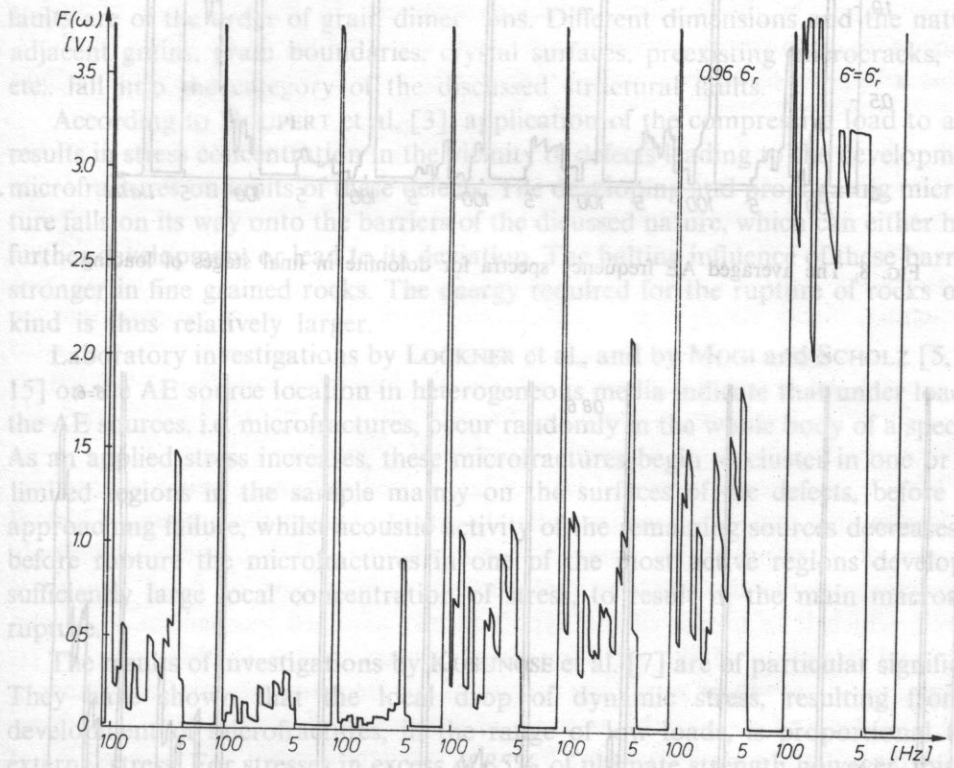

FIG. 7. The averaged AE frequency spectra for sandstone in final stages of loading

obtained data show that, as a result of long averaging time duration, it was difficult to distinguish the dominant frequency bands and thus to observe their evolution. However, some distinct shifts of the AE spectrum as a function of time was noticed.

Some of the averaged AE spectra for the sandstone specimen P1 are given in Fig. 7. This particular specimen had very low strength and failed at constant load of 2 tones in approx. 6 min time, which was accompanied by strong acoustic activity.

In the AE spectrum of that sample mostly low frequency components were present. Prior to failure, the characteristic obtained was flat, and next a domination of high frequency components was observed. For dolomite (Fig. 8), a growth of amplitudes of high frequency components was observed at approximately 0.7 of

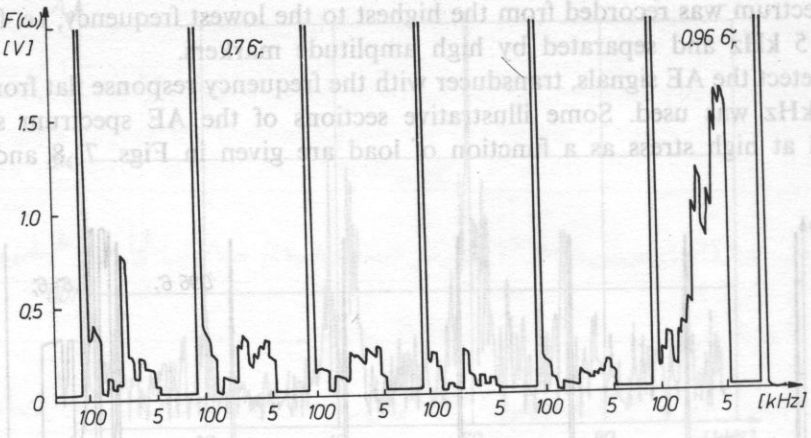

FIG. 8. The averaged AE frequency spectra for dolomite in final stages of loading

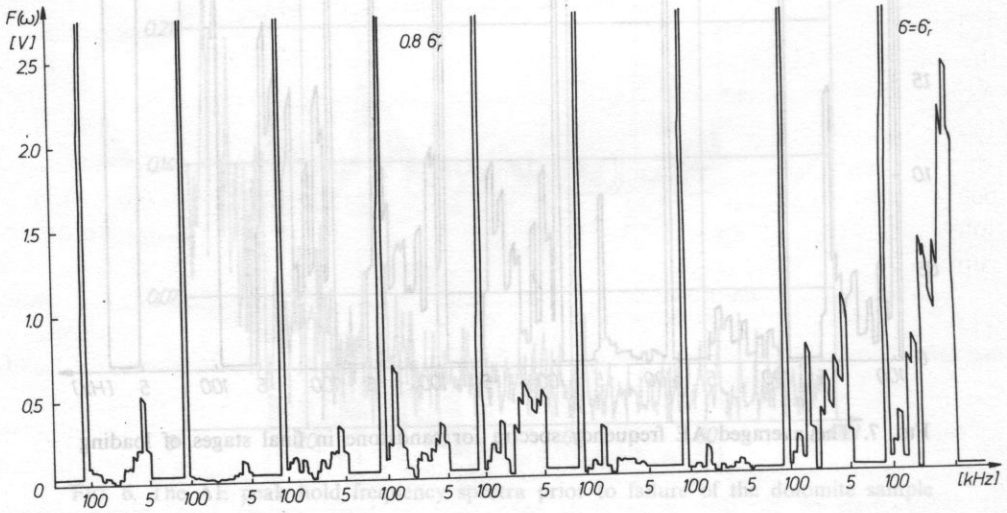

FIG. 9. The averaged AE frequency spectra for marble in final stages of loading

failure load, and next a considerable domination of amplitudes of low frequency components, prior to failure i.e. for 0.96 of failure load.

For marble (Fig. 9), also a growth of amplitudes of high frequency components was found for 0.8 of failure load, and next their diminution and growth of amplitudes of low frequency components immediately prior to failure. The obtained data indicate, that the evolution of the averaged AE signals is not fully consistent with the AE peak hold spectra evolution only in the case of sandstone samples.

5. Discussion and Conclusions

Process of the development and propagation of microfractures under external stresses, which lead to the inelastic deformation of rock and to the generation of acoustic waves, results in failure of brittle rocks. Rocks generally have large number of structural defects like discontinuities and unhomogeneities. Dimensions of these faults are of the order of grain dimensions. Different dimensions and the nature of adjacent grains, grain boundaries, crystal surfaces, preexisting microcracks, pores, etc., fall into the category of the discussed structural faults.

According to HOUPERT et al. [3], application of the compressive load to a rock, results in stress concentration in the vicinity of defects leading to the development of microfractures on limits of these defects. The developing and propagating microfracture falls on its way onto the barriers of the dicussed nature, which can either halt its further development or lead to its deviation. The halting influence of these barriers is stronger in fine grained rocks. The energy required for the rupture of rocks of that kind is thus relatively larger.

Laboratory investigations by LOCKNER et al., and by MOGI and SCHOLZ [5, 6, 11, 15] on the AE source location in heterogeneous media indicate that under load first the AE sources, i.e. microfractures, occur randomly in the whole body of a specimen. As an applied stress increases, these microfractures begin to cluster in one or more limited regions in the sample mainly on the surfaces of the defects, before stress approaching failure, whilst acoustic activity of the remaining sources decreases. Just before rupture the microfractures in one of the most active regions develope, at sufficiently large local concentration of stress, to result in the main macroscopic rupture.

The results of investigations by KUSUNOSE et al. [7] are of particular significance. They have shown that the local drop of dynamic stress, resulting from the development of microfractures, in the range of low loads, is proportional to the external stress. For stresses in excess of 85% of ultimate strength however, this drop is significantly larger than the external stress. This observation implies that the degree of stress concentration is unproportionally higher for higher external loads.

This dependency was confirmed experimentally by KUSUNOSE et al. [7] on the grounds of the observed enlargement of high frequency components in the AE waveforms for high loads. It was also shown that the propagation effect is not responsible of the spectrum shift i.e. that the frequency dependence of attenuation of acoustic waves does not contribute in the AE spectrum evolution as a function of load.

Concentration of sources of seismoacoustic signals in the region of rock mass fractures was observed also by ZUBEREK [17] in coal mines.

ISHIDA et al. [4] observed that in a time period preceding large earthquakes, a significant concentration of a foreshock seismic activity, which has form of small earthquakes, occurs around the future epicenter. It is characterized by consistently higher frequencies of peak spectral components in comparison with ordinary events. This fact seems to support a hypothesis of high progressive stress concentration

leading to the development of rock mass fractures and consequently to the significant local drop of dynamic stress.

Reconsidering the results of investigations cited, it can be assumed, that frequency spectrum of the AE event depends: on stress in the region of the AE source, on dimensions of the AE source; on a structure (degree of heterogeneity) of rock medium and on the AE source mechanism. Evolution of the dominant frequency bands in the acoustic emission spectrum, in the direction of higher frequencies as a function of increasing load, observed by the present authors, confirms a hypothesis of local stress concentration in a region of eventual failure plane.

The AE spectra of dolomites and sandstones with heterogeneous structure, manifested by significant dispersion of their physical parameters given Table 1, are characterized by large amplitude spectral density in the dominant frequency bands. Higher frequencies of the dominant components in the AE spectrum of dolomite seem to result from its more fine grained structure relative to sandstone and, consequently, higher strength and higher velocity of elastic wave propagation, see Table 1.

In general, the obtained data point out, that the frequency range up to 100 kHz is representative for spectrum evolution of the AE events of the tested dolomite and sandstone specimens, under uniaxial incremental compressive load.

In marble, as a consequence of lack of large sized unhomogeneities, microfractures develop in a minor degreee immediately prior to failure. On account of lack of occurrence of the considerable stress concentrations as well as microfractures, only the evolution of the discrete maximal spectral components of small density is observed, which is in favour of the hypothetically assumed mechanism. However, pronounced evolution of the AE long time average spectra is observed.

A very rapid growth of amplitude density of low frequency spectral components, immediately before failure of the majority of dolomite and of sandstone specimens, indicates the initiation of macroscopic fracture. The development and propagation of microfractures in the vicinity of the more strong defect, leads to rapid growth of the eventual failure plane. Generation of larger cracks occurs and/or coalescence of minor cracks into larger cracks takes place, leading to macroscopic failure. In that way the average size of the AE sources increases. Larger sources of the AE tend to generate AE events containing lower frequency components.

It seems that the shift of dominant frequency bands towards lower frequencies could be used as an indication of significant value in the prediction of failure of heterogeneous rocks. For final conclusion however, investigation of the AE spectra for large population of test specimens and statistical analysis of data are necessary.

Acknowledgements

The authors would like to express their thanks to Mr. DENIS, Mr. DURVILLE, Mr. GERARD, Mr. MARTINEAU, Mr. MASSIEU and Mr. THIEBAULT for the efficient assistance in various stages of the research work. This research was supported by the

Dept. Geologie et Materiaux du Laboratoire Central des Ponts et Chaussées et du Laboratoire regional de l'Est parisien and by grant C.P.B.P. 02.03 – from the Institute of Fundamental Technological Research, Polish Academy of Sciences.

References

[1] Y. P. CHUGH, H. R. HARDY, Jr., R. STEFANKO, *An investigation of the frequency spectra of microseismic activity in rock under tension*, Tenth Rock Mech. Sym. Austin, Texas, 1968, p. 79–113.

[2] S. A. FEDOTOW, A. A. GUSEW, S. A. BOLDYREW, *Progress of earthquake prediction in Kamchatka*, Tectonophysics, **14**, 279–286 (1972).

[3] R. HOUPERT, F. HOMAND-ETIENNE, J. P. TISOT, *Mecanismes de propagation de la rupture en compression dans les roches cristallines*, Bull. Soc. Geol. France, **28**, 6, 1583–1589 (1976).

[4] M. ISHIDA, H. KANAMORI, *Temporal variation of seismicity and spectrum of small earthquakes preceding the 1952 Kern County, California, earthquake*, Bull. Seism. Soc. Am., **70**, 2, 509–527 (1980).

[5] D. LOUCKNER, J. BYERLEE, *Acoustic emission and fault formation in rocks*, Proc. First Conf. on A.E./M.A in Geologic Structures and Materials, The Pennsylvania State University, Trans. Tech. Publ., 1977, p. 13.

[6] K. MOGI, *Source locations of elastic shocks in the fracturing process in rocks*, Bull. Earthq., Res. Inst., Tokyo Univ., **46**, 1103–1125 (1968).

[7] K. KUSUNOSE, K. YAMAMOTO, T. HIRASAWA, *Source process of microfracture in granite with reference to earthquake prediction*, Sci. Rep. Tohoku Univ., Ser. 5 Geophysics, **26**, 3-4, 111–121 (1980).

[8] M. OHNAKA, *Acoustic emission during creep of brittle rock*, Int. J. Rock Mech. Min. Sci. Geomech. Abstr., **20**, 3, 121–134 (1983).

[9] M. OHNAKA, K. MOGI, *Frequency dependence of acoustic emission activity in rock under incremental uniaxial compression*, Bull. Earthq. Res. Inst., Tokyo Univ., **56**, 67–89 (1981).

[10] M. OHNAKA, K. MOGI, *Frequency characteristics of acoustic emission in rocks under uniaxial compression and its relation to the fracturing process to failure*, J. Geoph. Res., **87**, B5, 3873–3884 (1982).

[11] M. C. REYMOND, *L'étude et les applications par procédés acoustique de la formation, la localisation et la propagation de fissures dans les milieux fragiles*, Revue d'Acoustique, **10**, 43, 284–293 (1977).

[12] M. C. REYMOND, *Etude de la fissuration des éprouvettes sous contraintes en laboratoire et des massifs rocheux en carriéres par une methode d'émission acoustique*, Rock Mechanics, **7**, 1, 1–16 (1975).

[13] M. C. REYMOND, J. BILLAUD, *Emission acoustique dans les roches calcaires à differentes echelles*, Revue d'Acoustique, **13**, 52, 20–25 (1980).

[14] Ph. SALA, *Etude experimentale de la fissuration et de la rupture des roches par emission acoustique. Application á l'étude de la sismogenèse*, These Dr. Ing. Université Scientifique et Medicale de Grenoble, 1982, p. 199.

[15] C. H. SCHOLZ, *Experimental study of the fracturing process in brittle rock*, J. Geoph. Res., **73**, 4, 1447–1454 (1968).

[16] T. UTSU, *Spatial and temporal distribution of low-frequency earthquakes in Japan*, J. Phys. Eart., **28**, 361–384 (1980).

[17] W. ZUBEREK, *Acoustic emission in rocks*, Uniwersytet Śląski, Katowice 1984, p. 66–73.

Received on May 24, 1988.

ARCHIVES OF ACOUSTICS
14, 1-2, 111-121 (1989)

PRELIMINARY ULTRASONOGRAPHIC STUDIES ON AN ELECTRONIC SYSTEM FOR FOCUSING AN ULTRASONIC BEAM

TOMASZ WASZCZUK, GRAŻYNA ŁYPACEWICZ

Department of Ultrasonics, Institute of Fundamental Technological Research, Polish Academy of Sciences
(00–049 Warszawa, ul. Świętokrzyska 21)

JAN SOMER

Biophysics, University of Limburg, 6200 MD Maastricht, the Netherlands

In conventional mechanical contact scanners the lateral resolution is inferior to the axial one. Improving the lateral resolution over a wide range of depth requires the use of variable focusing system. We choose the phase annular array system which may be used in obstetrics and gynaecology.

Measurements of the ultrasonic beam were carried out. Visualisations two different phantoms AIUM-100 and RMI-402 were performed during work: a typical B-scanner, and the annular array system. The results indicate a considerable increase in the lateral resolution when works the annular array system.

W typowych ultrasonografach rozdzielczość poprzeczna jest znacznie gorsza niż rozdzielczość podłużna. Poprawa rozdzielczości poprzecznej w całym badanym zasięgu wymaga stosowania różnego typu ogniskowania wiązki. Autorzy wybrali system ogniskowania wiązki ultradźwiękowej z wykorzystaniem wieloelementowej głowicy pierścieniowej. Taki system może znaleźć zastosowanie w ginekologii i położnictwie.

Przeprowadzono pomiary wiązki ultradźwiękowej zbudowanego systemu. Oceny rozdzielczości dla: a) typowej pracy ultrasonografu, b) pracy w systemie dynamicznego ogniskowania, przeprowadzono z wykorzystaniem dwóch wzorców AIUM-100 i RMI-402. Otrzymane wyniki pokazują wyraźną poprawę rozdzielczości poprzecznej podczas pracy systemu dynamicznego ogniskowania wiązki ultradźwiękowej.

1. Introduction

In ultrasonic diagnosis in medicine, the very essential parameters include the longitudinal and lateral resolution of the ultrasonic system. In investigation of a soft tissue by means of typical ultrasonograph the lateral resolution varies between 2 and 4 mm, whereas the longitudinal resolution is about 1 mm.

In the present state of the ultrasonic technique, the greatest impact on the resolution of the system is exerted by that of the ultrasonic probe. The lateral resolution of the probe can be improved by focusing the ultrasonic beam by means of a lens placed on the ultrasonic probe or by using a probe with an appropriately profiled concave transducer. A disadvantage of these methods is focusing only over a narrow depth range.

Focusing is possible along the whole observation range if a special multi-element ultrasonic probe is controlled by an appropriate electronic system.

The aim of this study is to show how the smaller width of the ultrasonic beam radiated by the probe affects the images obtained on the screen of the ultrasonograph.

2. Method

Electronic focusing along the whole range of depth is possible using one of two different types of ultrasonic probes: a linear array or an annular array [1, 2, 3]. In the case of interest, the conception was chosen in which a multi-element annular ultrasonic probe is controlled by an appropriate electronic system [4, 5, 6]. In view of the predicted use of the system for focusing an ultrasonic beam in obstetrics and gynaecology, 2.5 MHz was chosen as the resonance frequency of the probe, along with the range from 0 to 24 cm, and with the surface of the probe in contact with that of the investigated body. From theoretical analysis [7], an ultrasonic probe was designed and built, consisting of seven coaxial elements: a disk and six rings of piezoelectric ceramics. The disk diameter is about 10 mm and the external diameter of the last ring is about 40 mm. All the elements have the same surface area. An appropriate electronic system was designed and built for controlling the probe. The whole range from 0 to 240 mm was divided into five zones: zone I: from 0 to 50 mm, with only the disk transmitting, zone II: from 50 to 70 mm, with the focus at 60 mm, with the three central elements transmitting, zone III: from 70 to 90 mm, with the focus at 80 mm, zone IV: from 90 to 140 mm, with the focus at 110 mm, and zone V: from 140 to 240 mm, with the focus at 180 mm.

In zones III, IV and V all the elements transmit. During detection, dynamic focusing is ensured by the system, i.e., the focus is varied at the velocity of the ultrasonic wave propagation in a human body. For such a system, the 20 dB width of the ultrasonic beam was measured [6]. Throughout the range, i.e. 0–24 cm, the 20 dB width of the beam varies from 2.5 mm (over the range 40–120 mm) to about 6 mm (for the range 220–240 mm). All over the range under study, beam width changes are very regular. It was determined that for a 20 dB drop of the signal from the main lobe with respect to the maximum value, no side lobes can be seen.

The investigations of the whole system for dynamic focusing of an ultrasonic beam were carried out after it was connected to a USG-P30 ultrasonograph manufactured by Techpan. The imaged elements were two phantoms:

a) the phantom AIUM-100 (Fig. 1), and
b) the phantom RMI-402 (Fig. 2).

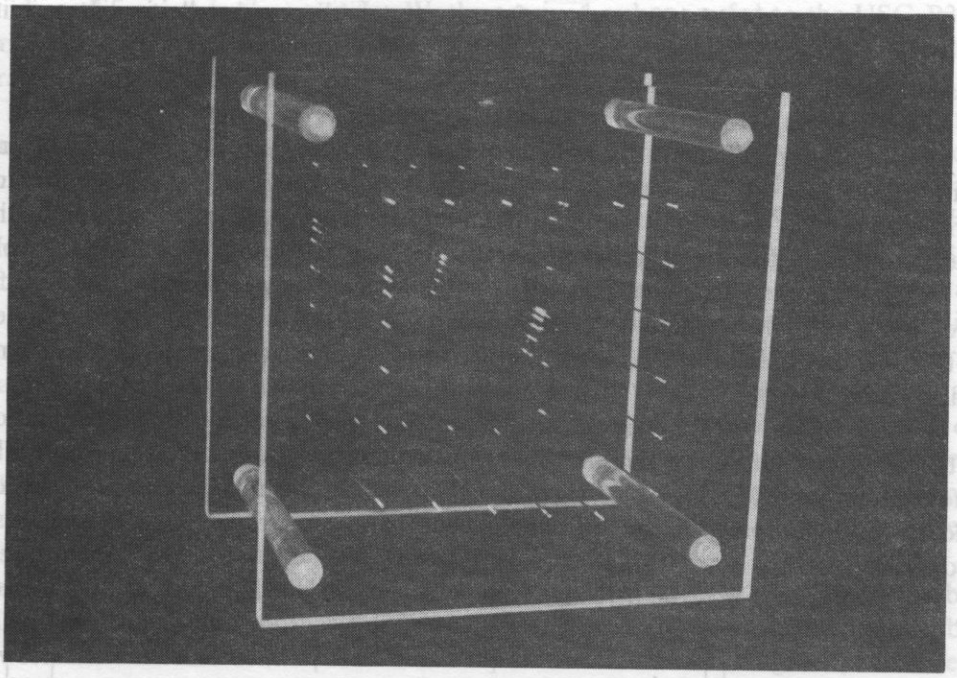

FIG. 1. Phantom AIUM-100

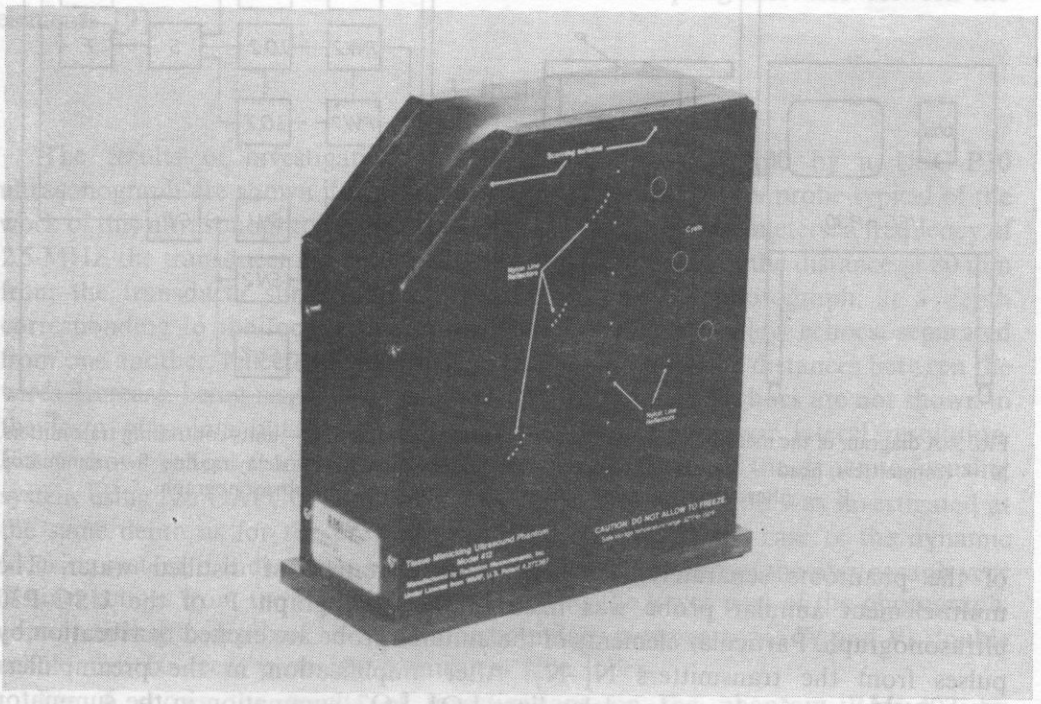

FIG. 2. Phantom RMI-402

The phantom AIUM-100 consists of appropriately disposed stell wires. It permits the determination of the longitudinal and lateral resolution and the accuracy of presentation on the ultrasonograph screen.

The phantom RMI-402 consists of:

a) three groups of nylon threads, disposed at different depths, 3, 7 and 12 cm, from the surface, with five threads in each group. The distance between the threads varies from 0.5, 1, 2 and 3 mm. These three groups of threads permit the determination of the longitudinal and transverse resolution of the ultrasonograph.

b) nylon threads distributed crosswise. The distance between each of the vertical threads is 2 cm. The horizontal threads are 3 and 4 cm apart. The threads distributed in this make it possible to evaluate the accuracy of presentation on the ultrasonograph screen.

c) three "cysts" with a diameter of 7.5 mm each. They permit the determination of the ability of maping of the internal body structures by the ultrasonograph. The whole phantom RMI-402 is filled with gel in which the ultrasound propagation velocity and damping of the ultrasonic beam are similar to those in a human body [8].

The system in which the investigations were carried out is shown in Fig. 3. Each

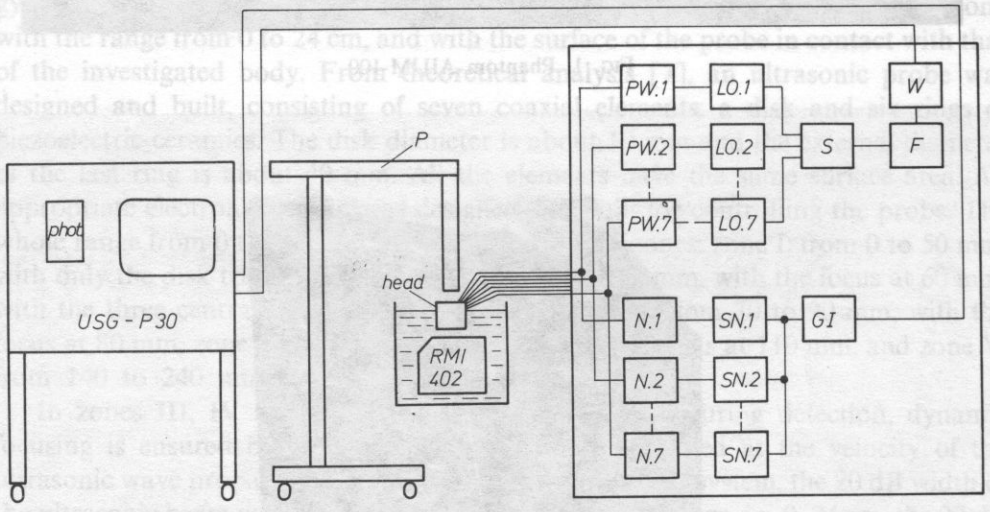

FIG. 3. A diagram of the measurement system: GI – pulse generator, SN – units controlling transmitters, N – transmitters, head – ultrasonic probe, PW – preamplifier, LO – delaying line, S – summator, F – filter, W – amplifier, P – pantograph of the ultrasonograph

of the phantoms separately was set in an container of distilled water. The multi-element annular probe was fixed in the pantograph P of the USG-P30 ultrasonograph. Particular elements of the annular probe are excited to vibration by pulses from the transmitters N_1–N_7. After amplification in the preamplifiers PW1–PW7, delaying in analog delay lines LO1–LO7, summation in the summator

S and amplification in the amplifier W, the received pubes are fed to the USG-P30. After appropriate electronic processing the detected signals are shown on the ultrasonograph screen.

In the course of the investigations the work of a USG-P30 ultrasonograph equipped with a typical probe was compared with the performance of the system for dynamic focusing of an ultrasonic beam. The investigations on the dynamic focusing system were carried out using two annular probes working at 2.5 MHz, with the same dimensions of particular elements: a probe manufactured by DAPCO-USA and a probe constructed in the Ultrasonics Department, Institute of Fundamental Technological Research, Polish Academy of Sciences. These probes are different in terms of constitution. The DAPCO probe is made of metaniobite piezoelectric ceramic material. The particular elements of the probe: the disk and successive rings are separated from one another by grooves filled with silicon rubber. The purpose of this is to decrease the mechanical coupling between elements of the probe. Compared with PZT-5 ceramic material, metaniobite is characterized by worse sensitivity and better matching to load, exerting a direct impact on the shape of the transmitted pulses. The probe built at the Ultrasonics Department was made of PZT-5 piezoelectric ceramic material. One side of the piezoelectric plate is fully covered by a silver electrode. On the other side of the plate, part of the silver which used to be between the elements of the probe was evaporated. There are no grooves between particular elements of the probe. Such a construction of the probe is supposed to decrease the harmful side lobes as the mechanical coupling increases between the elements [9].

3. Results

The results of investigations of the phantom AIUM-100 by a USG-P30 ultrasonograph are shown if Fig. 4. During the investigations, a probe typical of the work of this ultrasonograph was used. It has the following parameters: a frequency of 2.5 MHz, the transducer diameter of 20 mm and focal point of the distance of 80 mm from the transducer surface. In the central part of the photograph, at a depth corresponding to the focus, it is impossible to distinguish a few echoes, separated from one another, reflected from six wires in the phantom (the distances between the wires decrease, being respectively 5, 3, 2, 1 and 0.5 mm). The echoes are not shown in the form of points but as horizontal dashes, indicating poor lateral resolution. Fig. 5 shows echoes from the same phantom for the work of the dynamic focusing system using the DAPCO annular probe. The lateral resolution was investigated at the same depth as for the previous case, i.e., 7–8 cm. In the case of the dynamic focusing system, it is distinctly better, since in the central part of the photograph very distinct echoes from the six wires can be seen. In the lower part of the photograph, corresponding to depth of 13–14 cm (the boundary between zones IV and V), double echoes can be seen, probably because of side lobes.

Fig. 6 shows the results of investigations on the phantom RMI-402 by

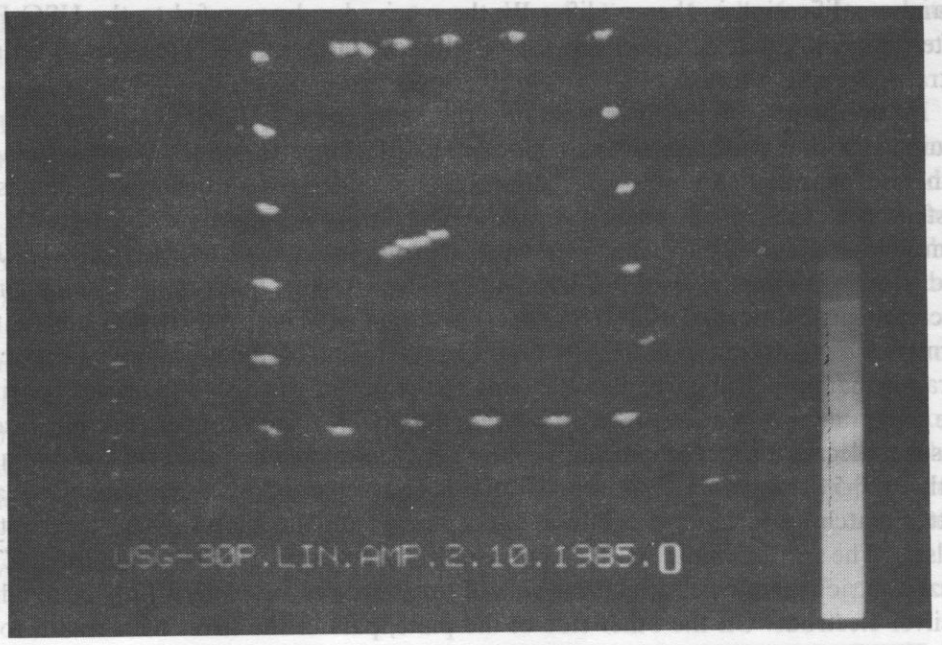

FIG. 4. Study on the phantom AIUM-100 by the USG-P30 ultrasonograph

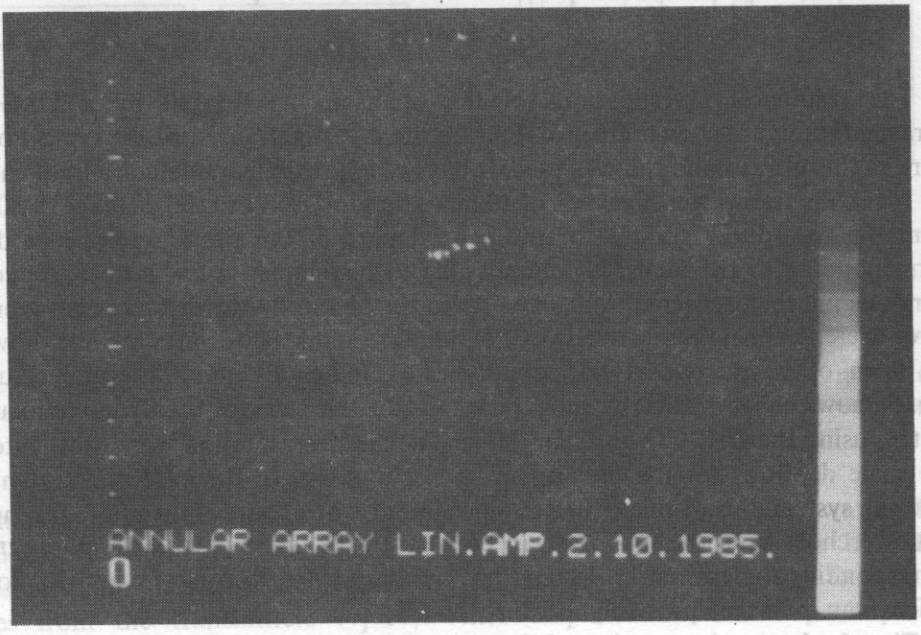

FIG. 5. Study on the phantom AIUM-100 by the dynamic focusing system

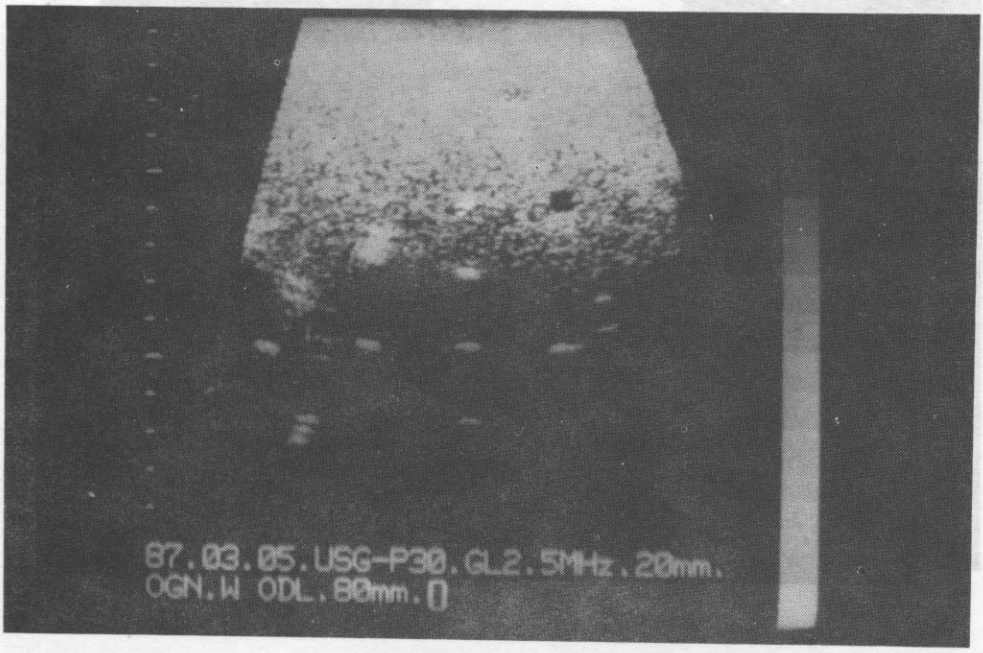

FIG. 6. Study on the phantom RMI-402 by the USG-P30 ultrasonograph

an USG-P30 ultrasonograph. All the elements of the phantom are visible, namely three cysts, all the threads in vertical and horizontal rows and three groups of five threads. The echoes from the threads can be seen as dashes rather than points.

Fig. 7 shows the results of investigations of the same phantom for the work of the dynamic focusing system using two different annular probes. The investigations were carried out using focusing in the zones during transmission and dynamic focusing during reception. In Fig. 7 a three cysts are visible, and so are all the threads in vertical and horizontal rows and three groups of five threads. The lateral resolution for structures situated over the range 0–5 cm is poorer than that for deeper-lying ones. This is caused by the fact that over the depth range 0–5 cm it is only the disk that works, and so there are no possibilities of electronic signal focusing.

For the probe made at the Institute of Fundamental Technological Research (Fig. 7b) one can see distinctly poorer echoes than those for the DAPCO probe. The image is more blurred. This results from much longer transmitted pulses. It also causes poorer lateral resolution of the system for work with this probe, compared to that involving the DAPCO probe.

In general, all the elements of the phantom RMI-402 are much more visible for the work of the dynamic focusing system compared with the typical work of the USG-P30 ultrasonograph [10, 11].

Fig. 8 shows the results of investigations of the phantom RMI-402 for the work of the dynamic focusing system for two annular probe, but for a constant focusing at transmission 110 mm and dynamic focusing at reception. Compared with the

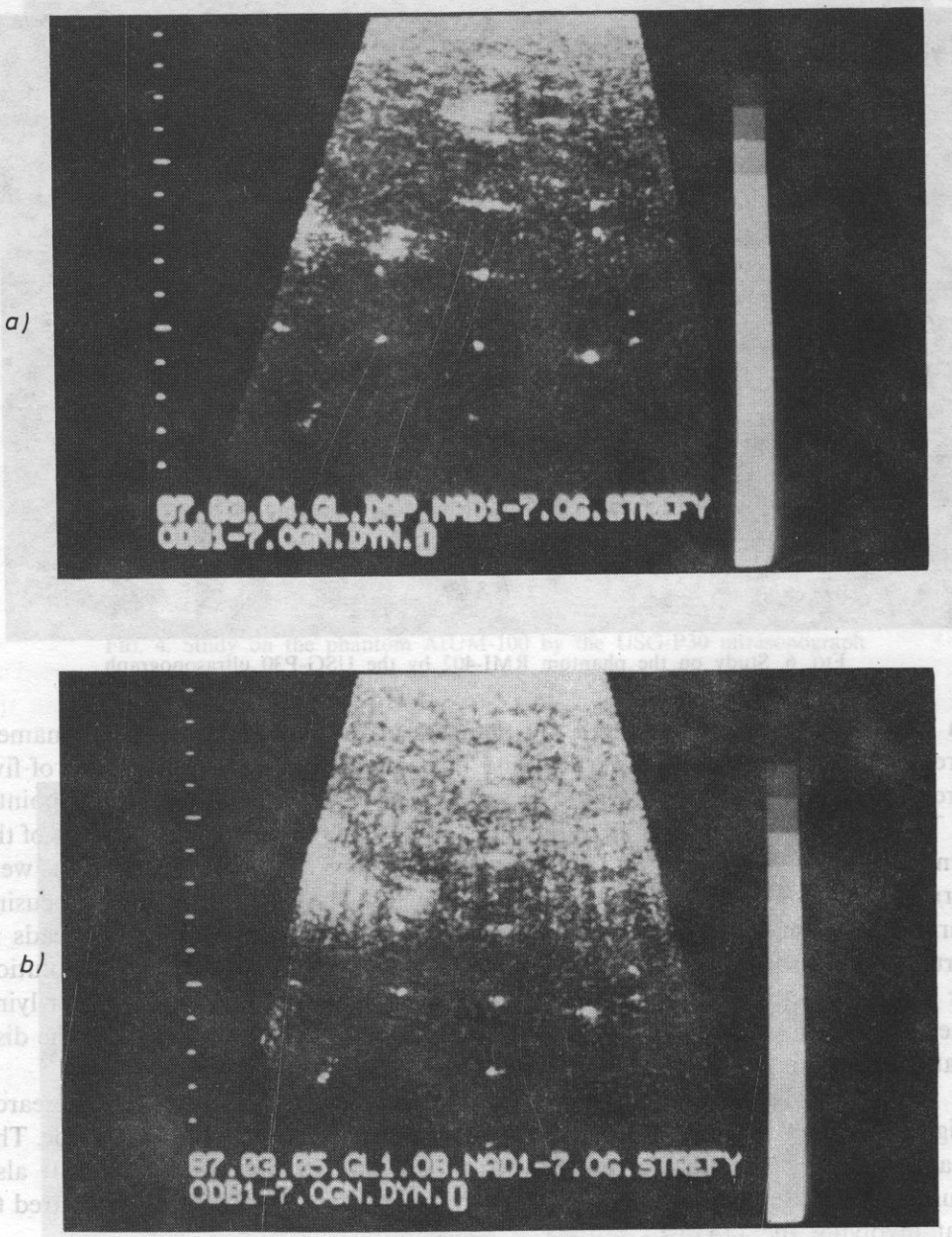

FIG. 7. Study on the phantom RMI-402 by the dynamic focusing system A — DAPCO probe, B — Institute of Fundamental Technological Research's probe

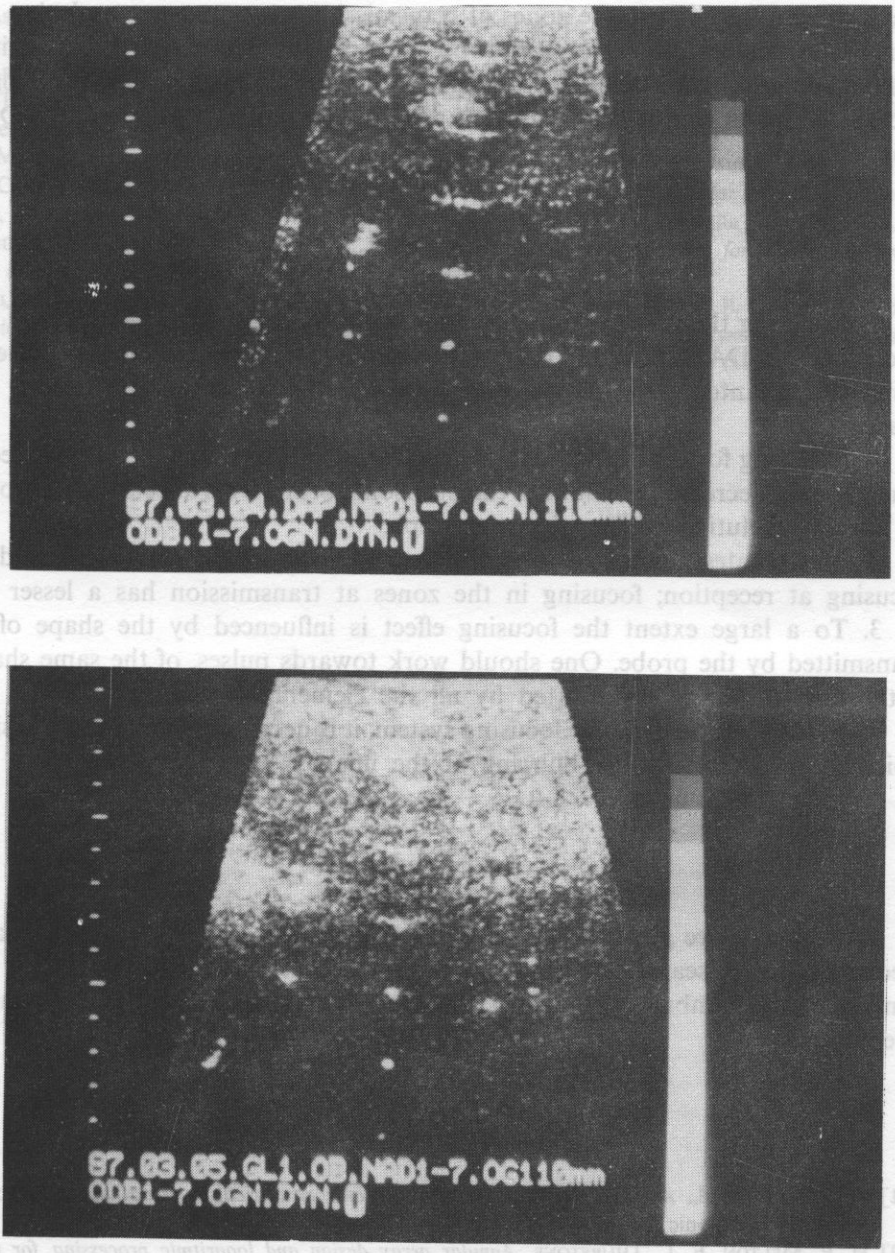

FIG. 8. Study on the phantom RMI-402 by the focusing system. A constant focus of 110 mm at transmission. Dynamic focusing at reception A – DAPCO probe, B – Institute of Fundamental Technological Research's probe

previous case focusing in the zones at transmission, some poorer resolution can be seen for structures closer to the probe. The probe produced by the Institute of Fundamental Technological Research is more sensitive than the DAPCO one, but because of longer transmitted pulses, its resolution is worse than that of the DAPCO unit.

4. Conclusions

Considering the results of investigations of the dynamic focusing carried out for two probes: of DAPCO and of the Institute of Fundamental Technological Research, using two phantoms AIUM-100 and RMI-402 the following conclusions can be drawn:

1. Focusing for drawn points at transmission and dynamic focusing at reception considerably decrease the width of the ultrasonic beam. This affects the improvement of lateral resolution of the ultrasonograph.

2. The greatest influence on improvement in lateral resolution has dynamic focusing at reception; focusing in the zones at transmission has a lesser effect.

3. To a large extent the focusing effect is influenced by the shape of pulses transmitted by the probe. One should work towards pulses, of the same shape but with short duration, transmitted by all the elements of the probe.

4. In the existing dynamic focusing system, it is necessary to increase the signal to noise ratio, decreasing the blurring of the image.

Acknowledgement

The authors are grateful to Prof. Dr L. FILIPCZYŃSKI, Institute of Fundamental Technological Research, Polish Academy of Sciences, Warsaw, and Dr A. HOEKS, University of Limburg, for discussion and valuable remarks as the study was prepared.

References

[1] G. KOSSOFF et al., *Annular phased arrays in ultrasonic obstetrical examinations*, Advanced Study Institute, Ultrasonic Diagnostics, Milan, June 1974.

[2] H. E. MELTON, F. L. THURSTONE, *Annular array design and logaritmic processing for ultrasonic imaging*, Ultrasound in Medicine and Biology, **4**, 1–12 (1978).

[3] O. von RAMM, S. W. SMITH, *Beam steering with linear arrays*, IEEE Transactions on Biomedical Engineering, **30**, 8 (1983).

[4] T. WASZCZUK, J. SOMER, *A system for dynamic focusing of an ultrasonic beam by annular transducers* [in Polish], Proc. XXVII Open Seminar on Acoustics, Warszawa-Puławy, September 1980.

[5] T. WASZCZUK, T. KUJAWSKA, J. SOMER, *Focusing of an ultrasonic beam by means of a piezoelectric annular array*, Archives of Acoustics, **3**, 3, 185–204 (1983).

[6] T. WASZCZUK, T. KUJAWSKA, J. SOMER, *Electronic focusing of the ultrasonic beam by means of an annular array system*, Archives of Acoustics, **9**, 1–2, 155–162 (1984).

[7] T. MARUK-KUJAWSKA, *Dynamic focusing of a ultrasonic beam by means of annular transducers* [in Polish], D. Sc. Thesis, Institute of Fundamental Technological Research, Polish Academy of Sciences, Warsaw 1980.

[8] S. H. MASLAK, *Comuted Sonography*, [ed] R. C. Sanders and M. G. Hill Ultrasound Annual 1985.

[9] D. A. CARPENTER, B. D. O'CONNOR, G. D. RADOVANOVICH, *Development of annular array transducer system*, Proceedings of the Fourth Meeting of the WFUMB'85 Sydney Australia July 1985, 274.

[10] M. ARDITI, W. B. TAYLOR, F. S. FOSTER, J. W. HUNT, *An annular array system for high resolution breast echography*, Ultrasonic Imaging, **4**, 1–31 (1982).

[11] R. PINI, L. FERRUICI, M. di BARI, B. GREPPI, M. CEROFOLINI, L. MASOTTI and R. B. DEVEREUX, *Two dimensional echocardiographic imaging in vitro comparison of conventional and dynamically focused annular array transducers*, Ultrasound in Medicine and Biology, **13**, 643–650 (1987).

Received on December 14, 1987.

ARCHIVES OF ACOUSTICS
14, 1-2, 123-142 (1989)

PRACTICAL APPLICATION OF THE PHENOMENON OF ACOUSTIC EMISSION IN ROCKS

WACŁAW M. ZUBEREK, LESŁAW CHODYŃ

Faculty of Earth Sciences of the Silesian University, Department of Applied Geology
(41–200 Sosnowiec, ul. Mielczarskiego 60)

Zjawisko emisji sejsmoakustycznej polegające na generowaniu fal sprężystych w czasie procesów dynamicznych znajduje szerokie zastosowanie przy rozwiązywaniu szeregu zagadnień geotechnicznych.

Uwzględniając podobieństwo procesów fizycznych, różnorodne zastosowania emisji sejsmoakustycznej sklasyfikowano w następujące grupy zagadnień:
– ocena stabilności wyrobisk i struktur geotechnicznych,
– przewidywanie momentu zniszczenia górotworu,
– inne zastosowania (jak np. do wyznaczania składowych głównych tensora naprężenia, który w przeszłości oddziaływał na skały, badanie zagrożenia lawinami, wykrywanie miejsc przepływu cieczy przez ośrodek porowaty itp.).

Oddzielnie przedstawiono lokalizację źródeł emisji sejsmoakustycznej traktując ją jako technikę pomiarów, która znajduje zastosowanie w ocenie stabilności, przewidywaniu momentu zniszczenia a także stwarza szerokie możliwości wykorzystania zjawiska emisji sejsmoakustycznej w geotechnice.

Dla każdej z grup zagadnień krótko opisano koncepcję zastosowań aktualny stan badań jak również czynniki ograniczające możliwość stosowania metody. Zastosowania zilustrowano najbardziej przekonywającymi przykładami z literatury.

Opis metod poprzedzono krótką analizą składu częstotliwościowego sygnałów sejsmoakustycznych w funkcji odległości od źródła w różnych typach skał.

Artykuł ma charakter przeglądowy i podsumowujący stan badań i został opracowany na podstawie obszernej literatury światowej.

1. Introduction

The notion acoustic emission (AE), which is also known as seismoacoustic, microseismic or geoacoustic, means the effect of elastic wave generation in rocks during dynamic processes. These processes may be caused by stresses within the rock body or certain unstable states.

Acoustic emission appears in solid and loose rocks as the result of plastic strains, microcracking, cracking, microcrack and crack growth or displacement of loose rock

particles. Elastic strain energy is released during these processes. Such sudden release of energy develops elastic waves in rock mass, which propagate from the source to the boundaries of the rock mass, and may be recorded as a signal or AE.

Energy and frequency of the generated signals depend on the scale of the phenomenon and the way of generation of the elastic waves in the source. Therefore, the AE can be observed in a very wide range of frequencies, beginning from low range – a fraction of Hz up to very high ultrasonic ones – several MHz (Fig. 1).

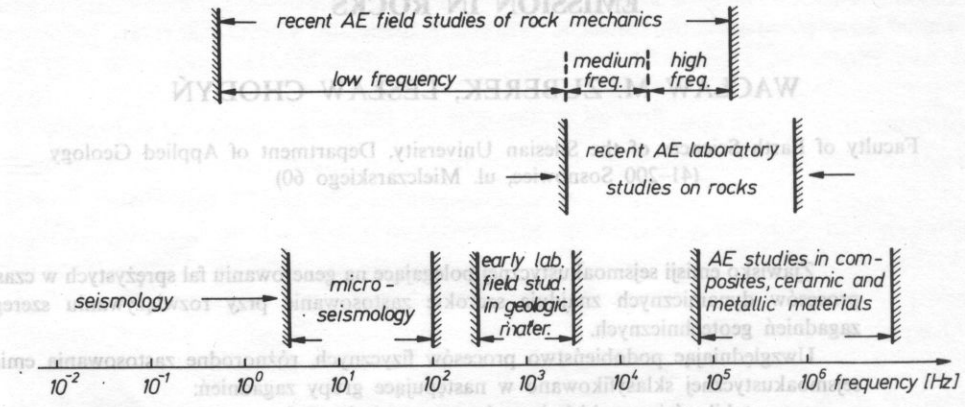

FIG. 1. Frequency range of various types of studies of acoustic emission in rocks and in related fields. Modified HARDY'S diagram [27]

Similarly wide is the range of energy of signals emitted from the source, which are fractions of Joule, for the weakest ones, up to millions of Joules for the most intensive bursts close to tremors. The boundary of acoustic emission in the low frequency range has not been clearly determined. However it is most often assumed above 20 Hz for the most intensive bursts (lower frequencies are also investigated) up to several MHz which can be observed during the weakest microdeformations of rocks. Hence the range of frequencies recorded by local seismological and AE networks is partly the same for the lowest frequencies. However, in general, the notion of acoustic emission covers signals of much higher frequency and much lower energy as the ones recorded by standard seismologic networks.

Various geotechnical applications of acoustic emission have been classified below in certain groups of problems, considering selected common physical features of the observed processes and the rules of using the effect of AE in practical cases, according to the concepts presented in earlier works [83, 84]. It should enable and make easier to obtain certain generalizations and comparisons of processes and applications that sometimes may seem apparently different.

2. Attenuation of AE events in rocks

Elastic waves that propagate in the rocks are attenuated which means irreversible loss of energy. As a measure describing the wave attenuation in rocks one can use undimensional Q factor defined as [1]:

$$\frac{1}{Q} = -\frac{1}{\pi}\frac{\Delta A}{A}, \tag{1}$$

where: A – amplitude of a wave with determined frequency, ΔA – amplitude reduction on the wave's way through the rock.

It can be determined that in a homogenous and isotropic medium an amplitude of a harmonic plane wave at a distance r, $A(r)$ is given by:

$$A(r) = A_0 \exp\left(-\frac{\pi \cdot f \cdot r}{v \cdot Q}\right) \tag{2}$$

where: A_0 – an initial amplitude of the wave (for $r = 0$), f – frequency of the wave, v – phase velocity.

It results from the equation (2) that attenuation of the wave increases together with the increase of frequency (if $Q = \text{const.}$).

Until now it has been assumed in seismology and seismic prospecting that, for different rocks $Q \cong \text{const}$ in the range of low seismic frequencies from 10^{-3} Hz to 10^2 Hz, and even up to 10^3 Hz. Typical Q values for rocks vary from about 10 up to 300. The values of the Q factor are higher for longitudinal waves than for shear ones [25];

$$\frac{Q_p}{Q_s} \cong 2.25 \tag{3}$$

(if sliding on intergranular boundaries is the main mechanism of attenuation)

The loss of the signal energy (depending on the wave length), as the result of attenuation, limits the distance up to which specified frequencies may be observed in the signal. It may be assumed that the rock mass acts on the elastic wave as a lowpass filter, therefore in larger distances we can observe in the signal mainly low frequencies, similar to the seismic ones. Thus the whole phenomenon of generation and propagation of elastic waves which develop in dynamic processes in the rock is usually called, in mining geophysics and rock mechanics, an effect of seismoacoustic or microseismic emission. The same phenomenon, in material sciences and acoustics, is called acoustic emission (AE).

Let us assume, that the maximum frequency of a signal f_{max} describes such a frequency that decrease of an amplitude, caused by attenuation, is equal 20 dB (higher frequencies will be attenuated more intensively). The dependence of f_{max} upon the distance r for rocks with different Q factor may be determined according to the formula (2), (for $Q = \text{const}$) which is presented in Fig. 2. An empiric

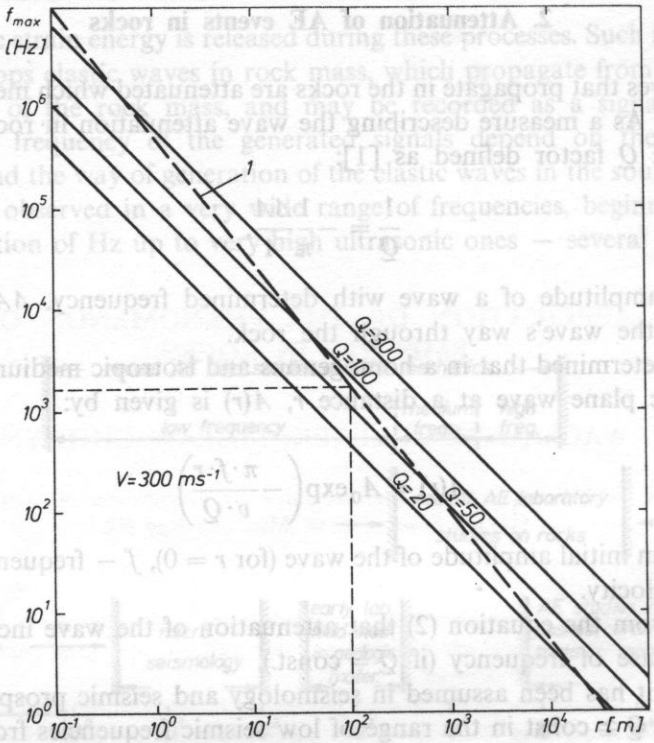

FIG. 2. Detection range r of AE signals as a function of maximum frequency f_{max} for a number of geological materials. Assumed wave velocity $v = 3000$ ms^{-1}. The empirical curve of AE detection range has also been plotted after HARDY [27] curve 1

relation of the range of AE signals as a function of frequency, according to HARDY [27] has been drawn in the diagram for the comparison.

A radius of emitted signal detection depends on a type of rocks; their state e.g. fracturing, a degree of pores and fissures filling (which determines the Q factor), and it is also — as it can be seen in Figure 2 — distinctly and quickly decreasing together with an increase of frequency. Therefore, only frequencies lower than 10^3 Hz can be observed at large distances from the source e.g. of the order 100 m. Actual investigations [25] indicate that in fact Q factor depends on frequency and for frequencies below 10 Hz it is increasing with frequency. It means that presented considerations should be treated only as a first approximation, and the detection distance has to be estimated in each specific case on the basis of accurate attenuation characteristic in the whole frequency range.

3. Stability of openings and geotechnical structures

According to Drucker's definition [68], as a stable system one can consider a system which configuration is determined by the history of loadings in such a way that small disturbances of conditions, under which the system exists, cause such

reaction of the system that no abrupt changes of configuration will occur. A system is unstable when small disturbances of conditions cause large and sudden reaction of the system which is connected with a dynamic transition to a new state of equilibrium, together with a sudden change of the system configuration and the transfer of a part of the potential strain energy into kinetic one.

When we consider the above definition and assume as a system a configuration of openings, their support and the surrounding rock mass, or certain natural elements and structural forms, then many apparently different phenomena, such as; rock bursts, sudden outbursts of gas and rocks, roof falls in mines, side walls slides, landslides of slopes, cavern and chambers collapses, failure of soil dams and embankments may be considered as a whole common group of problems connected with unstability of the system or the geotechnical structure.

The proposed application of AE to determine current stability of a system or a structure usually means periodical measurements of AE burst rate or another parameter of the emission to compare changes of this parameter in time. As it is assumed, when activity is low or it does not exist, the system is stable. High level of activity may indicate transformation of the system into an unstable state which makes necessary to undertake proper action increasing stability, or decreasing the existing hazard. This method is used to determine stability of mining openings [62, 63, 60, 67, 27, 28], as well as landslides of scarps and slopes, embankments and ramparts, underground water reservoires, repositories and caverns [26, 27, 38, 39, 40, 31, 66]. Occurrence of AE effect is strictly correlated with nonelastic deformations occuring in the rock mass. It also appeares that recording of the AE is more convenient and sensitive than traditional methods of deformation measurements, as even slight and local deformations of the rock mass may generate waves propagating from the source for relatively large distances.

On-time determination of stability may be also carried out using the level of artificially generated (AE) in the rock mass. Destressing blastings, concussion or concussion wining blastings, small and large diameter borehole drillings, mining by shearer loader, injections of water into rocks, and firing a standard blowing charge in small diameter boreholes are used for this purpose [82, 67, 7, 79, 80, 81, 55, 77, 78, 19].

It has been noted that high AE burst rate after blasting of the standard blasting charge and a long time period of the burst rate return to the level before blasting are connected with transformation of the system into an unstable state, while low burst rate and a short period of increased burst rate immediately after the blasting are typical for stable systems.

Some examples of the determination of stability based on artificially generated AE in the rock mass are presented in Fig. 3 [19]. The emission has been initiated in the rock mass by firing a standard blasting charge (1 kg of explosive) placed in a 3 m deep blast hole. A geophone, placed in the distance of 5 m from the blast hole in a bore hole 1.5 m deep, has been used as a detector of the AE. The curve 1 in Fig. 3 has been recorded in the undestressed part of the coal seam (unstable system), while the curve 2 in the same picture, in the destressed part of the coal seam (stable system).

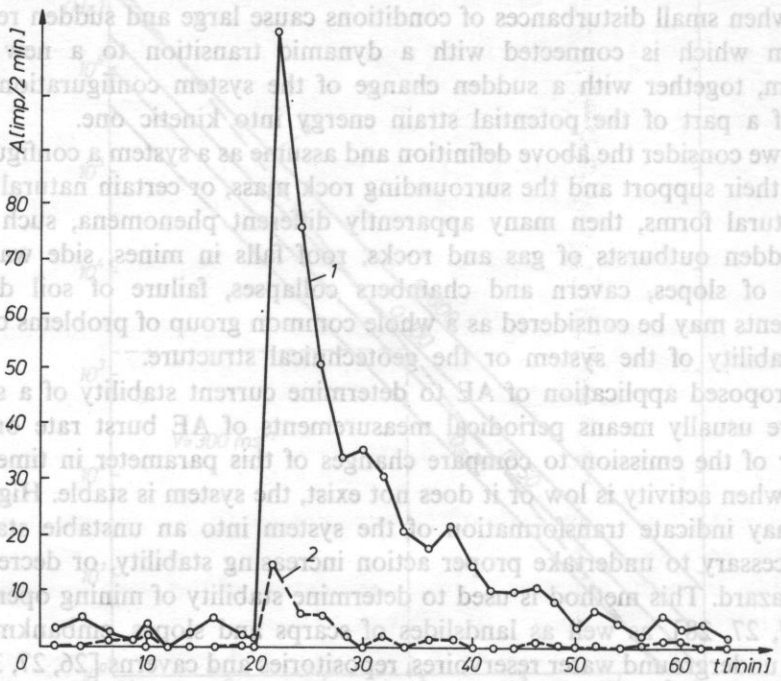

FIG. 3. AE burst rate after blasting in an underground mining face, coal seam 510 of the "Pokój" coal mine; 1 — in the undestressed part of the coal seam, 2 — in the destressed part of the coal seam (after CHACHULSKI and TROMBIK [19])

The level of AE burst and the maximum burst amplitude of the signals recorded during small diameter borehole drillings in a coal seam may also be indicators of stability. It was determined that high AE burst rate and high amplitude of the recorded signals are connected with the system transition into an unstable state. The AE burst rate distinctly correlates with flow-off of drillings from the borehole, and it is a more distinctive indicator of location of the exploitation stresses zone ahead of the working face [58, 67, 81].

Similarly, by means of the AE we can determine effectiveness and the transition time of the rock mass to the stable state after large diameter destressing drillings, injection of water or another liquid into the rock, dewatering, grouting or under — cutting of a scarp or a slope.

Certain ambiguity may appear during determination of openings stability caused, among others, by the facts that:

— definitions of a low and a high level of the AE burst rate are ambiguous, because they depend on the assumed detection threshold,

— it is necessary to consider only particular zones where occurrence of the emission is extremely important for determination of the stability,

– a high level of the AE burst rate is not always connected with unstability of the system or the structure.

However suitable practical experience may diminish and even eliminate these ambiguities.

The AE phenomenon is applied to continuous observation and stability control of mining openings, chambers and caverns, embankments of reservoires, landslides, scarps and sidewalls in open-pits and also rock mass subsidence due to previous mining activity. The method is unique because, using suitably sensitive equipment and the network of properly placed transducers, it may remotely and relatively early detect, localize and signalize changes occuring in the rock mass.

The example of AE application for stability estimation of the active landslide is presented in Fig. 4 [53]. The broken line presents AE burst rate which values increase about one month before the deformations measured geodetically on bench-marks installed in the landslide (solid line).

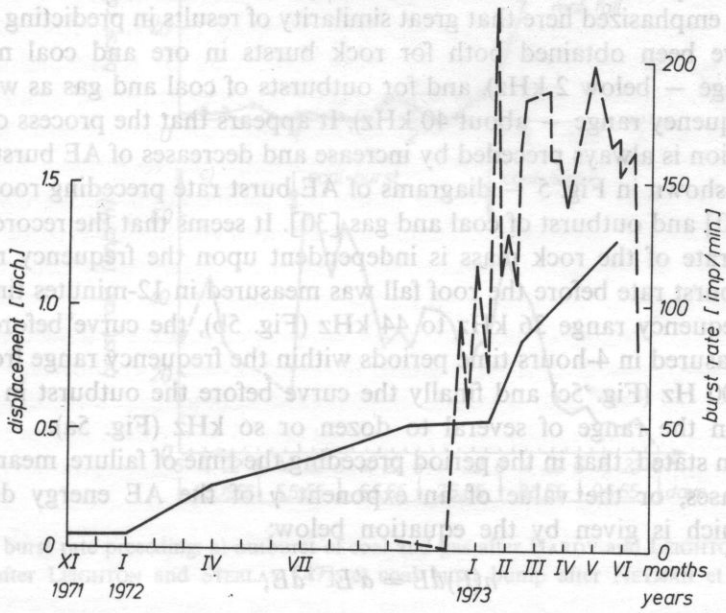

FIG. 4. Variations of AE burst rate broken line and displacement of the bench-mark solid line obtained during measurements in Thornton Bluffs slope, San Francisco penninsula, California USA after MC CAULEY [53]

4. Failure prediction

This problem is partly connected with the stability estimation of a system or a structure, but it is much more difficult, because the solution should include the following estimations (with appropriate accuracy):

– the place of failure,
– the time of failure,
– the area affected by the process of failure (the event magnitude).

Only determination of the above mentioned parameters is understood as failure prediction or prognosis of the failure moment. However it must be stated initially that despite great efforts and numerous investigations, which have been carried out for almost fifty years, and contradictory results, the problem of failure prediction has not been solved reliably and satisfactorily anywhere in the world yet. Nevertheless some results have been very encouraging and promising [61, 3, 76, 60, 42, 17, 16, 71, 8, 45, 44, 30, 48, 74, 73, 57, 20].

Some attempts have been made to determine these parametres when predicting earthquakes [4, 5, 56, 21]. However, there are great difficulties because of a limited detection range of the signals in the rock mass, especially at high frequencies. Therefore AE signals are sometimes recorded on the sea, directly above the focal zone of the earthquake, to diminish, as much as possible, high frequency attenuation.

It must be emphasized here that great similarity of results in predicting the failure moments have been obtained both for rock bursts in ore and coal mines (low frequency range – below 2 kHz), and for outbursts of coal and gas as well as roof falls (high frequency range – about 40 kHz). It appears that the process of the rock mass destruction is always preceded by increase and decreases of AE burst rate. The examples are shown in Fig. 5 – diagrams of AE burst rate preceding roof fall [47], rock burst [60] and outburst of coal and gas [30]. It seems that the recorded course of AE burst rate of the rock mass is independent upon the frequency range. The curve of AE burst rate before the roof fall was measured in 12-minutes time periods within the frequency range 36 kHz to 44 kHz (Fig. 5b), the curve before the rock burst was measured in 4-hours time periods within the frequency range from several Hz up to 1500 Hz (Fig. 5c) and finally the curve before the outburst in 5-minutes periods within the range of several to dozen or so kHz (Fig. 5a).

It has been stated, that in the period preceding the time of failure, mean energy of signals increases, or the value of an exponent γ of the AE energy distribution decreases, which is given by the equation below;

$$n(E)dE = a'E^{-\gamma}dE, \tag{4}$$

where: $n(E)dE$ – the number of AE signals with energy from E to $E+dE$, a', γ – distribution parameters.

It means the decrease of the exponent m value of the amplitude distribution of the AE given by the equation

$$n(a)da = Ka^{-m}da, \tag{5}$$

where: $a > 0$ – maximum amplitude of the signal, K, m – distribution parameters.

However it has not been possible to formulate unique criteria of prognosis and the problem of rockbursts, outburst of rocks and gases and roof falls prediction is still unsolved. Despite the numerous, quoted in the literature, examples of ap-

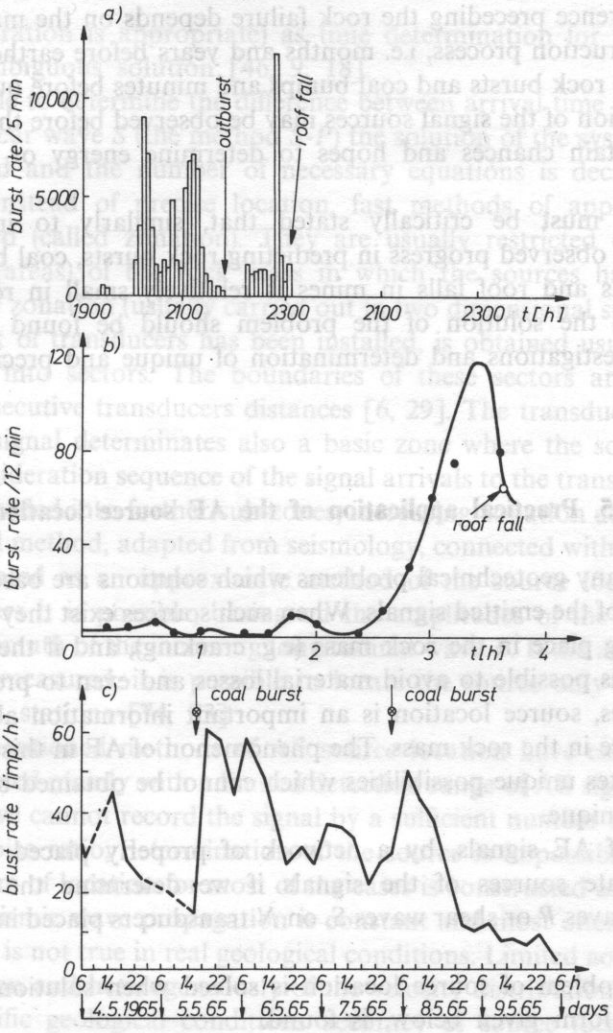

FIG. 5. AE burst rate preceding: a) outburst of coal and gas after HARDY and LEIGHTON [30], b) roof fall after LEIGHTON and STEBLAY [47], c) coal burst bump after NEYMAN et al. [60]

plication of this specific features of the AE to predict the time of failure, there are examples of sudden release of energy of a different course. There are also examples when after prediction the destruction does not occur.

Some new possibilities of interpretation can be obtained due to the AE signal source location and zonation and the possibility to observe changes in space and in time that occur in the rock mass. Such approach to failure prediction was proposed by B. T. BRADY [10, 11, 12, 13, 14, 15, 16, 17] according to his theory of soft inclusion. The results that have been obtained so far indicate that the time of

precursor occurrence preceding the rock failure depends on the magnitude and the scale of the destruction process, i.e. months and years before earthquakes, hours or even days before rock bursts and coal bumps and minutes before outbursts and roof falls. Concentration of the signal sources may be observed before the failure process. That makes certain chances and hopes to determine energy or the scale of the expected event.

However, it must be critically stated that, similarly to investigations on earthquakes, the observed progress in predicting rock bursts, coal bumps, outbursts of rocks and gas and roof falls in mines is relatively small in recent years. The authors suggest, the solution of the problem should be found mainly through fundamental investigations and determination of unique and precise definitions of the phenomena.

5. Practical application of the AE source location

There are many geotechnical problems which solutions are based mainly on the source location of the emitted signals. When such sources exist they indicate changes which are taking place in the rock mass (e.g. cracking), and if they are sufficiently early located it is possible to avoid material losses and even to prevent disaster. In some other cases, source location is an important information about the process which takes place in the rock mass. The phenomenon of AE in this type of practical application creates unique possibilities which cannot be obtained by other methods used in geotechnique.

Recording of AE signals, by a network of properly placed detectors makes possible to locate sources of the signals if we determine the arrival time of a longitudinal waves P or shear waves S, on N transducers placed in the area around the source.

Then, the problem of source location is solved when solution of N nonlinear equations, in a form given below, is found.

$$v(t_i - t) = [(x_i - x_0)^2 + (y_i - y_0)^2 + (z_i - z_0)^2]^{1/2} \tag{6}$$

where v – elastic wave propagation velocity P and S waves may be used, t – the time of the signal occurrence in the source related to the reference time, t_i – the wave arrival time on consecutive detectors, x_0, y_0, z_0 – Cartesian coordinates of the signal source, x_i, y_i, z_i – Cartesian coordinates of the detectors $i = 1 \ldots N$.

If it is assumed that the seismic wave velocity in rocks is constant and known then, to determine uniquely location of the source in three dimensional space, it is necessary to calculate four unknown values, which are source coordinates x_0, y_0, z_0 and the time of signal occurence in the source t.

If the system of equations (6) is solved by means of the method of P or S waves it is necessary to determine times when the signal reaches at least 5 stations (if the

network configuration is appropriate) as time determination for four transducers may give an ambiguous solution [46, 9, 18].

If it is possible to determine the difference between arrival time of a longitudinal wave *P* and a shear wave *S* (the method *S-P*) the solution of the system of equations may be modified and the number of necessary equations is decreased by one.

Sometimes, instead of precise location, fast methods of approximate source location are used (called zonation). They are usually restricted only to indicate certain regions (areas) of the rock mass in which the sources have appeared.

Signal source zonation (usually carried out in two dimensional space), in the area where a network of transducers has been installed, is obtained usually by dividing the whole area into sectors. The boundaries of these sectors are designated by bisectors of consecutive transducers distances [6, 29]. The transducer which is first reached by the signal determinates also a basic zone where the source must exist. Taking into consideration sequence of the signal arrivals to the transducers, the basic sector may be divided into further sub-zones, increasing zonation accuracy [29, 84].

An azimuthal method, adapted from seismology, connected with the *S-P* method may also be treated as an approximate method of the source location. Installing traxial transducers it is possible, basing on the amplitudes of the first arrivals, to determine the azimuth of the incoming longitudinal wave *P*. If the arrival time of the shear wave *S* is measured, it is possible to locate the source only from one of the three component stations [74, 73].

The above mentioned methods of AE source location have certain limitations which are connected mainly with a limited detection range of AE signals of relatively small energy. If we cannot record the signal by a sufficient number of transducers at a given signal/noise ratio, determination of the source is impossible. On the other hand an algorithm of location for most of the cases is constructed assuming that the velocity of the seismic wave propagation is constant and most often the same in all directions, which is not true in real geological conditions. Limited accuracy of arrival time determination and heterogeneously of the velocity distribution in rocks causes that in the specific geological conditions accuracy of source location is limited. However as experiments indicate, when accuracy of the arrival time determination is higher than 1 μs it is possible to obtain location accuracy up to several milimetres, and at the accuracy below 1 ms, up to several metres. This is usually sufficient for many geotechnical applications.

In case of the *S-P* method additional limitations may result from difficulties in determination of the time differences of the longitudinal and shear waves.

Some examples of application of AE sources location have been presented in Fig. 6 [81]. The sources of emission located after drilling of a destressing hole in a coal seam are presented there. Position of the signal sources shows the destressed part of the seam. As we suppose high accuracy of location was possible due to the small area of the investigated region, a large number of transducers and relative homogenity of the rock mass.

AE source location may be also used, in underground mining, to solve purely

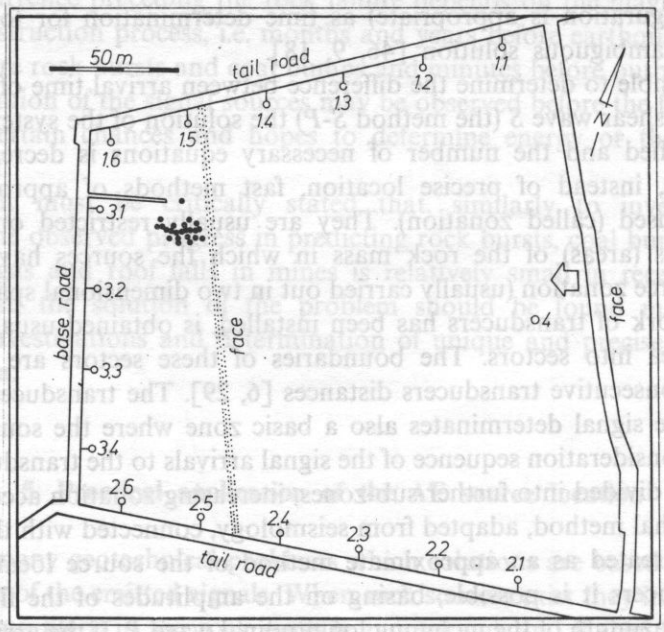

FIG. 6. The example of application of AE source location to determine destressed areas in the rock mass after destressing borehole drilling: o — locations of transducers, • — located AE sources (after WILL [81])

exploitation problems, e.g. control of roof cave developing in a room and pillar system of mining [64]. AE source location was applied to control natural reservoires of crude oil and gas [27, 26, 2] and also to test and control underground storage openings and caves e.g. for food, hot water, compressed air and radioactive waste. Higher AE burst rates the areas as well as where signals occur may show places where the rock mass is weaker and it is necessary to seal it. In some cases, testing of, e.g. natural underground reservoires of natural gas or compressed air, may be performed using so called overpressure, i.e. using pressure higher than the working pressure, and to record the rock mass reaction with source location of AE signals. If there are no signals during the test at overpressure it means proper sealing and ensures correct service of the reservoire at the lower working pressure.

Storage of radioactive waste, both solid and liquid, in underground workings is a separate problem. Such storage must be remotely controlled because of the possibility of high contamination of the environment in case of the growing process of the rock mass cracking. Radioactive waste storage is connected with emission of a large amount of heat, which causes thermal stresses in rocks. As a consequence, rocks may crack and sources of AE appear. A properly installed set of transducers enables remote control and the process observation in the storage [52, 51, 49, 33].

Location of sources of AE signals has been used to control hydraulic fracturing of rocks which is used in many cases e.g. to increase effective porosity of rocks and to recover crude oil and natural gas from a deposit, in geothermal heat plant construction and others. Growth of a macro-crack caused by influence of water injected under high pressure into a sealed part of a well is going discretly and it is acompanied by a large number of AE. Their sources cluster close to the macro--crack edge. Location of the signal sources enables to control currently the process of fracturing, observation of the direction of the macro-crack growth, determination of its magnitude and velocity of its growth, both in reservoire rocks and in the surrounding ones [50, 24, 65].

Application of location of AE signals at works on grouting of a rock mass, e.g. cement or special resin injections, is similar in its character [35]. In this case, the aim of location is to determine the range and velocity of movement of the injected medium in the rock mass.

The phenomenon of AE has also been used to observe movements of the thermal stress front in a process of underground fire flooding of heavy crude oil (to decrease its viscosity and to increase recovery of crude oil from the deposit) [22, 23]. Observing, by AE, the fire flooding and movement of its flame front, it is possible to control the process by regulation of oxygen or air inflow. Similar technique may be used to control a process of underground coal gasification [27]. Location of AE sources during this process enables to observe and control the process and to localize the range of gasification of the coal seam.

It must be stated that the possibility to locate sources of AE signals has caused lately large increase of interest in AE method, and distinguished growth of the range of applications of the effect in geotechnique.

6. Other applications

The examples of geotechnical applications of acoustic emission technique presented above, do not cover all possibilities of AE method. It should be added that the phenomenon connected with an effect of memory of maximum stresses in rocks (Kaiser effect) enables to determine maximum values a stress tensor main component, which influenced the rock in the past due to tectonic phenomena, mining or explosions [36, 32, 34]; as well as to determine preconsolidation pressure of the soil [39, 37, 54]. Despite the fact that results are very promising it is still necessary to explain how such factors as e.g. time, water content influence the effect of memory in rocks.

Fig. 7 presents an example of the course of AE cumulative count number during cyclic loads of samples of granular soil. The solid line represents cumulative count number in particular cycles of load as a function of the stress currently imposed, normalized in relation to the failure stress σ_F for the sample, while the dotted line marks maximum normalized stresses which have been imposed in particular load

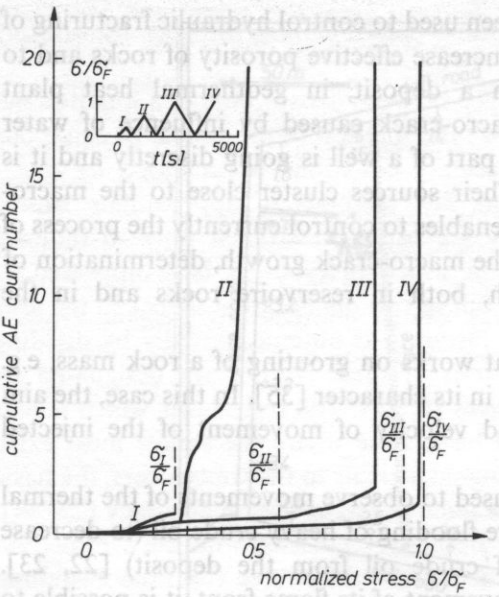

FIG. 7. The cumulative AE count number during cyclic loading of a granular soil sample. I, II, III and IV – the loading cycle number

cycles. One can notice two "stages" of AE course, connected with the memory effect of maximum stresses. Similar effect observed during investigations carried out on granite samples in cyclic load conditions is presented in Fig. 8 [41].

There are also attempts to apply acoustic emission to investigate snow avalanche hazard [69, 43]. It has also been successfully applied to investigate glaciers cracking [59]. The above examples may be considered as typical examples of geotechnical problems.

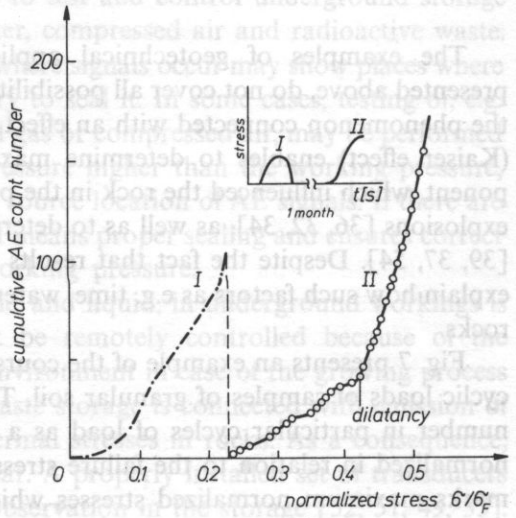

FIG. 8. The cumulative AE count number during cyclic loading of a granit sample (after KURITA and FUJI [41]). The loading path is presented in the upper part of the figure

Successful results have also been obtained during research of AE generated by a cone penetration of soils, to prepare a fast method of in situ soil penetration [75, 72]. It was found that the AE burst rate is strictly correlated with strength features of soils and it may be simply applied to distinguish layers of different soils as it has been presented in Fig. 9.

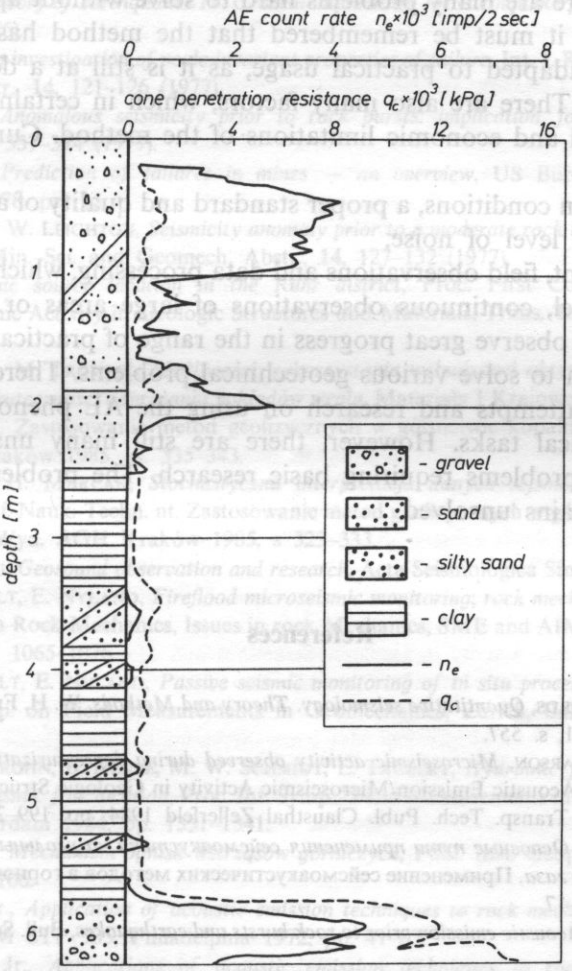

FIG. 9. Variations of the cone penetration resistance q_c and AE count rate n_e obtained during in situ cone penetration studies (after TANIMOTO and NAKAMURA [72])

Slightly different, but very practical, is the application of the AE to the detection of liquid seepage through porous rock. It has been observed that, flow of liquid through porous rock generates distinct signals which may be detected. As it appeared, there are good correlation between the level of the AE and the seepage velocity [35].

7. Conclusion

The presented examples prove distinctly that many geotechnical problems can be solved using the method of acoustic emission and there are vast potential possibilities of its application. It seems, it has already found permanent place in geotechnique, as there are many problems hard to solve without application of the AE effect. However it must be remembered that the method has not been fully developed yet and adapted to practical usage, as it is still at a development and improvement stage. There are also many factors, which in certain situations may cause both technical and economic limitations of the method. Currently the most important are:

– to obtain, in given conditions, a proper standard and quality of a received signal, especially at a high level of noise,

– costs of equipment, field observations and data processing, which may be high in case of multi-channel, continuous observations of large areas or structures.

Actually, we can observe great progress in the range of practical applications of the AE phenomenon to solve various geotechnical problems. There is also a lot of information about attempts and research on using the AE phenomenon to solve particular geotechnical tasks. However, there are still many unsolved technical aspects, as well as problems requiring basic research. The problem of the failure prediction also remains unsolved.

References

[1] K. Aki, P. G. Richards, *Quantitative seismology. Theory and Methods*, W. H. Freeman and Co., San Francisco 1980, v 1, s. 557.

[2] J. Albright, C. Pearson, *Microseismic activity observed during depressurization of an oil storage cavern in rock salt*, Acoustic Emission/Microseismic Activity in Geologic Structures and Materials, Proc. Third Conf., Transp. Tech. Publ. Clausthal Zellerfeld 1984, pp. 199–210.

[3] Н. Г. Анцуферов, *Основные пути применения сейсмоакустики на угольных пластах опасных по выбросам угла и газа*, Применение сейсмоакустических методов в горном деле, Изд. Наука, Москва 1964 с. 3–17.

[4] B. H. Armstrong, *Acoustic emission prior to rock bursts and earthquakes*, Bull. Seism. Soc. Am., **59**, 3, 1259–1279 (1969).

[5] C. F. Bacon, *Acoustic emission along the San Andreas fault in Southern Central California*, California Geology, **28**, 7, 147–154 (1975).

[6] A. Barański, J. Lipiński, E. Czech, Z. Holona, Z. Pilecki, H. Tomanek, *Rejonizacja impulsów w obserwacjach sejsmoakustycznych*, Publ. Inst. Geoph. Pol. Acad. Sci., M-8 (191), 267–280 (1986).

[7] H. Baule, M. V. M. S. Rao, *Seismoacoustic activity in a coal seam in relevance to destressing*, Rock Mechanics, **11**, 3, 177–187 (1979).

[8] W. Blake, *Evaluation of some rock burst precursor phenomena*, Acoustic Emission/Microseismic Activity in Geologic Structures and Materials, Proc. Third Conf. Transp. Tech. Publ., Clausthal-Zellerfeld 1984, s. 239–249.

[9] W. Blake, F. Leighton, W. I. Duvall, *Microseismic techniques for monitoring the behavior of rock structures*, US Bureau of Mines, Bulletin 665, Washington 1974; pp. 65.

[10] B. T. BRADY, *Theory of earthquakes* I. *A scale independent theory of rock failure*, Pageoph., **112**, 701–725 (1974).

[11] B. T. BRADY, *Theory of earthquakes II. Inclusion theory of crustal earthquakes*, Pageoph., **113**, 149–168 (1975).

[12] B. T. BRADY, *Theory of earthquakes III. Inclusion collapse theory of deep earthquakes*, Pageoph., **114**, 119–139 (1976).

[13] B. T. BRADY, *Theory of earthquakes IV. General implication for earthquake prediction*, Pageoph., **114**, 1031–1082 (1976).

[14] B. T. BRADY, *An investigation of scale invariant properties of failure*, Int. J. Rock Mech. Min. Sci. and Geomech. Abstr., **14**, 121–126 (1977).

[15] B. T. BRADY, *Anomalous seismicity prior to rock bursts: implication for earthquake prediction*, Pageoph., **115**, 357–374 (1977).

[16] B. T. BRADY, *Prediction of failures in mines — an overview*, US Bureau of Mines RI 8285, Washington 1978, pp. 15.

[17] B. T. BRADY, F. W. LEIGHTON, *Seismicity anomaly prior to a moderate rock burst: a case study*, Int. J. Rock. Mech. Min. Sci. and Geomech. Abstr., **14**, 127–132 (1977).

[18] A. CETE, *Seismic source location in the Ruhr district*, Proc. First Conf. on Acoustic Emission/Microseismic Activity in Geologic Structures and Materials, Trans. Tech. Publ., Clausthal, pp. 231–241.

[19] A. CHACHULSKI, M. TROMBIK, *Możliwości wykorzystania wzbudzonej aktywności sejsmoakustycznej dla określania skuteczności odprężania pokładów węgla*, Materiały I Krajowej Konferencji Naukowo-Technicznej nt. Zastosowanie metod geofizycznych w górnictwie kopalin stałych, Jaworze t. II. Wyd. AGH Kraków 1985, ss. 335–343.

[20] B. CIANCIARA, H. MARCAK, *Stochastyczna interpretacja danych sejsmoakustycznych*, Materiały I Krajowej Konf. Nauk.-Techn. nt. Zastosowanie metod geofizycznych w górnictwie kopalin stałych, Jaworze t. II, Wyd. AGH Kraków 1985, s 323–333.

[21] S. DONG, Y. LIU, *Geosound observation and research*, Acta Seismologica Sinica, **8**, 4, 115–120 (1986).

[22] M. B. DUSSEAULT, E. NYLAND, *Fireflood microseismic monitoring; rock mechanics implications*, Proc. 23 US Symp. on Rock Mechanics, Issues in rock Mechanics, SME and AIMM and Petr. Eng., New York 1982, pp. 1065–1076.

[23] M. B. DUSSEAULT, E. NYLAND, *Passive seismic monitoring of in situ processes for energy recovery*, Proc. Int. Symp. on Field Measurements in Geomechanics, Zurich, Balkema, Rotterdam 1984, s 81–92.

[24] D. FLACH, C. FROHN, B. HENTE, M. W. SCHMIDT, E. TAUBERT, *Hydraulic fracturing experiments in rock salt with seismic frac location*, Proc. Int. Symp. "Field Measurements in Geomechanics", Zurich, Balkema, Rotterdam 1984, pp. 1331–1341.

[25] S. J. GIBOWICZ, *Mechanizm ognisk wstrząsów górniczych*, Publ. Inst. Geoph. Pol. Acad. Sci M-13 (221) (1989) s. 106.

[26] H. R. HARDY Jr., *Application of acoustic emission techniques to rock mechanics research*, Acoustic Emission, ASTM STP 505, Philadelphia 1972, pp. 41–83.

[27] H. R. HARDY Jr., *Applications of acoustic emission techniques to rock and rock structures*; A state-of-the-art review, Acoustic Emissions in Geotechnical Engineering Practice, ASTM STP 750, Philadelphia 1982, pp. 4–92.

[28] H. R. HARDY Jr., *Application of acoustic emission/microseismic techniques to mine safety and design*, Proc. Int. Symp. on Mining Technology and Seience, Trans. Tech. Publ. and China Coal Industry Publ. House Clausthal–Zellerfeld, Beijing 1987, pp. 491–506.

[29] H. R. HARDY Jr., R. M. BELESKY, M. MRUGALA, E. J. KIMBLE, Jr., M. E. HAGER, *A study to monitor microseismic activity to detect sinkholes*, Final Report, Penn State Univ., NTI, Springfield Va 1986, p. 252.

[30] H. R. HARDY Jr., F. W. LEIGHTON, *Discussions*, Acoustic Emission/Microseismic Activity in Geologic Structures and Materials, Proc. Third Conf., Trans. Tech. Publ., Clausthal–Zellerfeld 1984, pp. 729–738.

[31] H. R. HARDY Jr., G. L. MOWREY, *Analysis of microseismic data from a natural gas storage reservoir*, Acoustic Emission/Microseismic Activity in Geologic Structures and Materials., Proc. Third Conf., Trans. Tech. Publ., Clausthal–Zellerfeld 1984, pp. 365–392.

[32] M. HAYASHI, T. KANAGAWA, S. HIBINO, M. MOTOZIMA, Y. KITAHARA, *Detection of anisotropic geo-stress trying by acoustic emission and non linear rock mechanics on large excavating caverns*, Proc. Fourth Congress of the Int. Soc. of Rock Mech. vol. 2, Montreux 1979, pp. 211–218.

[33] B. HENTE, G. GOMMLICH, D. FLACH, *Microseismic monitoring of candidate nuclear waste disposal sites*, Acoustic Emission/Microseismic Activity in Geologic Structures and Materials, Proc. Third Conf., Trans. Tech. Publ., Clausthal–Zellerfeld 1984, pp. 393–401.

[34] D. J. HOLCOMB, R. J. MARTIN III, *Determining peak stress history using acoustic emission*, Proc. US 26th Symp. on Rock Mechanics, vol. 2, Rapid City, Balkema, Rotterdam, Boston 1985, pp. 712–722.

[35] P. J. HUCK, R. M. KOERNER, *Acoustic emission monitoring of soil and rock grouting*, Acoustic Emission in Geotechnical Engineering Practice, ASTM STP 750, 1982, pp. 155–163.

[36] T. KANAGAWA, M. HAYASHI, H. NAKASA, *Estimation of spatial geo-stress components in rock samples using Kaiser effect of acoustic emission*, Proc. Third Acoustic Emission Symp., Central Res. Inst. of Electric Power Industry, Rep. E 375004, Tokyo 1976, pp. 1–22.

[37] R. M. KOERNER, A. E. LORD Jr., W. L. DEUTCH, *Determination of prestress in cohesive soils using AE*, J. of Geotech. Eng., **110**, 11, 1537–1548 (1984).

[38] R. M. KOERNER, A. E. LORD Jr., W. M. MCCABE, *Acoustic emission monitoring of soil stability*, Journal of the Geotechn. Eng. Div. ASCE, **104**, GT5, 571–582 (1978).

[39] R. M. KOERNER, W. M. MCCABE, A. E. LORD Jr., *Overview of acoustic emission monitoring of rock structures*, Rock Mechanics, **14**, 27–35 (1981).

[40] R. M. KOERNER, W. M. MCCABE, A. E. LORD Jr., *Acoustic emission behavior and monitoring of soils*, Acoustic Emission in Geotechnical Engineering Practice, ASTM STP 750, Philadelphia 1982, pp. 93–141.

[41] K. KURITA, N. FUJII, *Stress memory of crystalline rocks in acoustic emission*, Geophysical Research Letters, **6**, 1, 9–12 (1979).

[42] J. T. LANGSTAFF, *Hecla's rock burst monitoring system*, Mining Congress Journal, **1**, 46–52 (1977).

[43] J. D. LEAIRD, J. PLEHN, *Acoustic emission monitoring on avalanche prone slopes*, Acoustic Emission/Microseismic Activity in Geologic Structures and Materials, Proc. Third Conf., Trans. Tech. Publ., Clausthal–Zellerfeld 1984, pp. 449–466.

[44] F. LEIGHTON, *Microseismic monitoring and warning of rockbursts*, Rockbursts and Seismicity in Mines, The South Afr. Inst. of Min. and Met. Symp. Series no. 6, Kelvin House, Johannesburg 1984, pp. 287–295.

[45] F. LEIGHTON, *Microseismic activity associated with outbursts in coal mines*, Acoustic Emission/Microseismic Activity in Geological Structures and Materials, Proc. Third Conf., Trans. Tech. Publ., Clausthal–Zellerfeld 1984, pp. 467–477.

[46] F. LEIGHTON, W. BLAKE, *Rock noise source location techniques*, US Bureau of Mines RI 7432, Washington 1970, pp. 18.

[47] F. LEIGHTON, B. J. STEBLAY, *Applications of microseismics in coal mines*, Proc. First Conf. on Acoustic Emission/Microseismic Activity in Geologic Structures and Materials, Trans. Tech. Publ., Clausthal 1977, pp. 205–229.

[48] P. MACDONALD, K. M. BROWN, *A microseismic monitoring of an outburst-prone coal seam*, Acoustic Emission/Microseismic Activity in Geologic Structures and Materials, Proc. Third Conf., Trans. Tech. Publ., Clausthal–Zellerfeld 1984, pp. 479–497.

[49] E. L. MAJER, M. S. KING, T. V. MCEVILLY, *The application of modern seismological methods to acoustic emission studies in a rock mass subjected to heat*, Acoustic Emission/Microseismic Activity in Geologic Structures and Materials, Proc. Third Conf., Trans. Tech. Publ., Clausthal–Zellerfeld 1984, pp. 499–516.

[50] E. L. MAJER, T. V. MCEVILLY, *Stripa acoustic emission experiment*, Proc. XVII Workshop on

Hydraulic Fracturing Stress Measurements, US Geological Survey Open File Report, Monterey 1982, pp. 569–581.

[51] E. L. MAJER, T. V. MCEVILLY, *Seismic monitoring of a heated underground repository*, Earthq. Notes, **54**, 1, 31 (1983).

[52] E. L. MAJER, T. V. MCEVILLY, *Acoustic emission and wave propagation monitoring at the spent fuel test*: Climax, Nevada, Int. J. Rock Mech. Min. Sci. and Geomech. Abstr., **22**, 4, 215–226 (1985).

[53] M. L. MCCAULEY, *Monitoring slope stability with acoustic emission*, Proc. First Conf. on Acoustic Emission/Microseismic Activity in Geologic Structures and Materials, Trans. Tech. Publ., Clausthal 1977, pp. 257–269.

[54] J. J. MCELROY, R. M. KOERNER, A. E. LORD Jr., *An acoustic jack to assess in situ rock behaviour*, Int. J. Rock Mech. Min. Sci. and Geomech. Abstr., **22**, 1, 21–29 (1985).

[55] B. M. MCKAVANAGH, J. R. ENEVER, *Developing a microseismic outburst warning system*, Proc. Second Conf. on Acoustic Emission/Microseismic Activity in Geologic Structures and Materials, Trans. Tech. Publ., Clausthal–Zellerfeld 1980, pp. 211–225.

[56] K. MOGI, *Earthquakes as acoustic emission — 1980 Izu Peninsula earthquake in particular*, J. of Acoustic Emission, **1**, 1, 37–44 (1982).

[57] P. MOTTAHED, J. B. VANCE, *Correlation between high frequency acoustic emission and stress redistribution in potash mining*, Stability in Underground Mining II, AIMM and Petr. Eng., 1984, pp. 251–265.

[58] I. NAKAJIMA, Y. WATANABE, T. FUKAI, *Acoustic emission during advance boring associated with the prevention of coal and gas outbursts*, Acoustic Emission/Microseismic Activity in Geologic Structures and Materials, Proc. Third Conf., Trans. Tech. Publ., Clausthal Zellerfeld 1984, p. 529 548.

[59] K. G. NEAVE, J. C. SAVAGE, *Icequakes on the Athabasca Glacier*, J. Geoph. Res., **75**, 8, 1351–1362 (1970).

[60] B. NEYMAN, Z. GRABIS, M. TROMBIK, W. ZUBEREK, *Wyniki badań ciśnienia i tąpań metodami sejsmoakustycznymi w kopalni „Bobrek"*, Prace GIG, Komunikat nr 464, Katowice 1969, s 26.

[61] L. OBERT, W. DUVALL, *Use of subaudible noises for the prediction of rock bursts*, Part II, US Bureau of Mines, RI 3654, Washington 1942, p. 22.

[62] L. OBERT, W. I. DUVALL, *Microseismic method of determining the stability of underground openings*, US Bureau of Mines Bull., 573, Washington 1957, p. 18.

[63] L. OBERT, W. I. DUVALL, *Rock mechanics and the design of structures in rock*, John Wiley and Sons Inc., New York, London, Sydney 1967, p. 650.

[64] M. S. OUDENHOVEN, R. E. TIPTON, *Microseismic source locations around block caving at the Climax molybdenum mine*, US Bureau of Mines RI 7798, Washington 1973, p. 13.

[65] C. PEARSON, J. N. ALBRIGHT, *Acoustic emission during hydraulic fracturing in granite*, Acoustic Emission/Microseismic Activity in Geologic Structures and Materials, Proc. Third Conf., Trans. Tech. Publ., Clausthal–Zellerfeld 1984, pp. 559–575.

[66] A. PENNING, H. VAN DER KOGEL, R. M. KOERNER, F. M. SCHENKEVELD, *Acoustic emissions during slope failure*, Proc. Int. Symp. on Field Measurements in Geomechanics, v. 2, Zurich, Balkema, Rotterdam, 1984, pp. 749–763.

[67] И. М. ПЕТУХОВ, В. А. СМИРНОВ, В. Ш. ВИНОКУР, А. С. ДАЛЬНОВ, *Геофизические исследования горных ударов*, Недра, Москва 1975, с. 33–56.

[68] M. D. G. SALAMON, *Rock mechanics of underground excavations*, Proc. Third Congress of ISRM, National Acad. of Sci., Washington 1974, v. 1, B, pp. 951–1099.

[69] R. A. SOMMERFELD, *Acoustic emission from unstable snow slopes*, Proc. Second Conf. on Acoustic Emission/Microseismic Activity in Geologic Structures and Materials, Trans. Tech. Publ., Clausthal–Zellerfeld 1980, pp. 319–329.

[70] F. D. STACEY, *Physics of the earth*, John Wiley and Sons, New York, Santa Barbara, London, Sydney, Toronto 1977, pp. 300–307.

[71] B. J. STEBLAY, *Progress in the development of a microseismic roof fall warning system*, Proc. Tenth

Annual Inst. on Coal Mining Health, Safety and Research, Virginia Polytechnic Institute and State Univ., Blacksburg Va 1979, pp. 177–195.

[72] K. TANIMOTO, J. NAKAMURA, *Use of AE technique in field investigation of soil*, Acoustic Emission/Microseismic Activity in Geologic Structures and Materials, Proc. Third Conf., Trans. Tech. Publ., Clausthal–Zellerfeld 1984, pp. 601–612.

[73] A. VAN ZYL BRINK, D. M. O'CONNOR, *Research on the prediction of rockbursts at Western Deep Levels*, J. of the South Afr. Inst. of Min. and Met., **83**, 1, 1–10 (1983).

[74] A. VAN ZYL BRINK, D. M. O'CONNOR, *Rock burst prediction research-development of a practical early warning system*, Acoustic Emisssion/Microseismic Activity in Geologic Structures and Materials, Proc. Third Conf., Trans. Tech. Publ., Clausthal–Zellerfeld 1984, pp. 269–282.

[75] W. C. B. VILLET, J. K. MITCHELL, P. T. TRINGALE, *Acoustic emission generated during the quasi-static cone penetration of soils*, Acoustic Emission in Geotechnical Engineering Practice, ASTM STP 750, Philadelphia 1982, p. 174–193.

[76] Д. ВИНОГРАДОВ, *Акустические наблудения процессов разрушения горных пород*, Изд. Наука, Москва 1964, с. 84.

[77] Y. WATANABE, I. NAKAJIMA, *Acoustic emission activity in bed rock surrounding underground working faces in deep level coal seams*, Advances in Acoustic Emission, Proc. of Int. Conf. on Acoustic Emission, Dunhart Publ., Knoxville, Tennessee 1981, pp. 307–322.

[78] Y. WATANABE, I. NAKAJIMA, K. ITAKURA, *The fracturing activity prior to coal or rock outburst in cross-measure drivages*, Acoustic Emission/Microseismic Activity in Geologic Structures and Materials, Proc. Third Conf., Trans. Tech. Publ., Clausthal–Zellerfeld 1984, p. 613–631.

[79] M. WILL, *Seismoacoustic activity and mining operations*, Acoustic Emission/Microseismic Activity in Geologic Structures and Materials, Proc. Second Conf., Trans. Tech. Publ., Clausthal–Zellerfeld 1980, pp. 191–209.

[80] M. WILL, *Measurement and on line evaluation of seismic seam-reactions during test – and destressing – drilling*, Acoustic Emission/Microseismic Activity in Geologic Structures and Materials, Proc. Third Conf., Trans. Tech. Publ., Clausthal–Zellerfeld 1984, p. 633–646.

[81] M. WILL, *Seismic observations during test drilling and destressing operations in German coal mines*, Rockburst and Seismicity in Mines, The South Afr. Inst. of Min. and Met. Symp., Series no. 6, Kelvin House, Johannesburg 1984, p. 231–234.

[82] W. ZUBEREK, *Sejsmoakustyczna charakterystyka pękania calizny węglowej pod wpływem strzelań wstrząsowych*, Prace GIG, Komunikat nr 593, Katowice 1973, p. 38.

[83] W. M. ZUBEREK, *Wykorzystanie efektu emisji sejsmoakustycznej w geotechnice*, Publ. Inst. Geophys. Pol. Acad. Sci. M-11 (217) (1988) s. 178.

[84] W. M. ZUBEREK, M. DZIUROWICZ, L. CHODYŃ, *Zastosowanie emisji sejsmoakustycznej w geotechnice*, Prz. Górn. 11-12, 32-36 (1987).

Received on March 14, 1988.